
AFRL-RY-WP-TR-2016-0193

# PERFORMANCE PREDICTION OF CONSTRAINED WAVEFORM DESIGN FOR ADAPTIVE RADAR

**Aaron M. Jones**

**Radio Frequency Exploitation Technology Branch**
**Layered Sensing Exploitation Division**

**NOVEMBER 2016**
**Final Report**



**AIR FORCE RESEARCH LABORATORY**
**SENSORS DIRECTORATE**
**WRIGHT-PATTERSON AIR FORCE BASE, OH 45433-7320**
**AIR FORCE MATERIEL COMMAND**
**UNITED STATES AIR FORCE**

# NOTICE AND SIGNATURE PAGE

Using Government drawings, specifications, or other data included in this document for any purpose other than Government procurement does not in any way obligate the U.S. Government. The fact that the Government formulated or supplied the drawings, specifications, or other data does not license the holder or any other person or corporation; or convey any rights or permission to manufacture, use, or sell any patented invention that may relate to them.

This report was cleared for public release by the USAF 88th Air Base Wing (88 ABW) Public Affairs Office (PAO) and is available to the general public, including foreign nationals.

Copies may be obtained from the Defense Technical Information Center (DTIC) (http://www.dtic.mil).

AFRL-RY-WP-TR-2016-0193 HAS BEEN REVIEWED AND IS APPROVED FOR PUBLICATION IN ACCORDANCE WITH THE ASSIGNED DISTRIBUTION STATEMENT.

//signature//

*AARON M. JONES, Project Manager
Radio Frequency Exploitation Technology Branch
Layered Sensing Exploitation Division

//signature//"

GREGORY A. CAZZELL, Chief
Radio Frequency Exploitation Technology Branch
Layered Sensing Exploitation Division

//signature//"

JACQUELINE A. TOUSSAINT-BARKER, Chief
Layered Sensing Exploitation Division
Sensors Directorate

This report is published in the interest of scientific and technical information exchange, and its publication does not constitute the Government's approval or disapproval of its ideas or findings.

*Disseminated copies will show "//signature//" stamped or typed above the signature blocks.

# REPORT DOCUMENTATION PAGE

*Form Approved*
*OMB No. 0704-0188*



| 1. REPORT DATE *(DD-MM-YY)* | 2. REPORT TYPE | 3. DATES COVERED *(From - To)* |
|---|---|---|
| November 2016 | Doctoral Thesis | 01 April 2012 – 30 June 2016 |

**4. TITLE AND SUBTITLE**
PERFORMANCE PREDICTION OF CONSTRAINED WAVEFORM DESIGN FOR ADAPTIVE RADAR

**5a. CONTRACT NUMBER**
In-House

**5b. GRANT NUMBER**

**5c. PROGRAM ELEMENT NUMBER**
6.1

**6. AUTHOR(S)**
Aaron M. Jones

**5d. PROJECT NUMBER**
2311

**5e. TASK NUMBER**
N/A

**5f. WORK UNIT NUMBER**
N/A

**7. PERFORMING ORGANIZATION NAME(S) AND ADDRESS(ES)**
Layered Sensing Exploitation Division
Radio Frequency Exploitation Technology Branch (AFRL/RYAP)
Air Force Research Laboratory, Sensors Directorate
Wright-Patterson Air Force Base, OH 45433-7320
Air Force Materiel Command, United States Air Force

**8. PERFORMING ORGANIZATION REPORT NUMBER**
AFRL-RY-WP-TR-2016-0193

**9. SPONSORING/MONITORING AGENCY NAME(S) AND ADDRESS(ES)**
Air Force Research Laboratory
Sensors Directorate
Wright-Patterson Air Force Base, OH 45433-7320
Air Force Materiel Command
United States Air Force

Air Force Office of Scientific Research
875 N. Randolph, Suite.325
Arlington, VA 22203

**10. SPONSORING/MONITORING AGENCY ACRONYM(S)**
AFRL/RYAP

**11. SPONSORING/MONITORING AGENCY REPORT NUMBER(S)**
AFRL-RY-WP-TR-2016-0193

**12. DISTRIBUTION/AVAILABILITY STATEMENT**
Approved for public release; Distribution is unlimited.

**13. SUPPLEMENTARY NOTES**
PAO Case Number: 88ABW-2016-3170, cleared 27 June 2016. A dissertation submitted in partial fulfillment of the requirements for the degree of Doctor of Philosophy in Engineering at Wright State University, Dayton, OH. Report contains color.

**14. ABSTRACT**

Traditional radar sensing paradigms consider relatively benign noise and interference operational environment. Today's radars, however, face an ever increasingly complex operational environment, exacerbated by the numerous mission/modes, number and type of targets, non-homogeneous clutter and active interferers in the scene. Thus, the ability to adapt ones transmit waveform to optimally suit the needs for a particular radar tasking and environment becomes mandatory. This requirement brings with it a host of challenges to implement, including the basic decision of what to transmit.

In this dissertation, we will discuss five original contributions that aid in the decision making process of an adaptive radar in selection what to transmit. We investigate the signal-to-noise-and-interference ratio (SINR) performance for a multi-constrained waveform design in the presence of colored interference. We set-up and numerically solve two optimization problems that maximize the SINR while applying a novel waveform design technique that requires the signal be an ordered subset of eigenvectors of the noise and interference covariance matrix. The significance of the work is the observation of the non-linearity in the SINR performance as a function of the constraints.

We then derive two new performance models, one for the constrained waveform SINR and one for the basis-dimension of the eigenvectors of the noise and interference covariance matrix required to achieve a particular modulus constraint. Radar waveforms typically require a constant modulus (constant amplitude) transmit signal to efficiently exploit the available transmit power. However, recent hardware advances and the capability for arbitrary (phase and amplitude) designed waveforms have forced a re-examination of this assumption to quantify the impact of modulus perturbation from phase-only signals.

Lastly, we develop the role of the integrated sidelobe (ISL) parameter for adaptive radar signal design as it pertains to SINR performance. We seek to further extend the state of the art by developing two new performance models for the integrated sidelobemetric. First, the corresponding SINR degradation, from optimal as the ISL constraint is applied and second, the basis dimension of the noise and interference covariance matrix required to generate the waveform. Included are Monte Carlo simulation trials designed to measure the impact of ISL on SINR.

**15. SUBJECT TERMS**
performance prediction, waveform design, fully adaptive radar

| 16. SECURITY CLASSIFICATION OF: | | | 17. LIMITATION OF ABSTRACT: | 18. NUMBER OF PAGES | 19a. NAME OF RESPONSIBLE PERSON (Monitor) |
|---|---|---|---|---|---|
| a. REPORT | b. ABSTRACT | c. THIS PAGE | | | Aaron M Jones |
| Unclassified | Unclassified | Unclassified | SAR | 170 | 19b. TELEPHONE NUMBER *(Include Area Code)* N/A |

# PERFORMANCE PREDICTION OF CONSTRAINED WAVEFORM DESIGN FOR ADAPTIVE RADAR

A dissertation submitted in partial fulfillment
of the requirements for the degree of
Doctor of Philosophy in Engineering

by

AARON M. JONES
B.S., Wright State University, 2007
M.S., Wright State University, 2011

---

2016
Wright State University

WRIGHT STATE UNIVERSITY

GRADUATE SCHOOL

June 28, 2016

I HEREBY RECOMMEND THAT THE DISSERTATION PREPARED UNDER MY SUPERVISION BY Aaron M. Jones ENTITLED Performance Prediction of Constrained Waveform Design for Adaptive Radar BE ACCEPTED IN PARTIAL FULFILLMENT OF THE REQUIREMENTS FOR THE DEGREE OF Doctor of Philosophy in Engineering

Brian D. Rigling, Ph.D.
Dissertation Director

Frank W. Ciarallo, Ph.D.
Director, Ph.D. in Engineering Program

Robert E. W. Fyffe, Ph.D.
Vice President for Research and
Dean of the Graduate School

Committee on
Final Examination

Brian D. Rigling, Ph.D.

Muralidhar Rangaswamy, Ph.D.

Christopher Baker, Ph.D.

Fred D. Garber, Ph.D.

Zhiqiang Wu, Ph.D.

ABSTRACT

Jones, Aaron M., Ph.D. Engineering, Engineering Ph.D. Program, Department of Electrical Engineering, Wright State University, 2016. *Performance Prediction of Constrained Waveform Design for Adaptive Radar.*

Today's radars face an ever increasingly complex operational environment, intensified by the numerous types of mission/modes, number and type of targets, non-homogeneous clutter and active interferers in the scene. Thus, the ability to adapt ones transmit waveform, to optimally suit the needs for a particular radar tasking and environment, becomes mandatory. This requirement brings with it a host of challenges to implement including the basic decision of what to transmit. In this dissertation, we discuss six original contributions, including the development of performance prediction models for constrained radar waveforms, that aid in the decision making process of an adaptive radar in selecting what to transmit.

It is critical that the algorithms and performance prediction models developed be robust to varying radio frequency interference (RFI) environments. However, the current literature only provides toy examples not suitable in representing real-world interference. Therefore, we develop and validate two new power spectral density (PSD) models for interference and noise, derived from measured data, which allow us to ascertain the effectiveness of an algorithm under varying conditions.

We then investigate the signal-to-interference-and-noise ratio (SINR) performance for a multi-constrained waveform design in the presence of colored interference. We set-up and numerically solve two optimization problems that maximize the SINR while applying a novel waveform design technique that requires the signal be an ordered subset of eigenvectors of the interference and noise covariance matrix. The significance of this work is the observation of the non-linearity in the SINR performance as a function of the constraints. This inspires the development of performance prediction models to obtain a greater understanding of the impact practical constraints have on the SINR.

Building upon these results, we derive two new performance models, one for the constrained waveform SINR and one for the basis-dimension of the eigenvectors of the noise and interference covariance matrix required to achieve a particular modulus constraint. Radar waveforms typically require a constant modulus (constant amplitude) transmit signal to efficiently exploit the available transmit power. However, recent hardware advances and the capability for arbitrary (phase and amplitude) designed waveforms have forced a re-examination of this assumption to quantify the impact of modulus perturbation from phase only signals. The models are validated with measured data and through Monte Carlo (MC) simulation trials.

Lastly, we develop the role of the integrated sidelobe (ISL) parameter for adaptive radar waveform design as it pertains to SINR performance. We seek to further extend the state-of-the-art by developing two new performance models for the integrated sidelobe metric. First, the corresponding SINR degradation, from optimal as the ISL constraint is applied and second, the basis dimension of the noise and interference covariance matrix required to generate the waveform. With our approach, we are able show exceptional ability to predict the impact to SINR as we tighten the ISL constraint in the waveform design. For all performance models, we include Monte Carlo simulation trials designed to measure the impact of ISL on SINR as well as compare performance when measured data is used to represent the interference and noise covariance matrix.

# Abbreviations and Symbols

Throughout this dissertation numerous abbreviations and symbols are used. While the definitions can be found in surrounding text, this section provides a quick reference.

| | |
|---|---|
| ACF | Autocorrelation Function |
| ACS | Autocorrelation Sequence |
| AF | Ambiguity Function |
| AFRL | Air Force Research Laboratory |
| AR | Auto-regressive |
| BAA | Broad Agency Announcement |
| CDF | Cumulative Distribution Function |
| CM | Cumulative Modulus |
| DARPA | Defense Advanced Research Projects Agency |
| DAWG | Digital Arbitrary Waveform Generator |
| DFT | Discret Fourier Transform |
| DOF | Degree of Freedom |
| DSP | Digital Signal Processing |
| ET | Envelop Tracking |
| FAR | Fully Adaptive Radar |
| FFT | Fast Fourier Transform |
| FM | Frequency Modulation |
| GHz | Gigahertz |
| Hz | Hertz |
| I + N | Interference and Noise |
| ISL | Integrated Sidelobe |
| ISLR | Integrated Sidelobe Ratio |
| KL | Kullback-Leibler |
| LFM | Linear Frequency Modulation |
| MATLAB | Matrix Laboratory |
| MC | Monte Carlo |
| MDL | Minimum Description Length |
| ML | Maximum Likelihood |
| MLE | Maximum Likelihood Estimates |
| MHz | Megahertz |
| MP | Marčenko-Pastur |
| MPC | Micro Power Conversion |
| MPSL | Minimum Peak Sidelobe Sequence |
| OTA | Over-the-air |
| PAPR | Peak-to-average-power Ratio |
| PDF | Probability Density Function |
| PeCAN | Periodic Cyclic Algorithm New |

List of Abbreviations (cont.)

| | |
|---|---|
| PMF | Probability Mass Function |
| PSD | Power Spectral Density |
| PSL | Peak Sidelobe |
| PSLR | Peak Sidelobe Ratio |
| RCS | Radar Cross Section |
| RF | Radio Frequency |
| RFI | Radio Frequency Interference |
| RMB | Reed Mallett Brennan |
| RMT | Random Matrix Theory |
| RX | Receive |
| SINR | Signal-to-Interference-and-Noise Ratio |
| SWORD | Signal Waveform's Optimal Under Restriction Design for Active Sensing |
| TX | Transmit |
| UHF | Ultra High Frequency |
| WLOG | Without Loss of Generality |

# List of Symbols and Notation

| | |
|---|---|
| $\approx$ | Denotes an approximate quantity |
| $(\cdot)^{\mathrm{H}}$ | Hermitian form of an argument |
| $\mathbf{E}\{\cdot\}$ | Expectation operator |
| $\|\cdot\|_p$ | p-norm of an argument |
| $\nabla$ | Gradient vector |
| $\underline{\mathrm{s}}_n$ | The $n^{th}$ entry of a column vector |
| $\mathrm{Re}\{\cdot\}$ | Real component of complex argument |
| $\mathrm{Im}\{\cdot\}$ | Imaginary component of complex argument |
| $\mathcal{H}$ | Hermitian matrix |
| $\mathbb{H}$ | Hessian operator |
| $(\cdot)^*$ | Optimal solution |
| $\odot$ | Hadamard operator |
| $\sim$ | A probability density |
| $\mathrm{vec}(\mathbf{X})$ | Vectorize operator |
| diag | Diagonal matrix |
| $\lceil\cdot\rceil$ | Ceiling operator |
| $\lfloor\cdot\rfloor$ | Floor operator |
| tr | Trace of a matrix |
| $(\cdot)^{-1}$ | Inverse operator |
| $\|\cdot\|$ | Absolute value |
| $\hat{(\cdot)}$ | Estimate |
| s.t. | subject to |
| $\dim(\cdot)$ | dimension of the argument |
| $\in$ | denotes membership in a set |
| $\mathbb{R}$ | set of real numbers |
| $\mathbb{I}$ | set of imaginary numbers |
| $\mathbb{C}$ | set of complex numbers |
| LHS | Left hand side of an equation |
| $\min$ | minimization |
| $\sqrt{\cdot}$ | square-root of an argument |
| $\sqrt[p]{\cdot}$ | p-th root of an argument |
| $\mathcal{F}$ | Fourier Transform |
| $\prod$ | Product operation |
| $\mathcal{O}(\cdot)$ | Computational complexity |
| $\Gamma(\alpha)$ | Gamma function evaluated at $\alpha$ |
| $\leq$ | Less than or equal to |
| $\gtrsim$ | Approximately greater than |
| $(\cdot)^T$ | Transpose operator |
| $\cong$ | Asymptotically equivalent |
| $\int_a^b$ | Bounded integral |
| $\partial$ | Partial derivate |
| $\prod$ | Product |

## List of Symbols and Notation (cont.)

| | |
|---|---|
| $\bigotimes$ | Kronecker |
| $\forall$ | For all |
| $\rightarrow$ | Tends to |
| $\lim$ | Limit |

# Contents

# List of Figures

# List of Tables

# Acknowledgment

It is my pleasure to thank those who helped effectuate this dissertation project, without whom it would not have been possible.

I am indebted to many of my current and former colleagues especially former Branch Chief, Dr. Jeffrey H Sanders and Senior Technical Advisor, Dr. Muralidhar Rangaswamy of the RF Exploitation Branch within AFRL. Both of whom can be attributed to the advancement of this technology, providing valuable technical guidance and affording me the time to pursue its completion. Thank you.

Additionally, I would like to thank Mr. Michael J. Callahan, Dr. Jason T. Parker and the additional members of the AFOSR Fully Adaptive Radar STAR Team comprised of Dr. Pawan Setlur, Dr. Sandeep Gogineni, Dr. Tariq Qures Hi and Mr. Sean O'Rourke. All of whom have contributed, in their own way, to my professional and sometimes personal development.

I owe sincere gratitude to my dissertation advisor, Dr. Brian D. Rigling, who has committed countless hours in the classroom, in the office and in personal correspondence to my technical development. Dr. Rigling is a true teacher, evident by his patience, knowledge and genuine selflessness to assist in others growth and achievement. I also thank Dr. Christopher Baker, Dr. Fred Garber and Dr. John Wu for their participation on the dissertation committee.

Lastly, I would like to pay tribute to my family, especially my beautiful wife, Lesley. Without their support, confidence and encouragement, it would be difficult to appreciate this accomplishment.

Dedicated to

Lesley and Cameron and Michael and Ashley Rose

# Chapter 1

# Introduction

This chapter includes introductory material that provides context for the research and gives a brief synopsis of each of the novel contributions described in the dissertation. First, in section 1.1, we give a broad overview of the intentions for the dissertation. Section 1.2 provides motivation to pursue this important research area. Section 1.3 describes performance models and gives an example and use-case for radar. Section 1.4 discusses each of the novel contributions. Section 1.5 gives the outline of the dissertation. Section 1.6 reviews the notation used throughout the document. Finally, section 1.7 summarizes the Chapter.

## 1.1 Overview

In this dissertation, we endeavor to improve answering the basic question of what to transmit for an adaptive radar. We accomplish this objective by advancing our understanding of how constraints on radar waveforms affect the SINR performance with six novel contributions in the areas of performance prediction models, interference and noise covariance matrix modeling and new waveform design approaches.

Waveform design and optimization is a highly developed field with applications in radar, communications, imaging, etc., for both commercial and military communities. This

is, in part, inspired by the fact that the ability of a system to transmit arbitrary waveforms provides a unique flexibility to improve sensing performance by optimizing the design degrees of freedom (DOF) for a specific task [4, 5]. Additionally, a key advantage of an adaptive waveform design system, versus a waveform static system, is that it theoretically allows improved operation in dynamically changing environments, such as those that modern radar systems face.

Waveform diversity has its roots dating back as far as the 1930s, where history recalls the development of waveforms with varying chirp rates [6]. In 1953, the definition of the narrowband radar ambiguity function (AF) was formulated by P. M. Woodward [7, 8]. This instrument has proved to be an important and intricate tool in waveform design, as noted in [9]. In fact, this dissertation is partially inspired by the famous Woodward quote, having a ubiquitous feeling for all radar waveform design (and performance prediction) researchers, that is found at the end of the book [7] and is as follows:

> *The reader may feel some disappointment, not unshared by the writer, that the basic question of what to transmit remains substantially unanswered.*

This sentiment is further exacerbated today with the increases in the number modes, missions, and operational environments that current (and future) radar systems face, an example of such a system is given in [10].

The advent of the matched filter (or pulse compression) technique allowed longer pulse lengths and ability to resolve closely spaced targets as a function of the waveform bandwidth [11, 12]. However, this invention created an additional concern for radar waveforms designers, namely, range sidelobe levels and its corollary, how to suppress them. In this dissertation, we consider a design methodology to observe the signal-to-interference-and-noise ratio performance as a function of the sidelobe suppression and develop quick-to-compute performance prediction models to aid in the decision making process of an adaptive radar. We employ this novel waveform diversity approach to allows intuitive, and analytical, development of performance prediction models for constrained radar waveform

design.

Significant operational challenges exist for modern radar systems, such as, scene topography, increasing number of targets, decrease in size of targets and the congested/contested spectrum, among others. These concerns lead us, inexorably, to the conclusion that simply interrogating the scene is no longer sufficient. The radar (and thus the transmit waveform) must adapt to its environment and, therefore, understanding the impact of practical constraints is a prerequisite.

## 1.2 Motivation

Radar waveform design techniques typically focus on maximizing the SINR [13–15] while satisfying some practical constraint quantified by a suitable measure (e.g., Doppler tolerance, peak side-lobe ratio (PSLR) and/or integrated side-lobe ratio (ISLR), bandwidth, energy, etc.). Success is claimed when the waveform achieves improved SINR, relative to the current best technique. However, what is ignored, or not fully understood, is the degradation in SINR, from optimal, when the constraint is allowed to be tightened or loosened.

Currently, no performance models exists that discuss relationships between waveform constraint and SINR performance. This motivates research to focus on developing the relationships (i.e., performance prediction models) between practical constraints for radar waveforms and the SINR performance that is critical for detection. The lack of understanding leads us to develop innovative practical models with an intuitive approach to understanding the complex relationships of constraints and SINR performance. Specifically, in this dissertation, we will focus on the waveform modulus and the range sidelobe constraints[1].

Adaptive systems can use performance prediction models to make informed, responsive decisions on what to transmit based on the needs of the system and the operational

[1]This work first featured in; A. M. Jones, B. D. Rigling, and M. Rangaswamy, *Motivations to develop performance prediction for adaptive radar*, in NAECON. IEEE, June 2015.

environment. Designing waveforms and *enforcing constraints without this understanding is a shortsighted approach for adaptive radar waveform design* due to the nonlinearity of the SINR performance for practical constraints [16].

We are further motivated by recent advances in hardware capability to generate arbitrary (phase and amplitude) design waveforms. The need to re-examine the usual assumption of phase-only or constant modulus signal design for radar is warranted and can be attributed to a confluence of recent events. For example, the Defense Advanced Research Projects Agency (DARPA) has made significant progress in the Micro-scale Power Conversion (MPC) program that desires, among other goals, to advance high efficiency RF power amplifier technology via envelope tracking (ET) of the transmission, see DARPA BAA-11-33. They note in [17] that many present and future RF systems employ complex modulation techniques with high peak-to-average-power ratio (PAPR) and the power amplifiers operate well below peak output a majority of the time, wasting valuable and limited, energy resources. Begin able to employ ET in a fixed and highly limited power environment (e.g. airborne platform) could imply additional devices or sensors could run simultaneously or if battery powered, extended operational time. Also, the community has witnessed significant advances in digital arbitrary waveform generators, giving rise to the possibility of a broad range of transmit signal classes [13, 18].

### 1.2.1 Adaptive Sensing

As a possible concept of operations, we consider the challenging RF sensing paradigm (see Figure 1.1) where a sensing system must contend with multiple types of topography (such as urban, rural, suburban and littoral, or combinations within a single sortie), many different types of targets (ground movers, airborne and space platforms, for example) and the shrinking RF spectrum (i.e., contested/congested) limiting the available frequencies for clean transmission. These concerns together necessitate optimal use of available resources

to maximize system performance.

Under these assumptions, it would be advantageous to consider use of a Fully Adap-

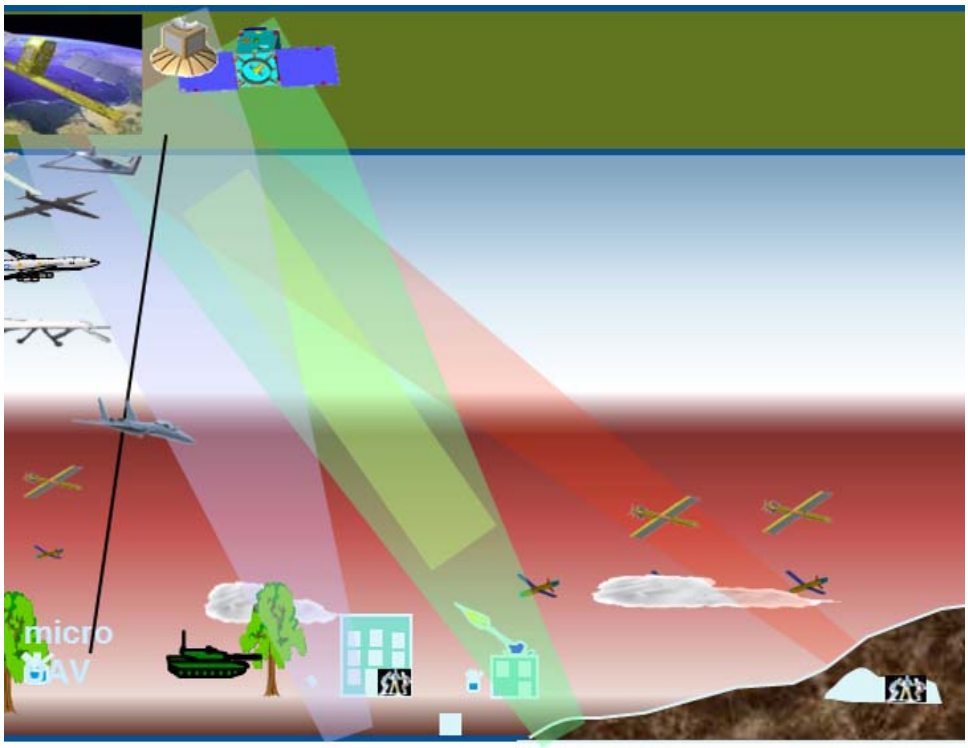


Figure 1.1: Challenging RF sensing paradigm.

tive Radar (FAR) or cognitive radar [19, 20] to overcome the limitations of fixed transmission. However, one of the many implementation challenges of the FAR is estimating how the waveform will perform as the constraints are changed to suit the mission/mode/environmental needs.

A direct application for performance prediction models is the Fully Adaptive Radar (see Figure 1.2), which we define as:

**Definition 1** ***Fully Adaptive Radar Construct:***

*A broad system architecture that exerts all available degrees of freedom (DOF) on transmit and receive to provide closed-loop feedback optimization of system performance for all possible missions/modes and environmental concerns.*

We highlight how performance models can aid in the decision making process of what to transmit for an adaptive system in the following sections.

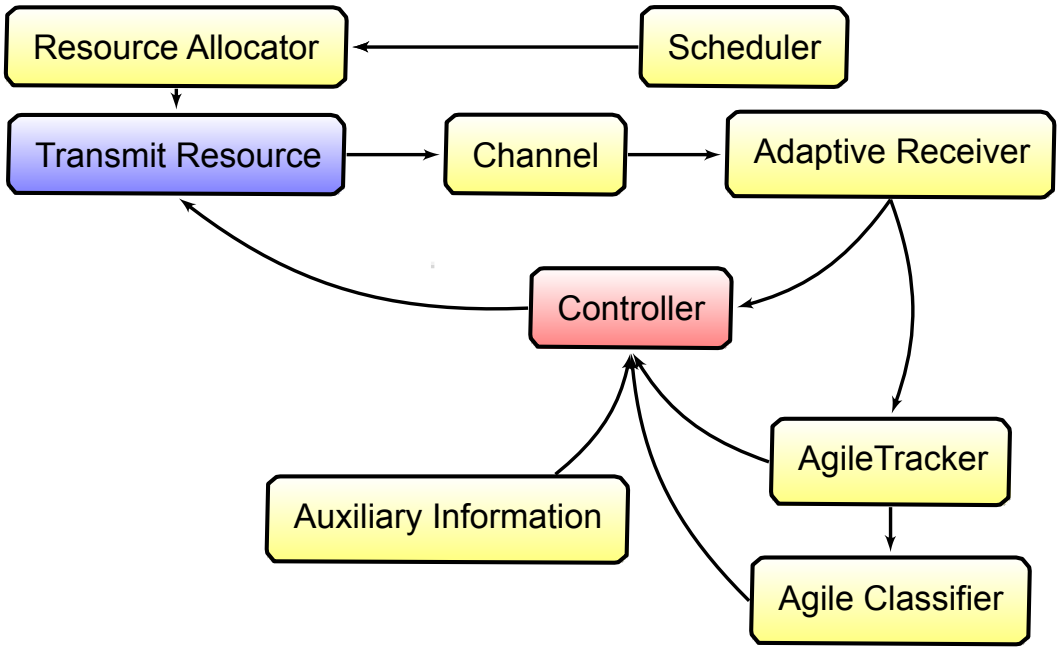


Figure 1.2: Fully Adaptive Radar Construct [1]

### 1.2.2 Motivations for Performance Models for Radar

**Gross Lack of Understanding of How Practical Constraints on the Waveform Effect Detection Performance**

Possibly the most convincing argument to develop performance models is the lack of understanding in how constraints influence SINR performance. Intuitively, we have an understanding that forcing constraints on the waveform design limits the DOF to maximize SINR performance. However, it seems misguided then, to arbitrarily place a constraint without fully comprehending the consequence to the detection performance.

Again, adaptive systems can use performance models to make informed, responsive

decisions on what to transmit based on the needs of the system and the operational environment. Designing waveforms and forcing constraints without understanding the consequences is a shortsighted approach due to the nonlinearity of the SINR performance.

**Adaptive Technologies Require Insight**

The use of an adaptive system allows the radar to smartly adjust to a wide variety of non-stationary environments. However, to truly close-the-loop, the radar must be adaptive on transmit [19]. This would imply we understand how to change the transmit waveform to be better suited for the environment under test, to do so; we (the radar waveform designers) need to provide the direction of adaptation. This could include a multitude of dimensions, including the sidelobe levels and the modulus. We caution, the absence of performance models to aid in the decision of what to transmit for FAR limits the responsiveness of the directivity we can provide to the adaptive system.

**Solving High-Dimensional Optimization Problems in Real-Time is Currently a Challenge**

Lastly, we are motivated to develop performance models due to the computational burden of solving large dimension optimization problems. Compute power is a primary concern in time/space limited environments (like that of an on-board airborne computer system) and the adaptive radar is no exception. We note, for example the adaptive matched filter has $\mathcal{O}(M^3)$ (where $M$ is dimensionality of the problem), the adaptive tracker given $L$ points of data and $K$ target models, the computational cost of data association is $KL$, and additional cost can come from incorporation of a priori information pertaining to a given scenario in the form of information storage, communication, retrieval overhead as well as the cost of cuing databases in real time. Thus, even a simple instantiation of the FAR/cognitive system becomes computationally intensive. Reducing training data support is imperative to ameliorate over this important problem.

For the use-case of adaptive radar we ask, can we limit the search space to identify the desirable transmit waveform? Thus, providing relief for the curse of dimensionality on the computing resources. With the development of performance models for waveform design, we can give the radar a rough estimate of performance and achieve in limiting the search space.

## 1.3 Example of a Performance Model

As shown notionally in Figure 1.4, the interference and noise (I + N) characteristics play an important role in the SINR performance that is further compounded by the constraints applied to the waveform design. As an example, estimation of the interference and noise in the radar channel is necessary for adaptive radar to be effective. Detailed in [21], the Reed-Mallot-Brennan (RMB) rule (i.e. performance model) accurately denotes the number of training data samples required ($\approx$ 2N, where N is the problem dimensionality) to get within 3dB of the optimal (clairvoyant) covariance estimation for adaptive receive filter design. This is an effective performance model for radar that with rigorous mathematical tractability provided insights into the data needs for covariance estimation to perform space-time adaptive processing. Although not a guarantee, this model gives the average training data requirement for a specific case of an I + N environment under certain assumptions.

The model significantly reduces the amount of information needed to predict performance, in this case you only need to know the dimension of the problem to get an estimate of the data needs, where, in reality you would need to acquire the actual sample covariance matrix to compute the true data needs. The model has traded accuracy for speed and, over time, has proved a useful model. It is our goal to achieve a similar level of utility for the performance prediction models for constrained radar waveform design.

### 1.3.1 Typical Waveform Constraints

For practical radar, we are limited by the hardware capabilities as to what is possible to be transmitted. However, with the advent of digital arbitrary waveform generators (DAWG's) and envelope tracking technologies, we are in new territory enabling near absolute flexibility on transmit. Nevertheless, concerns persist. For example, finite energy on-board an airborne platform, low SINR targets being missed by high range-sidelobes or near-in targets masked by high PSLR. As an example, in Figure 1.3 we observe the issues when sidelobe concerns are omitted from the transmit waveform design process. This loosely illustrates how ignoring the integrated sidelobes can result in target misses at the radar receiver output.

Similarly, the peak-to-average power ratio of the transmit waveform is of critical

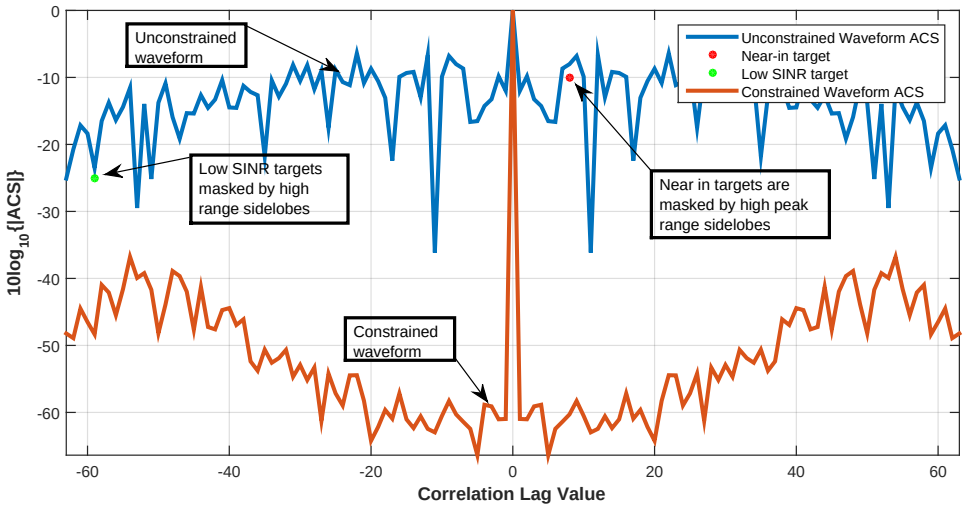


Figure 1.3: Illustration of the consequences when range sidelobe concerns are omitted (and considered) in the waveform design process to maximize SINR.

importance for the radar designer. Of course, the maximum supply voltage is finite in any system and it is understood that more power on target increases the chances that the return signal is detected, but modulating the amplitude of the waveform will limit the over-all transmit power. Therefore, efficient use of the available supply voltage on transmit becomes

part of the waveform design criteria. Other constraints exist; however, range-sidelobes and power usage are the primary concerns for the radar waveform designer.

### 1.3.2 Use-case for Performance Prediction Models and Adaptive Radar

The use-case for performance models considered in this dissertation is the radar detection problem in the presence of colored noise and interference. Mentioned in the introduction, the challenging RF sensing paradigm (Figure 1.2) is exacerbated by the number and types of targets and the contested, congested spectrum. We note that simply interrogating the scenes is no longer sufficient, the radar must adapt. But, how to know best where to put the DOF in the waveform design problem, maximizing SINR, minimizing ISL or efficient use of energy? Or some combination of all three (or others)? And, what are the consequences to one if emphasis is placed on another? Answering these questions, broadly, is the product of performance prediction models, derived in this dissertation.

In Figure 1.4, we give a notional example of how we can use performance models for adaptive radar waveform design using spectral efficiency [22] to describe the environment. The Figure illustrates the loss in SINR as the constraint (modulus or range-sidelobes in this case) is applied for a particular spectral efficiency scenario. Understanding the trade-off between SINR and the constraint can help avoid over constraining the waveform design and unnecessarily relinquishing SINR performance .

### 1.3.3 Current Solutions Being Worked

A significant gap exists in the understanding of how constraints place on the waveform design affect the SINR performance. We note that performance prediction for radar waveform designs developed in this dissertation, are not design techniques, but rather, a tool to provide guidance to the waveform designer. In Figure 1.5 we suggest strategies in which performance modeling can support the waveform design process managed by the controller in the FAR scheme. We expand upon the trade-off in the waveform computation strategy

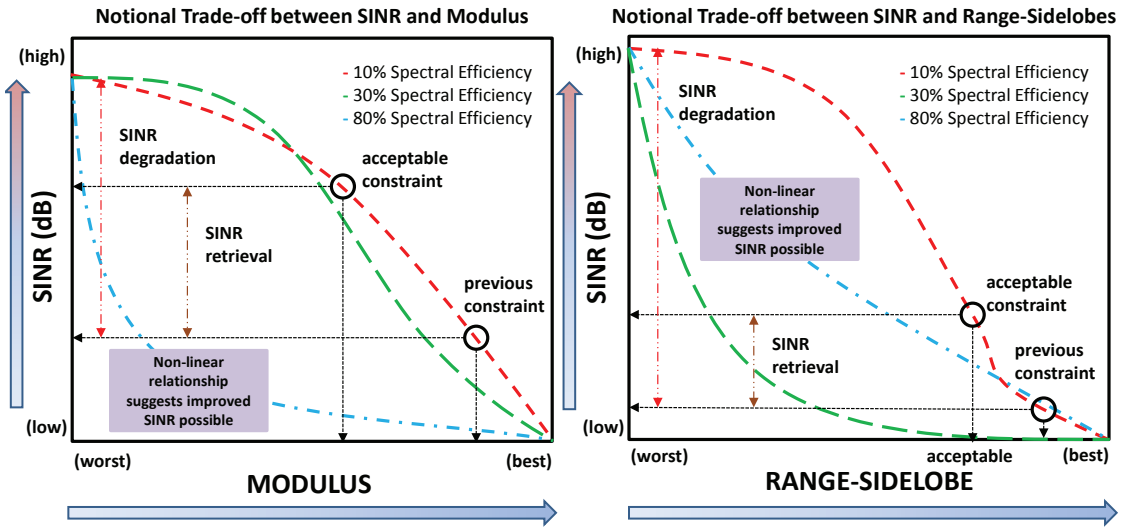


Figure 1.4: Notional example of the trade-off between constraints and SINR for adaptive radar waveform design.

between a fixed (non-adaptive, decided prior to the mission) providing fast computation (non-existent, in this case) and the constrained optimization without smart initialization requiring the highest of computations. We see performance models can provide support in all the strategies mentioned and the theorized benefit when the models are effective.

In [16, 23, 24] they examine development of performance models for range-sidelobe and modulus constraints, both jointly and individually. It is shown a nonlinear relationship exists between the application of the waveform constraint and the performance degradation, from optimal. This is a novel result and suggests that fewer DOF can be placed to meet the constraints if the designer is willing to release limited control over the design and these can be re-purposed towards SINR maximization.

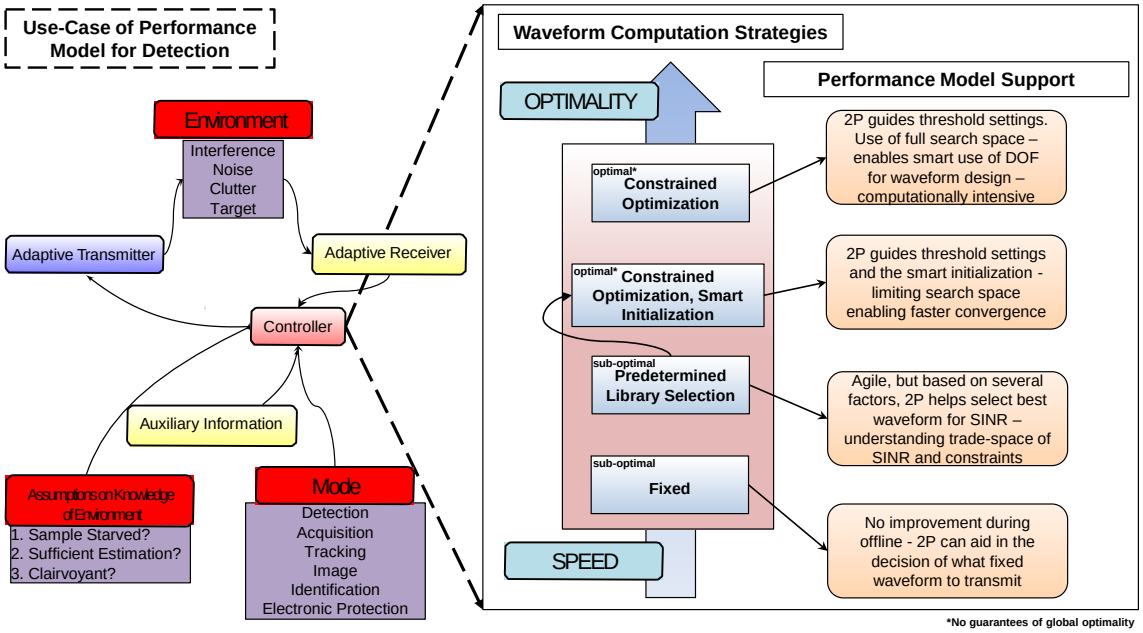


Figure 1.5: Illustration of the role performance models play in aiding the decision making process of an adaptive radar.

## 1.4 Contributions

This dissertation includes six significant novel contributions, culminating in original interference and noise models, new signal designs and advanced performance models for adaptive radar. These contributions are introduced in the following sections.

### 1.4.1 Data Models (new and legacy)

In this dissertation, we make use of three important data models to represent the interference and noise covariance matrix. We note that conventional models for representing power spectral densities, and their corresponding covariance matrices, fall short in characterizing the statistical properties and other features for both the noise and signal bands. This leaves algorithm designers limited resources to perform realistic Monte Carlo analysis. In this dissertation, we develop a new practical technique, derived from measured data, to generate unique instantiations of radio frequency interference in urban North American

environments. Additionally, we make novel use of a general utility I + N model not previously used for waveform design analysis. Portions of this Chapter have been previously published in [25].

Current approaches to estimating RFI (see Figure 1.6) involve either the collection of spectral data in various environments to characterize the interference or the use of aggregation tools, such as TV Fool$^{TM}$, which provide analysis of over-the-air (OTA) broadcasts [2]. These approaches can be costly, cover only a limited bandwidth, or limited to only a few instantiations. Additionally, modeling colored interference and noise covariance matrices, with desired power spectral density (PSD) traits, is useful for waveform design, development, and analysis [26]. Many attempts in literature employ what is mathematically convenient but not necessarily accurate in representing real-world interference [15, 27]. As such, only conjecture that performance trends seen in toy examples will translate to representative data is possible. This is a risky assumption.

The first I+N model considered is that most commonly seen in the waveform design

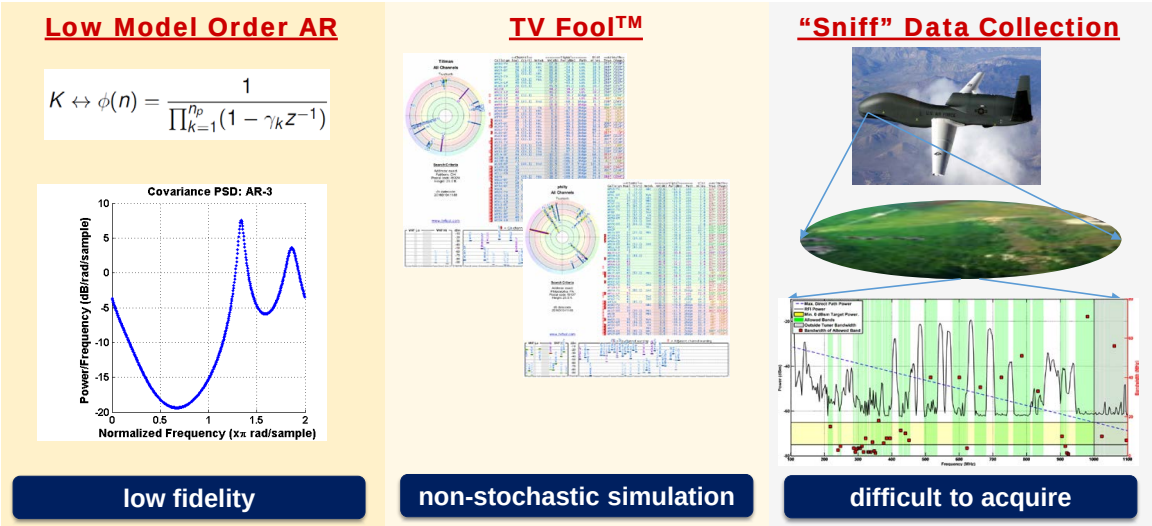


Figure 1.6: Current approaches to synthetic RFI generation and data collection challenges.

literature, a toy example used to show performance differences in various design techniques, the low model-order auto-regressive (AR) model. This model is useful for its ease

of generation in Monte Carlo analysis, but, as we will show, is not a statistically accurate model for real-world data.

Second, we consider a model with general utility gives that has convenient asymptotic properties, like a closed-form representation of the eigen-spectrum and ease of generation, but, may not be suitable for all scenarios.

Lastly, we derive, from measured data, two synthetic PSD models by employing a novel approach where a two-state Markov chain is used to define the spectral transitions from signal-and-noise present to noise-only and vice versa. We then modify the sequence with signal and noise specific amplitude distributions to arrive at the synthetic PSD. This is advantageous over current approaches in multiple ways. First, we are able to exploit the unique underlying phenomenology inherent to the UHF bands' power spectral content. Second, the technique requires limited computing power and time, and therefore is also cost effective.

These models allow us to illustrate the dependence on the scenario in SINR degradation as a function of the constraints. It is desirable to use real-world scenarios to provide accurate performance estimates, not just toy examples. Details are found in Chapter 3

### 1.4.2 Eigen-Basis Analysis of Modulus and Sidelobe Constrained Radar Waveform Design

The second unique contribution is an algorithm to develop a qualitative understanding the role the Eigen-basis of the colored noise and interference covariance matrix plays in constrained radar waveform design. We jointly constrain the modulus and range-sidelobes to show the trade-off between each constraint and the SINR performance. We accomplish by solving a cascade of optimization problems that are analyzed through Monte Carlo simulation trials. This requires a structured approach to the design of the waveform and well defined definitions of the constraints and I + N. This work has been previously published in [16].

We investigate the impact of constraints on the basis dimension of the I + N covariance matrix eigen-space used to represent the desired signal (via discrete *Karhunen-Loève* expansion [28]) . As expected, when constraints are applied to the waveform, a larger basis is required to meet the design needs. Next, we derive relationships between the constraint definitions used in this analysis and more familiar constraints, peak-to-average-power ratio (PAPR) and PSLR. We also prove or disprove the convexity of the constraints. Careful consideration must also be given to the initialization of the optimization problems, for, as we will show, the sidelobe constraint is non-convex and the solution will be dependent on the starting waveform.

Additionally, in this contribution, we develop a novel approach for constrained waveform design for detection performance analysis. This research advances our understanding of the impact of constraints to SINR under the assumption of accurate representation of the second order statistics of the noise and interference covariance. Of course, actual SINR will depend on many others factors; target location, radar cross-section (RCS), and carrier frequency among others. This new algorithm could be employed to improve the decision making capability of an adaptive system and reduce real-time through-put requirements. The details are found in Chapter 4.

### 1.4.3 SINR Performance Prediction for Modulus and Energy Constrained Waveform Design

The third novel contribution, previously submitted for publication [29], is the development of a performance model for SINR as we apply modulus constraints on the radar waveform design. Of course, constraints on waveform design are manifestations of the operational paradigm. For example, the peak-to-average power, where unity would be a constant modulus waveform, prevents a large power scaling due to the nonlinearity of a radar systems power amplifier and simplifies recognition of the target distortion on receive while also ensuring efficient use of dynamic range. Typically, a constant modulus waveform design is

used to prevent this power loss. Here, we relax this requirement to investigate the effect on SINR in non-phase only designs with finite energy.

This effort requires development of a new, simplified function to represent the modulus perturbation from phase only waveforms. Next, we employ asymptotic results from random matrix theory (RMT) to derive accurate performance prediction of the SINR given a modulus constraint. In addition, in this section we develop innovative performance models for the SINR as a function of the modulus for two classes of colored interference environments and a random interference environment. We also report barriers for developing additional analytical results for this approach. Therefore, Monte Carlo computer simulations and measured data are used to validate the analytical findings. Details can be found in Chapter 4.

### 1.4.4 Cumulative Modulus Performance Models for Energy Constrained Waveform Design

The forth distinct contribution of this dissertation is the derivation and analysis of a new performance model to estimate the cumulative modulus (CM). This derivation is a function of the eigen-basis dimension of the interference and noise covariance matrix required to generate the waveform. Motivated by the well-known optimal design solution for SINR, the Rayleigh solution or the minimum eigenvector waveform, we implement a formulation where a linear combination of the eigenvectors of the noise and interference covariance matrix comprises the waveform. Under the Rayleigh solution, the waveform is defined by a single eigenvector, but applying waveform constraints implies additional eigen-dimensions must be spanned. In doing so, we point out; any waveform may be viewed as a linear combination of the eigenvectors of the interference and noise covariance matrix.

The novel performance prediction model developed gives a generalized first-order approximation of the eigen-basis dimension (i.e. the approximate minimum number of eigenvectors) required to achieve a certain waveform modulus. Understanding these per-

formance trades can improve/enhance the decision making process of an adaptive system. Lastly, we observe and report the performance response for several representative interference types and validated against measured data. Details are found in Chapter 4

### 1.4.5 SINR Performance Prediction for Sidelobe Constrained Waveform Design

The fifth significant contribution we propose is a new model for the SINR performance when a sidelobe constraint is applied on the waveform design. For this contribution, we discuss the role of the integrated sidelobe parameter for adaptive radar signal design as it pertains to SINR performance. We do so by undertaking a design methodology that, again, limits the basis dimension of the waveform while placing a finite energy constraint on the optimal ISL solution. Next, we will develop new equations to predict the SINR performance when a sidelobe constraint is applied for various interference classes. Monte Carlo simulation trials and measured data are designed to measure the impact to SINR on the ISL and validate the accuracy of the models. This material has been accepted for publication in [24]. Details are found in Chapter 6.

### 1.4.6 ISL Performance Models for Constrained Waveform Design

Lastly, to complete the research, we propose the sixth unique contribution be development of a model of the ISL constraint as a function of the eigen-basis dimension of the interference and noise covariance matrix required to generate the waveform. We have developed an analytical result for the expected ISL as a function of multiple variables that we validate against synthetic data. The integrated sidelobe constraint as a signal design criteria has been studied in great depth [3, 30–34] and we note its important role in multiple radar functions, including reducing the number of false alarms, improving multiple target resolution and efficient spreading of the energy contained within the signal. Others have

investigated performance models for similar metrics, integrated sidelobe ratio and peak-sidelobe ratio but limited the data models of noise and interference modeled to Bernoulli distributions [35, 36].

The literature also mentions several design methodologies for limiting sidelobe levels, including; periodic autocorrelation function technique that has zero sidelobes [37], and similarly a cyclic technique PeCAN [14, 34] or a competing technique Signal Waveform's Optimal Under Restriction Design for Active Sensing (SWORD) [15], among others. However, the progressive consequence to SINR when synthesizing waveforms with these techniques is unclear. We demonstrate the accuracy of the performance prediction models through use of measured interference and noise data to generate the covariance matrix. A majority of this work has been submitted for publication in [38]. Details can be found in Chapter 6.

## 1.5 Outline of Dissertation

Each Chapter will begin with a brief synopsis and end with a brief conclusion. In Chapter 2, we conduct a review of relevant past literature, with emphasis on waveform design algorithms, applications and challenges to fully adaptive radar, asymptotic results in random matrix theory and other mathematical tools, and radar performance models. For Chapter 3, we derive interference and noise covariance matrix models and explain the potential advantages and pitfalls for each model when used to evaluate waveform design performance. We discuss our initial results and observations for the jointly constrained waveform design problem in Chapter 4. In Chapter 5, we discuss research that develops performance prediction models to quantify the impact on SINR when an amplitude constraint is placed on a radar waveform design. Our research on SINR performance for range-sidelobe suppressed waveforms is given in Chapter 6. Then, in Chapter 7, we discuss possible avenues for future research. Finally, in Chapter 8 we summarize the dissertation and offer some

closing remarks followed by the comprehensive Bibliography and related appendices. A chapter dependency chart is given is Figure 1.7 to allow the readership to select only the components of interest.

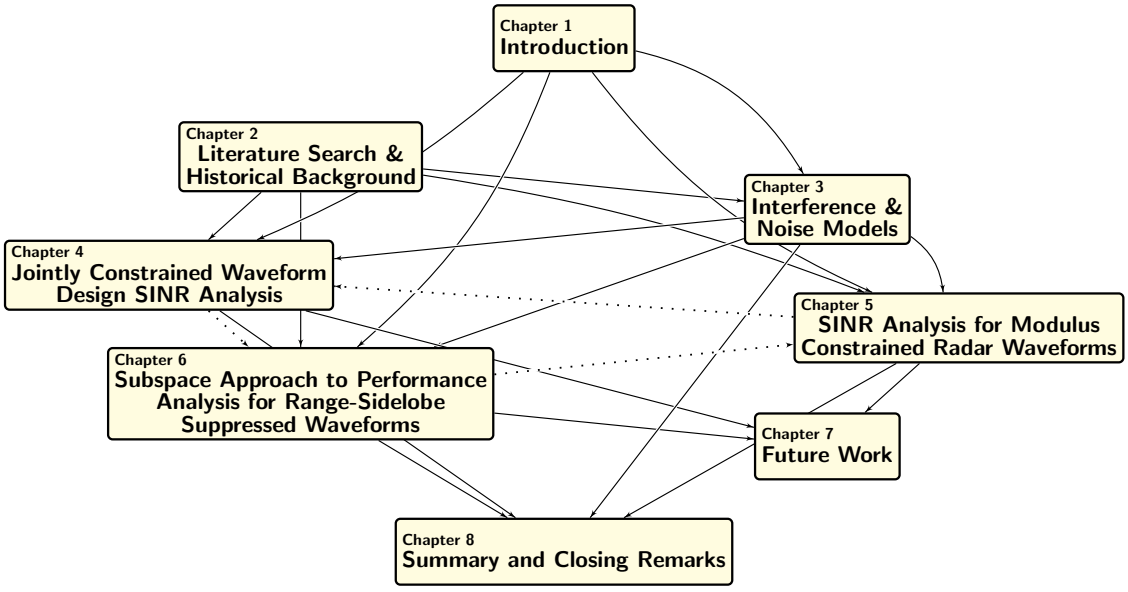


Figure 1.7: Chapter dependency chart.

## 1.6 Notation

The following notation will be used throughout the Dissertation. We denote column vectors as underlined lowercase letters. The $n^{th}$ entry of a column vector $\underline{\mathrm{s}}$ is characterized $\underline{\mathrm{s}}_n$. Matrices are shown using **boldface** capital letters. Scalar quantities are as capital letters. $\mathrm{Re}\{\cdot\}$ and $\mathrm{Im}\{\cdot\}$ represent the real and imaginary components of a complex argument, respectively. The Hermitian operator is given as $(\cdot)^H$, while the expectation operator is $\mathbf{E}\{\cdot\}$. The $\mathrm{L}_2$ and $\mathrm{L}_4$ norms are represented as $\|\cdot\|_2$ and $\|\cdot\|_4$, respectively. The optimal solution is denoted as $(\cdot)^*$. The partial derivative operator is indicated by the $\partial$ identifier with the gradient as $\nabla$ and the Hessian denoted $\mathcal{H}$. The Hadamard operation is given by the $\odot$ symbol while $\sim$ denotes a probability density.

The optimal solution is denoted as $(\cdot)^*$. The vec operator on a matrix stacks the columns of the matrix in a single column vector, such that, for $\mathbf{X} = \left[\begin{smallmatrix} a & b \\ c & d \end{smallmatrix}\right]$, $\text{vec}(\mathbf{X}) = [acbd]^T$.

## 1.7 Chapter Summary

This chapter included several background items that provide context for the research described in the dissertation. This included a description of the six novel contributions of the dissertation, the notation, conventions and several definitions used in the document. We also motivated the use of performance models in an adaptive system. We also gave an example and use-case, with notional illustrative example, for performance models of SINR as constraints are applied to waveform..

Performance models can be successful in addressing the top concerns. Knowing the SINR performance is a function of the interference and noise, it is imperative to have accurate knowledge, or an accurate model, of the statistics in order to develop a useful tool.

In summary, we have motivated the use of performance prediction for radar waveform design for detection. We have given a detailed use-case and discussed the primary reasons for performance models for adaptive radar.

# Chapter 2

# Literature Search and Historical Background

In this chapter, we present a focused literature search and discuss some of the relevant historical background in waveform diversity and design. Due to the limitations of prior work in performance prediction, we consider the historical work in design to help guide the focus of the performance prediction efforts. We note that waveform diversity and design has witnessed a widespread resurgence over the last 10-15 years. This is evidenced by the increase in number of articles, books, funding increases, special sessions in conferences and workshops, and special issues on selected topics in waveform diversity [13, 39, 40]. While extensive literature exists in the areas of waveform diversity and optimization with emphasis towards improving many typical functions of radar (e.g., detection, automatic target recognition, imaging, electronic warfare, etc.), it is impractical to review these topics entirely. Therefore, to avoid confusion and dilution of the primary contributions, we limit the discussion to constrained radar waveform design and the SINR performance.

In section 2.1 we mention some of the broader and more foundational materials. Section 2.2 gives a review of common types of radar waveforms and their applications. We discuss current radar performance models and the need for the development of additional

models in section 2.3. A cursory review of the concepts of Fully Adaptive Radar (FAR) is in section 2.4. In section 2.5 we review useful conclusions derived from random matrix theory (RMT), other mathematical tools. We then discuss current data modeling techniques for colored interference and noise in section 2.6. Finally, we summarize the chapter in section 2.7.

## 2.1 Broad Background Material

There have been numerous books written on different aspects of waveform design for radar. Some of the more popular and fundamental texts in the field of signal design and radar include [6, 13, 41–46]. These texts provide a detailed examination of the rich history of waveform design for radar and we employ the definition of waveform diversity from [45] as

> *Adaptivity of the radar waveform to dynamically optimize the radar performance for the particular scenario and tasks.*

There have also been several survey papers on various topics in waveform design for radar. For example, Stoica et al., provide a good discussion of the use of transmit code sequences for range resolution and detection [47]. In 2009, Sira [48] wrote on adapting the transmit waveform to match the sensing task and environment. In 2009, Calderbank [49] wrote on waveform diversity in signal processing and the control of DOF in the radar illumination pattern. Lastly, we mention the 2009 paper by Benedetto, et. al [9] that mentions the important role the ambiguity function plays in phase-coded waveforms.

## 2.2 Review of Review Waveform Designs

Early radar systems employed the linear frequency modulated (LFM) or chirp waveform or the simple pulsed waveform [50, 51]. Since this time, an abundance of techniques have been developed for which there are many applications. In the sections that follow, we explore and define many common types of radar waveforms and their application to this dissertation.

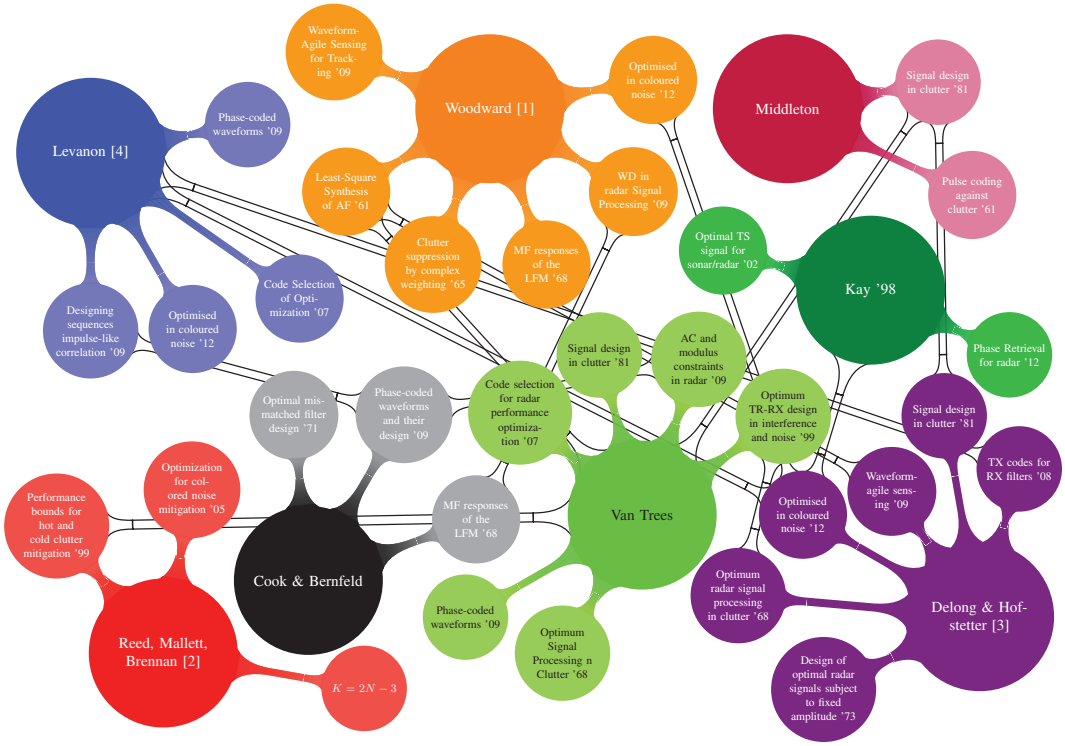


Figure 2.1: Seminal contributors in waveform and filter design for radar and inspired additional works.

### 2.2.1 Binary Coding Techniques

Phase-coded sequences, such as binary code sequences, are attractive because they are straightforward to generate in a radar transmitter [47]. They can provide considerable sidelobe suppression (e.g. Barker [52]), although no known sequence takes on satisfactorily small values for practical tasks. Other examples of binary phase codes include the minimum peak sidelobe (MPSL) sequence or the chaotic sequence, such as that described in [53]. However, these codes offer limited DOF for adaptation in colored interference environments and therefore offer limited SINR performance improvement. For additional information and examples (e.q. Golay or Gold), we refer to the following [9, 54–57].

### 2.2.2 Polyphase Techniques

Polyphase waveforms are described as those that allow any possible phase values for the waveform. These signals, evidently, offer additional flexibility in designing the sidelobes over a binary code, are constant amplitude, and again, straightforward to generate in a radar transmitter [47]. Many examples exists of polyphase waveforms for various applications, some of the more popular are the generalized Barker sequence, the P1, P2, P3 and P4 sequences, Zadoff-Chu sequence, Frank codes and the nonlinear FM [37, 58–60]. These waveforms provide good results for thumbtack ambiguity function response. Additional work has been completed on sidelobe design for practical concerns in [34, 61].

### 2.2.3 Modulus or PAPR Constrained Waveform Design

Of course, the aforementioned Binary and Polyphase techniques assume a constant modulus signal, but, in this section, we give a discussion of the literature on waveform designs when the amplitude, is explicitly considered. In 1973, Mesiya [62] first discussed the need for phase only waveforms because the transmitter in most modern systems should operate in power saturated mode to obtain maximum average power. Since then, much research

has focused on the optimal design, given restrictions and environmental concerns, of phase only signals [63–66]. Patton discussed the joint role of the modulus and the ambiguity function in [27, 33]. In this dissertation, we consider to consequences when allowing the modulus to adjust and relate the cumulative modulus to the PAPR in Chapters 4, 5.

### 2.2.4 Range Sidelobe Suppression Constraints

An important practical aspect of radar waveform design is the suppression of range sidelobes [67]. Pulse compression can simultaneously provide good range resolution (bandwidth dependent) and allow for additional power on the target by increasing the pulse length [9, 41, 68] while maintaing resolution properties. It has been shown that on receive, the application of frequency domain windowing can reduce the time sidelobes [43, 69], but in this dissertation, we are focused on the transmit design to achieve lower range sidelobes and the SINR performance hit. Additional work relating to the minimization of the energy outside the main lobe of the waveform can be found in [30, 31, 34, 70]. In this dissertation, we develop performance prediction models for ISL suppression, details are found in Chapters 4, 6.

### 2.2.5 Waveform Design for Clutter Suppression

The radar detection problem could be defined as the challenge of separating the objects of interest (targets) from the objects not of interest (clutter) by illuminating the scene with a particular waveform [45]. The best waveform to solve this problem is decidedly unknown. There is however, a diverse and abundant history of possible waveform solutions. Included in this are published techniques from information theoretic perspectives [71,72], joint transmit and receive designs [73–79] and signal dependent clutter designs [61, 76, 80, 81]. Another vein of research considers the waveform design from the perspective of multiple pulses for clutter mitigation, with examples in [82–85]. Lastly, several papers have been published that consider knowledge aided designs [86], nearly optimal designs [87] and ac-

tive and passive clutter jointly considered [32]. In this dissertation, we use an eigen-basis waveform design technique to imply SINR maximization in the presence of colored interference.

### 2.2.6 Additional Selected Topics in Waveform Design

As radar technology has improved, we have seen the sophistication of the waveform and the design techniques also increase. This section gives a cursory overview of some topics and concepts available in the literature that we felt help give a more complete picture for motivating performance prediction models of constrained waveforms.

In 1961, Sussman discussed use of the AF shaping to the needs of the system [30]. Other work has been completed on designing the waveform to be similar to a desired waveform [54]. We have adaptive pulse diverse waveform designs for sonar and radar applications [88, 89]. In [90] they discuss the congested spectrum challenge with a sparse frequency waveform design technique. In [91–93], they discuss adaptive signal design to improve target recognition. Lastly, considerable waveform innovation and novel approaches have been developed and analyzed, while not appropriate to discuss in detail in this dissertation proposal, we refer to the following papers [94–99].

## 2.3 Radar Waveform Performance Models

This section is devoted to discussing the current models available for radar and the apparent absence of performance models for constrained waveform design. We begin with the practical models of the radar target scattering statistics, known as Swerling models [100]. They describe multiple statistical models for various target types. These models have been proven extremely useful for statistical analysis for detection/estimation theory development [67].

Another example of a performance model used in radar is the necessary sample sup-

port required to estimate the second-order interference and noise statistics of background clutter. This is known colloquially as the Reed Mallett Brennan (RMB) rule [21]. This model provides a practical estimate of the training data required for adaptive arrays to be effective against avoiding noise and interference.

Of course, statistical models for the noise and interference are prevalent in almost all waveform development techniques, as the Gaussian approximation is ubiquitously declared.

We note a considerable absence in the literature for performance modeling of constrained waveform design. In fact, the only work (that we are aware of) is on sidelobe predictions for spectrally-disjoint radar waveforms [35, 101]. This lack of previous work in the field of performance models for constrained radar waveform design points to the novelty of this dissertation.

## 2.4 Fully Adaptive Radar

Modern radar systems are becoming increasingly more flexible in their ability to perform multiple missions/modes [19]. This is evidenced by the digitization of the RF back end, (i.e. its moving closer to the aperture [102]). To take full advantage of the hardware advances, the Fully Adaptive Radar (FAR) construct allows sophisticated DSP techniques to prevail in exploitation of the received signal. Also, on transmit, digital arbitrary waveform generators provide a mechanism to move away from rigid, conventional, although historically effective, waveforms [5].

For our purposes, we can more succinctly define the FAR as: *a closed loop feedback controller from the receiver to the transmitter* [4]. The challenge is how to best optimize all of the available DOF on transmit and receive to maximize radar performance. Of course, then, a critical component of the FAR construct is the adaptive waveform design capability for optimal performance. However, due to the large number of free parameters, it becomes

readily apparent that the the closed-loop operation comes at a significant computational burden [103].

In this dissertation, we develop performance prediction on the effects of constraints on the waveform SINR to aid in the decision making process of what to transmit for FAR.

## 2.5 Random Matrix Theory and Mathematical Tools

Most of the derivations and performance prediction models outlined in the previous sections use mathematical conclusions and asymptotic results from random matrix theory literature. In this section, we briefly discuss some of the relevant results and other tools used throughout the dissertation.

A seminal paper on the asymptotic limits of eigen-values distributions was published in 1972 by Marčenko-Pastur. The eigen-spectrum is derived from this distribution and used in certain SINR performance models in this proposal [104]. This is unique in that a closed-form expression for the eigen-spectrum is available[1].

In 1972, Gray inspected the asymptotic eigenvalue distribution of toeplitz matrices [105, 106]. Also, Gray published a useful book on matrix theory and linear algebra that provides several insights in [107]. Lastly, for the complex derivatives and matrix differentiation, we refer to the following [108, 109] for techniques and helpful conclusions.

## 2.6 Interference and Noise Covariance Matrix Models

We will review, in detail, the three I + N covariance models used for Monte Carlo analysis in the following chapter. Here, we discuss current approaches to estimating RFI which, involve either the collection of spectral data in various environments to characterize the interference or the use of aggregation tools, such as TV Fool$^{TM}$, which provide analysis of

[1]The closed-form expression for the eigen-value distribution is an asymptotic result on the average eigenvalues as the dimension of the covariance matrix approaches $\infty$.

over-the-air (OTA) broadcasts [2]. These approaches can be costly, cover only a limited bandwidth, or limited to only a few instantiations. Additionally, modeling colored interference and noise covariance matrices, with desired power spectral density (PSD) traits, is useful for waveform design, development, and analysis [26]. Many attempts in literature employ what is mathematically convenient but not necessarily accurate in representing real-world interference [15, 27].

For example, use of an low $n^{\text{th}}$ order auto-regressive (AR) model of the interference is easy generate, but, as we show, not statistically similar to actual spectra ( or possess representative features). This questions the utility of the AR-model to yield useful conclusions from analysis. Another key issue motivating the development of spectra generation techniques is the need for rapid algorithm development where access to synthetic data can improve modeling and simulation analysis. These concerns are addressed in this dissertation with multiple new data models developed for improved practicality.

## 2.7 Chapter Summary

In this chapter, we reviewed the background literature in our areas of research. While doing so, we observed a considerable absence in the literature for performance modeling of SINR for constrained radar waveform design. This is a significant concern as radars become more agile on transmit and will require a deeper understanding of how the performance will react when forced to constrain the transmit waveform.

Additionally, we make use of a field of mathematics not typically seen in radar, Random Matrix Theory. The asymptotic results of this field provide a general framework to compute close-form expressions of the eigen-values of the covariance matrices, and thus, initial analytical results are possible. We will refer back to sections of this Chapter throughout the dissertation when needed.

# Chapter 3

# Interference and Noise Models

One of the challenges in the development of performance prediction models for waveform SINR (as a function of the constraints) is the selection of the interference and noise covariance matrix model, as mentioned previously. Typically, a toy example of the interference and noise covariance is used for theoretical development, owing to the simplicity to generate in MATLAB [110] and ease of use, not what is actually representative of real world data.

Still, many situations in algorithm development require the use of Monte Carlo techniques to ascertain the effectiveness of an algorithm under varying conditions. We consider, for example, the perspective of radars operating in complex operational environments (see figure 1.1) where, when not thoroughly considered, RFI can degrade the detection performance of the system and/or limit the effective operating bandwidth [111]. For perspective, in figure 3.1 we give the spectrum survey data for a mid-size metropolitan area [2] from 100MHz to 1GHz. We note the complexity in the environment must be considered in waveform design and performance prediction to be effective.

Therefore, it is critical that the algorithms be robust to varying narrowband RFI environments. In this Chapter, we develop the covariance matrix structure and eigen-spectrum approximations for three unique interference and noise classes used in Chapters 4, 5, 6 to

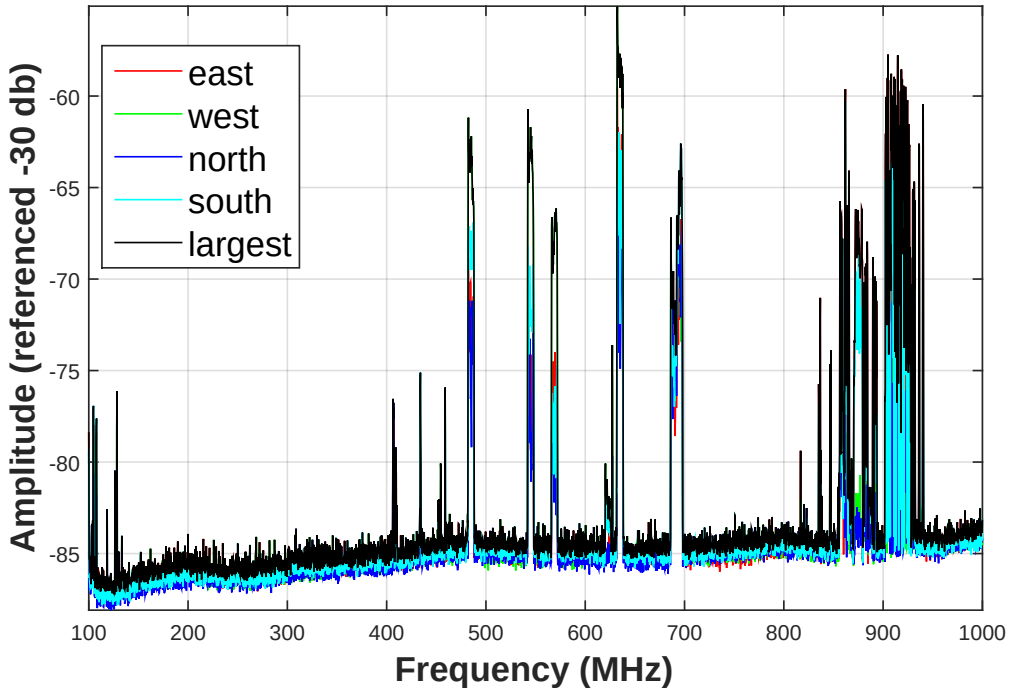


Figure 3.1: Tillman-Pit spectrum survey data [2].

derive the performance prediction models and perform the analysis.

In section 3.1 we discuss the oft-used low-order auto-regressive model. Next, in section 3.2, we employ a novel use of a random matrix that possesses a closed-form expression for the eigen-spectrum of its covariance matrix. Then, we report a new result in synthetic data generation that is derived from measured data in section 3.3. We compare and contrast each model and summarize in section 3.4. Parts of this chapter are included in a journal paper [29] which was submitted for publication in 2016. Final results were published in [25].

## 3.1 Auto-Regressive Model

In this section, we define the low model order AR colored interference covariance matrix model and the approximation of its eigen-spectrum. To generate the covariance, we use

an auto-regressive process driven by Gaussian white noise whose auto-correlation function (ACF) can be represented by a decay function. We note this model to have low fidelity however, relative to practical power spectral densities (as shown in future sections), but will use to perform Monte Carlo analysis due to its prevalence in current literature. The received interference and noise model is then given as:

$$X_k = \sum_{p=1}^{P} \phi_p X_{k-p} + \epsilon_k, \tag{3.1}$$

where $P$ is the model order, $k$ the lag position, $\phi_p$ the model coefficients and $\epsilon_k$ the driving white noise with distribution $\mathbb{CN}(0,1)$. The auto-correlation of the time series ($R_{XX}(m) = E\{X(k)X(k-m\}$) defines the covariance matrices, given as $\mathbf{K}_{AR}$. This all-pole model will generate spectrally peaky RF colored environments and the magnitude of the coefficients $\phi_p$ describes how correlated the samples are in time.

In this dissertation, we consider two variants. First, a highly correlated $\text{AR}_{\text{high}}$ model and then, a weakly correlated $\text{AR}_{\text{low}}$ model. The highly correlated corresponds with pole locations ($\theta_p$) whose magnitudes are uniformly distributed over $0.75 \leq |\theta_p| \leq 0.9$ with uniform phase. The weakly correlated corresponds to pole locations whose magnitudes are uniformly distributed over $0.1 \leq |\theta_p| \leq 0.25$, also with uniform phase distribution. We compare the eigen-spectrum for each correlated model against the MP spectrum for length $M = 64$ signal size (correlated eigen-spectrums are empirically computed as the average of 1000 realizations). and we display the results in Figure 3.5 for the MP, $\text{AR}_{\text{low}}$ and $\text{AR}_{\text{high}}$, both of model order 3. The eigen-values are sorted in ascending order and we recognize the MP as a balanced model for the eigen-spectrum when compared against the AR.

Additionally, one of the most attractive properties of the AR model to represent a PSD, and thus a covariance matrix, it its ease of generation. The low model order AR PSD is a useful tool to compare between two waveform design algorithms and constraints. However, we will show in subsequent sections that this model deviates from measured data

(for certain bands) and therefore, yields misleading representations of SINR performance for the waveform.

This model is used in Chapter 4 to prove out initial results prior to running analysis with more representative covariance models.

## 3.2 Random Interference Covariance Matrix Definition

In this section we discuss the Marčenko-Pastur (MP) model, a general utility model predicated upon an asymptotic result from random matrix theory. This models considers the case when prior information about the interference and noise spectrum is not available and a balanced model of the eigen-spectrum is required.

Therefore, to generalize the covariance data representation, we use an asymptotic result reported in random matrix theory literature that states, in the limit of large data, that the statistical behavior of eigenvalues of large ($M \gtrsim 32$) random Hermitian matrices (see (6.13) for description), under the assumption of a full-rank covariance with $\sum_{k=1}^{M} \lambda_k = M$ (equivalent to assuming constant noise power), conforms to the following Marčenko-Pastur (MP) density when the matrix is square, a requirement for our analysis:

$$p_{\Lambda}(x) = \frac{\sqrt{4x - x^2}}{2x}, x \in (0, 4]. \tag{3.2}$$

This is an empirical distribution and, we refer the reader to [104] for further details. Applying the inverse transform sampling method [112] to (3.2), a closed-form representation of the CDF, thus a mechanism to compute the expected eigenvalues is possible. We define the CDF as:

$$\mathcal{M}(x) = \int_0^x p_{\Lambda}(z)dz, \tag{3.3}$$

$$= \frac{1}{2\pi}\left(\sqrt{4x - x^2} - 2\arcsin\frac{4 - 2x}{4}\right) + \frac{1}{2}, \tag{3.4}$$

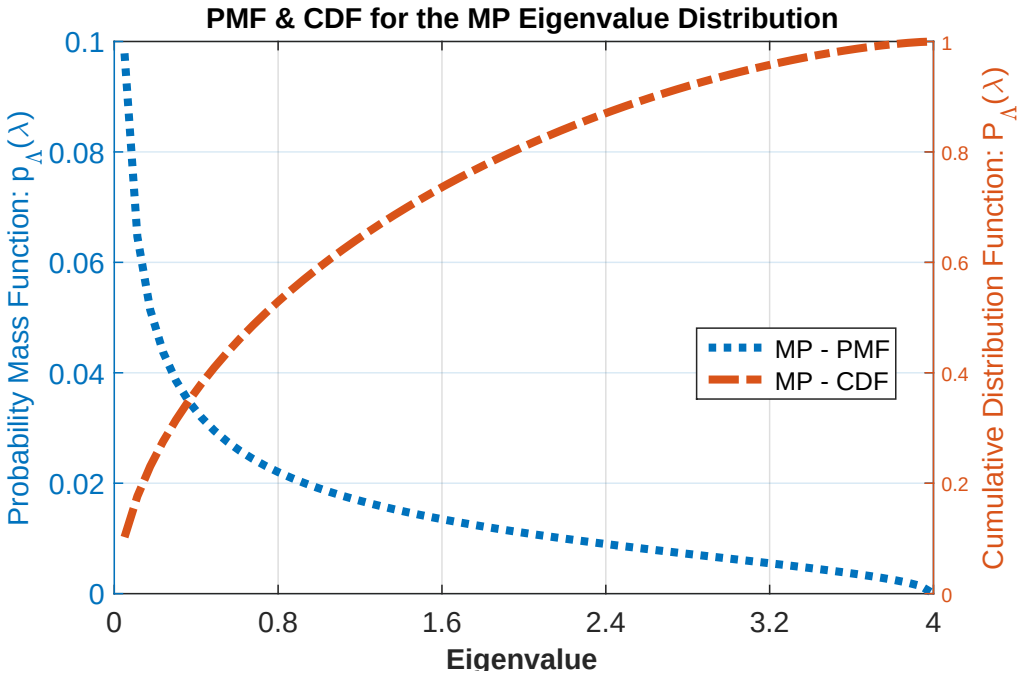


Figure 3.2: (left axis) Probability Mass Function for the Marčenko-Pastur asymptotic result ($M = 64$). (right axis) The associated Cumulative Distribution Function for the Marčenko-Pastur eigen-spectrum.

This data model is unique due to the closed-form expression of the eigen-value distribution. This will allow for simplified development of the SINR models in the future Chapters. See Figure 3.2 for depiction of this density (left axis) and the corresponding cumulative distribution function (right axis). For analytical tractability, we use this model to represent the eigen-spectrum of a generic interference and noise covariance matrix enabling demonstration of the expected cumulative modulus as a function of the eigen-basis. Additionally, in the practical case where no information about the noise and interference statistics is available, this model would provide initial estimates of the eigen-spectrum, and thus performance.

The covariance, for this data, is defined as

$$\mathbf{K}_{\text{MP}} = \frac{1}{M}\mathbf{Z}\mathbf{Z}^H, \tag{3.5}$$

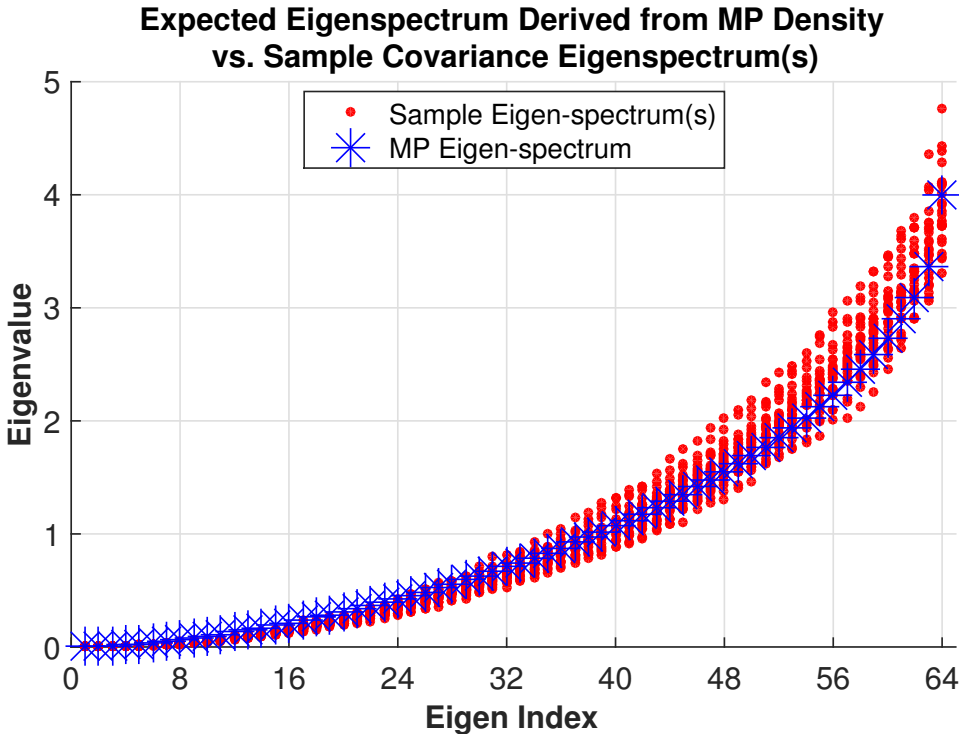


Figure 3.3: Asymptotic Marčenko-Pastur eigen-spectum, derived from the density in (3.2) with sample covariance eigen-spectrum generated from 25 random instantiations of the data matrix for $M = 64$, for comparison.

where elements $\mathbf{Z}_{ij}$ are $\mathbb{CN}(0, \frac{1}{\sqrt{M}})$.

As an example, in figure 3.3, we show 25 realizations of the eigen-spectrum of the random matrix along with the theoretical asymptotic distribution for M $= 64$. This model will be used extensively in Chapters 5 and 6 to show how the eigen-spectrum of the I + N covariance matrix interacts with the SINR performance.

Using (3.2) to compute the survival function (complimentary CDF), $\mathcal{S}(x) = 1 - \mathcal{M}(x)$, we can compute the inverse survival function, $\mathcal{Z}(x)$ to describe the eigen-spectrum

for discrete, $x$, where $x \in (0, 4]$, as

$$\mathcal{Z}(x) = \mathcal{S}^{-1}(x) \tag{3.6}$$

$$= \Big(1 - \mathcal{M}(x)\Big)^{-1} \tag{3.7}$$

$$= \frac{2}{\pi}\Big(2 \arcsin \frac{4 - 2x}{4} + \pi - \sqrt{4x - x^2}\Big). \tag{3.8}$$

Then, to obtain the eigen-spectrum for an $M$-dimensional covariance, we generate $M$ uniformly sampled values of $x$ and transform with the function, $\mathcal{Z}$ to obtain eigen-values ($\underline{\lambda}$) that have MP PMF.

For some additional analysis, shown in Figure 3.4 is the MP eigen-spectrum ($\mathcal{Z}(x)$) as well as sample eigen-spectrum from $25$ random instantiations for $M = 256$. Also, we compare the eigen-spectrum of the MP model against measured data. The measured data is interference and noise data collected with system parameters listed in table 6.1 for an air-to-ground radar operating at X-band. The standardized eigenvalues on a log scale are shown against the theoretical model. We will use the eigen-value models to develop the performance prediction models and validate agains the measured data set.

Table 3.1: Interference and Noise Measurement Specifications

| **Parameter** | **Value** |
|---|---|
| Bandwidth | 1 GHz |
| Minimum Frequency | 9.2 GHz |
| Maximum Frequency | 10.2 MHz |
| Pulses | 256 |
| Fast-time Samples | 256 |
| Sample Rate | 3 GHz |
| Number Channels | 1 |

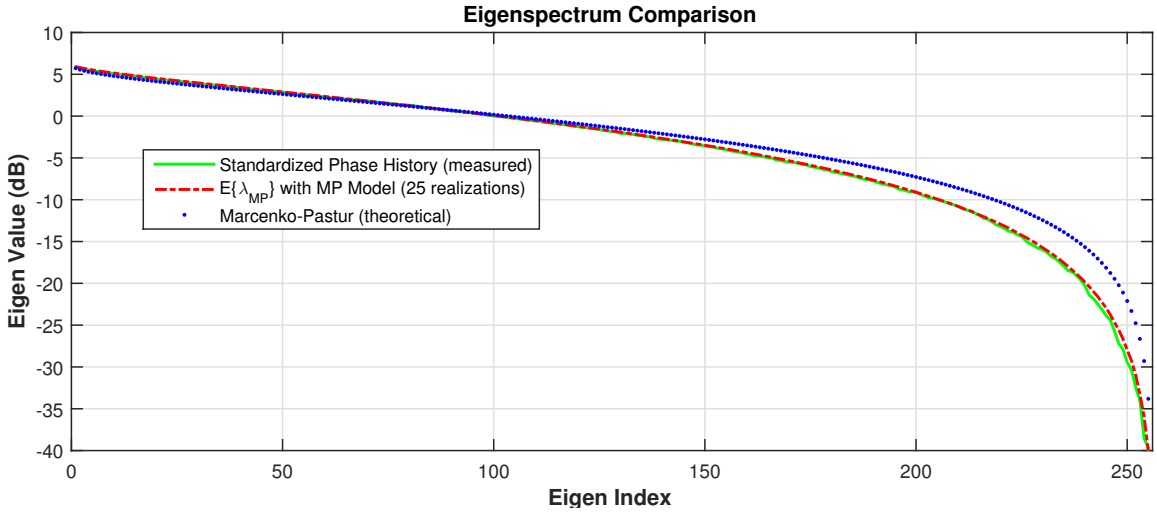


Figure 3.4: Eigen-spectrum comparison of theoretical Marčenko-Pastur (3.2), sample covariance eigen-spectrums generated from 25 random instantiations of (6.13), and eigen-spectrum of measured data with collection specifics in Table 6.1 for $M = 256$, for comparison.

### 3.2.1 MP Comparison to the AR Model

We compare the eigen-spectrum for each correlated model against the MP spectrum for length $M = 64$ signal size (correlated eigen-spectrums are empirically computed as the average of 1000 realizations). We display the results in Figure 3.5 for the MP, $\text{AR}_{\text{low}}$ and $\text{AR}_{\text{high}}$ covariance matrix definitions. The similarities suggest that the MP model is a good representation for certain data and allows for a convenient mathematical model of the eigenvalues.

In Figure 3.6, representative power spectral densities for a single instantiation of the three classes of interference mentioned, are displayed. As expected, the MP has a large dynamic range, owing this to its aversion to any particular frequency, while the $\text{AR}_{\text{low}}$ has distinct Fourier components based on the pole location but the overall distribution is still "flatter" than the $\text{AR}_{\text{high}}$ whose model coefficients would place poles closer to the unit circle giving deeper nulls and higher peaks.

However, for these covariance representations to be useful in developing performance models for SINR and cumulative modulus, the eigen-spectrum, in the expectation, must

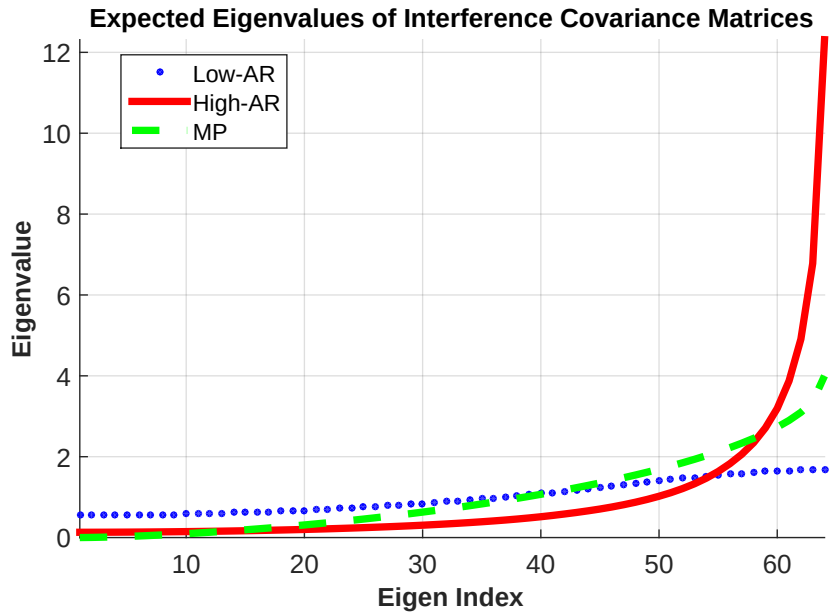


Figure 3.5: Expected eigen-spectrum for three interference classes from 1000 realizations; low magnitude coefficient AR-3, high magnitude coefficient AR-3 and Marčenko-Pastur. AR models have precedent in representing certain radar data [3].

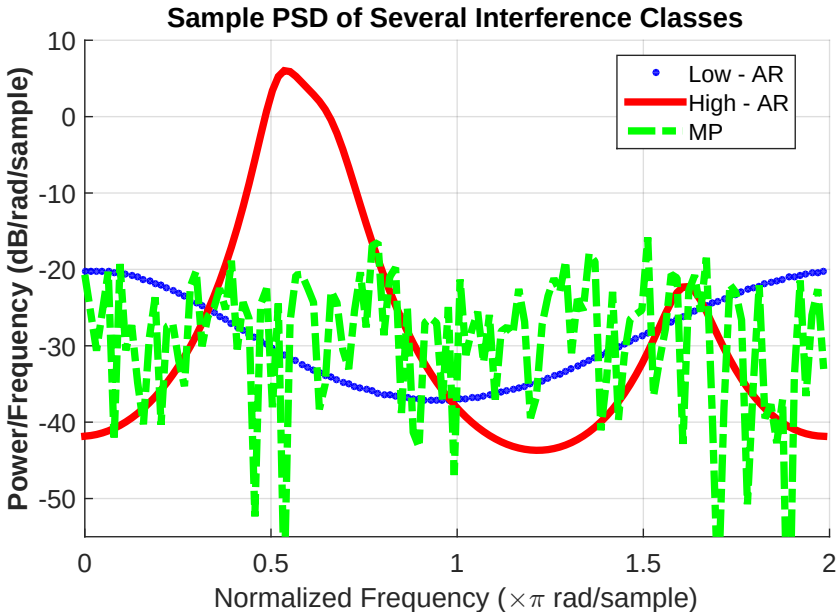


Figure 3.6: Representative PSD for three unique classes of interference. 1. Weakly correlated AR data model. 2. Highly correlated AR model. 3. Marčenko-Pastur data model.

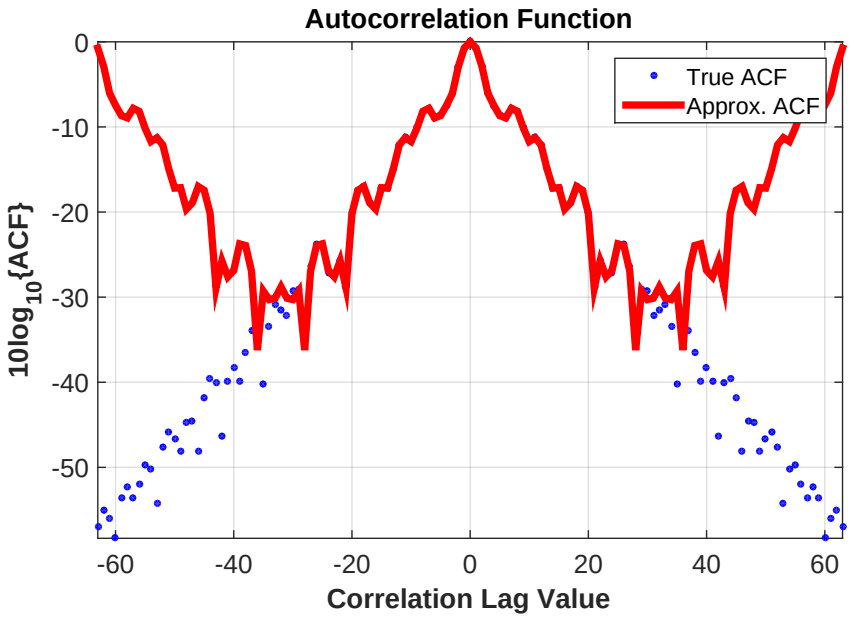


Figure 3.7: Single instantiation of circulant approximation ACF and corresponding covariance magnitudes. Autocorrelation function of example covariance matrix compared with the circulant approximation, ($M = 64$).

be known to a high confidence. Unfortunately, little is known about the probability-mass-function (PMF) of eigen-values for covariance matrices whose underlying physical model is based on an AR-process.

To overcome this limitation, though out the dissertation, we approximate the eigen-values of correlated interference covariance matrices by invoking Szego's Theorem. The theorem states that, asymptotically, the distribution of eigenvalues of an autocorrelation matrix approach the power spectrum as the dimension of the matrix increases, full description found in [113, 114]. For our purposes, this is convenient given the AR model. Although, in order for this approximation to be valid, the eigenvectors of the covariance matrix must be samples of a complex exponential (i.e. discrete Fourier transform (DFT) matrix). Not typically the case for AR models, we are forced to approximate the covariance via a circulant matrix which has been proven to be asymptotically equivalent in a certain sense [105, 106].

In Figure 3.7 and 3.8 we give an example comparing an M=64 (relatively short) signal

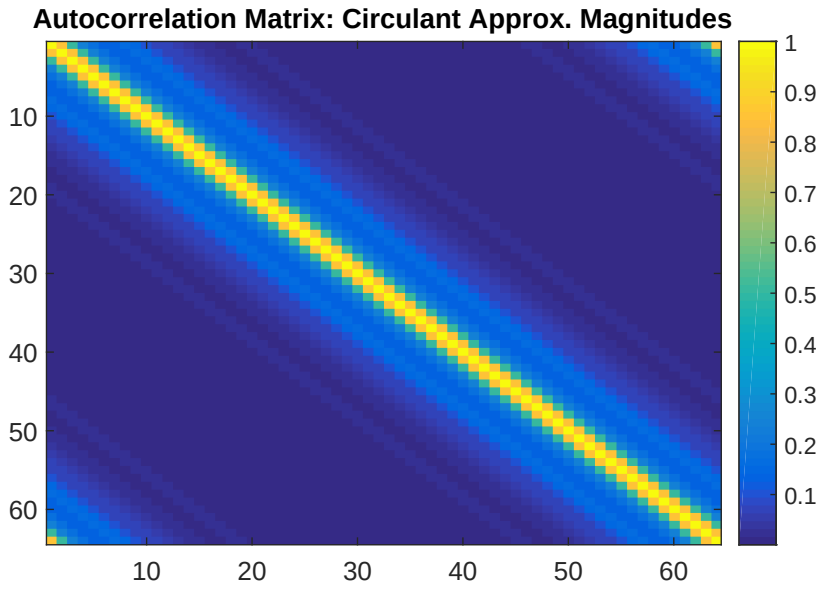


Figure 3.8: Single instantiation of circulant approximation ACF and corresponding covariance magnitudes. Covariance matrix magnitudes for the circulant approximation. Note, the errors in the approximation reside at large lag values.

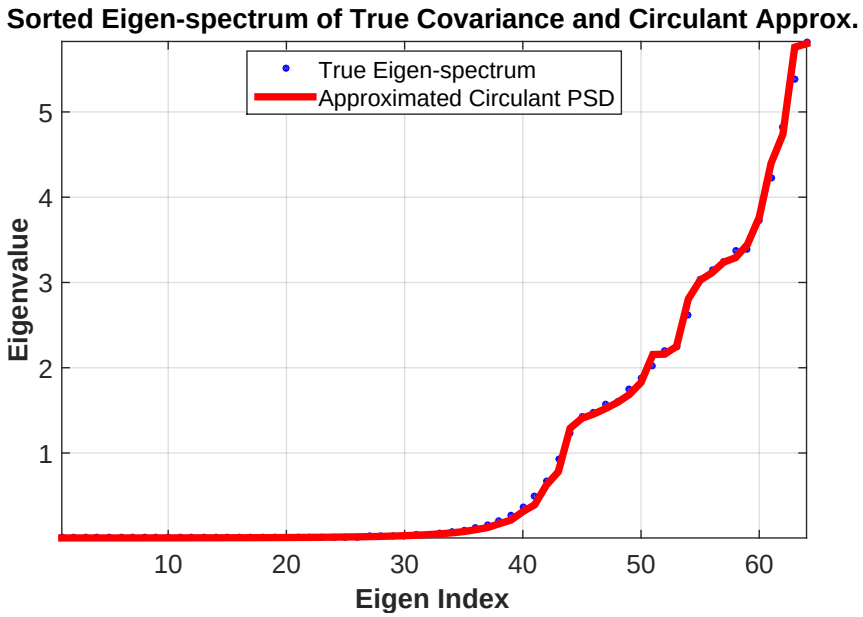


Figure 3.9: Eigen and power spectrum comparison for single instantiation of the clairvoyant and circulant approximation of the interference and noise covariance matrix. Single instantiation of the $\text{AR}_{\text{high}}$ covariance eigen-spectrum with the approximated spectrum from the circulant matrix and the sorted PSD, ($M = 64$).

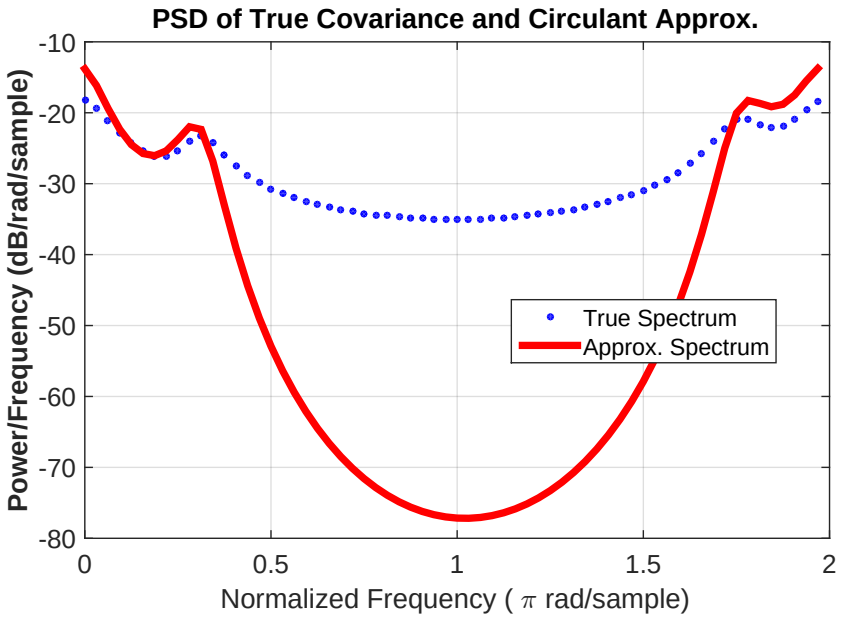


Figure 3.10: Eigen and power spectrum comparison for single instantiation of the clairvoyant and circulant approximation of the interference and noise covariance matrix. Comparison of the PSD for the clairvoyant and the circulant approximation. Higher power frequencies are represented more accurately than lower power frequencies.

with its circulant approximation. The figure gives the autocorrelation function of a representative $AR_{low}$ covariance matrix with its circulant approximation and the covariance matrix magnitudes for the circulant approximation. Additionally, in Figure 3.9 we give the sorted eigen-spectrum for the known covariance and the corresponding estimate via the sorted PSD and in Figure 3.10, a comparison of the PSD for a single instantiation. The approximation, even for this relatively short signal, is accurate in the eigen-spectrum and will act as a useful model in this context and the approximation improves as the signal length increases.

## 3.3 Synthetic RFI Development

Finally, in this section, we derive two new synthetic PSD models[1] by employing a novel approach where a two-state Markov chain is used to define the spectral transitions from signal

[1] Accepted for publication in the 2016 RadarCon, [25]

present to noise-only and vice versa. We then modify the sequence with signal and noise specific amplitude distributions to arrive at the synthetic PSD. This is advantageous over current approaches in multiple ways. First, we are able to exploit the unique underlying phenomenology inherent to the UHF bands' power spectral content. Second, the technique requires limited computing power and time, and therefore is also cost effective.

### 3.3.1 Problem Statement and Signal Model

Evaluation of algorithms for RF systems operating in statistically stationary but geographically varying (i.e., different urban environments) UHF bands requires affordable, simple generation of representative urban RFI based on real-world data characteristics.

Let's say, for example, we could assume the signal and noise are complex, independent, stationary and ergodic Gaussian random processes. These assumptions would give a general Gaussian model described as

$$\underline{\mathrm{x}} = \underline{\mathrm{s}} + \underline{\mathrm{n}} \tag{3.9}$$

where $\underline{\mathrm{s}} \sim \mathbb{CN}(\mu_s, \sigma_s^2\mathbf{I})$ and $\underline{\mathrm{n}} \sim \mathbb{CN}(0, \sigma_n^2\mathbf{I})$.

Since we are interested in modeling the PSD, we note this implies the power spectrum analyzer output to be $\chi^2$ distributed with $1$ complex degree of freedom. However, the signal is confounded by real-world effects such as channel fading, indirect path contributions, etc. [115]. Additionally, as more noise sources are multiplexed, the noise distribution is similarly confounded. Such concerns manifest, in a statistical sense, by a move away from the expected $\chi^2$ distribution. Representing the difference from the model and real-world distributions is a major concern of this dissertation.

### 3.3.2 Model Development

Our objective is simple, to remain in the class of easy to generate and convenient models, like those currently employed and discussed in the previous sections, while improving upon the statistical similarity of the model to real-world interference (i.e, entropy reduction) and the inclusion of other desirable features of the PSD. We, therefore, leave higher-order effects modeling to others.

In the following sections we discuss two models. First, a model developed using a systematic approach that is statistically similar to the measured data sets, denoted **Model 1**. The second model (**Model 2**), uses a more ad hoc approach based on reasonable conjecture that the signal distribution posesses additional features not allowed by **Model 1**. The following sections discuss each of the four steps in the technique to produce synthetic PSD's in the UHF band and, in the case where no measurement data is available, we have provided the necessary parameters to reproduce our results.

### 3.3.3 Rank Determination

To begin, as is the case in many signal processing problems involving radar, detection of the number of signals (embedded in additive noise) is an important issue. For our concerns, when given a sample PSD data set, we desire to know the number of frequency bins that have a signal present. Accurate estimation of the number of occupied bins allows separation of the signal subspace from the noise to derive statistical properties from the measured data.

To accomplish, we apply the principles discussed in [116] that allow determination of the number of signals present after assertion of an asymptotic result on the measured PSD data sets by invoking *Szego's* Theorem. The theorem states that, *asymptotically, the distribution of eigenvalues of an autocorrelation matrix approaches the power spectrum as the dimension of the matrix increases*. A full description can be found in [113, 114].

For our signal and noise model, whose estimated eigenvalues are denoted $\hat{\lambda}_i = l_i, i =$

$1, \ldots, k$, it is reasonable to use the minimum description length (MDL) technique to compute the rank of the signal subspace for a given data set. We recount the definition for MDL for Gaussian distributed data [116]:

$$\text{MDL}(\hat{\lambda}) = -\log\left\{\frac{\rho}{\eta}\right\} + \frac{1}{2}k\log(N) \tag{3.10}$$

where $\rho = \prod_{i=k+1}^{p} l_i^{1/(p-k)}$ and $\eta = \frac{1}{p-k}\sum_{i=k+1}^{p} l_i$, the geometric and arithmetic mean, respectively and $p$ is the problem dimensionality. Parameter $k$ is the number of free adjusted parameters, and $N$ is the number of observations. This strategy can be applied to any measurement set where the Gauss-Gauss signal model assumption is appropriate.

### 3.3.4 Shifted Gamma Distribution

Next, for **Model 1**, we appoint a shifted gamma distribution to represent the signal and noise amplitudes of the PSD (where under the Gaussian signal model, a $\chi^2$ distribution would prevail, a special type of the Gamma). The distribution has shape parameter $\alpha$, scale parameter $\beta$, and shift parameter $\gamma$ such that it is generically described by the density function:

$$G_{\alpha,\beta,\gamma}(x) = \frac{x^{\alpha-1}}{\Gamma(\alpha)\beta^{\alpha}}\exp\{-\frac{x}{\beta}\} + \gamma \tag{3.11}$$

where $x \in (0, \infty)$ and $\Gamma(\alpha)$ is the gamma function evaluated at $\alpha$. The gamma distribution is more flexible than a $\chi^2$ distribution, owing to the non-integer possibilities of the parameters, and permits higher fidelity variations to represent the distributions. We also note, gamma and shifted gamma distributions have been used for probability modeling in many fields [117].

For **Model 1**, we assume $\alpha$, $\beta$, and $\gamma$ are deterministic, for both the signal and noise amplitude models, and can compute the maximum likelihood estimate (MLE) of the parameters for a given measurement set. The subscript $(\cdot)_1$ is used when referring to **Model 1** and the superscript $(\cdot)^{s,n}$ denotes signal or noise, respectively.

With regards to **Model 2**, we again use shifted Gamma distributions to describe the signal and noise amplitude distributions, with subscript $(\cdot)_2$. The noise model remains unchanged. However, where in **Model 1** we assert the shape, scale and shift parameters to be deterministic, in **Model 2** we claim, ad hoc, that the shape and shift are actually uniformly distributed. Use of this approach is further motivated by observing the PMF/CDF of each of the individual signal bands as determined by the MDL. In figure 3.11, it is evident that, while we could reasonably assume each came from a similar distribution, the parameters for each vary substantially. That is, we define new variables $\Theta_2^s \sim U[\alpha_{min}, \alpha_{max}]$

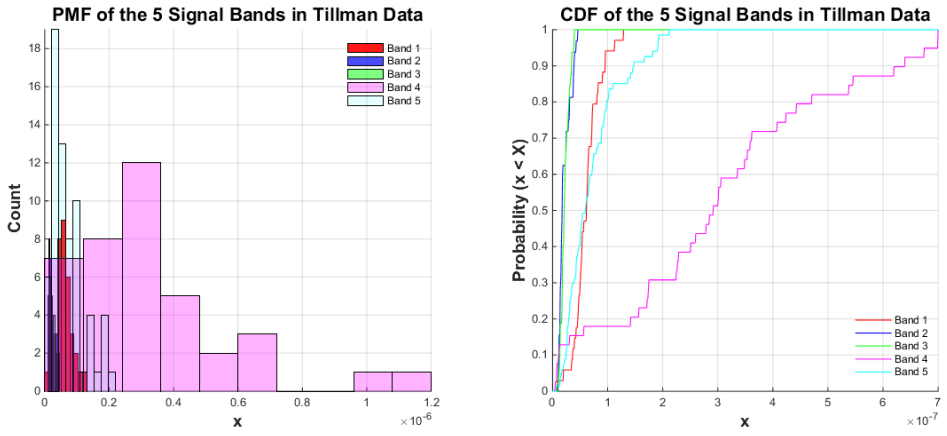


Figure 3.11: PMF/CDF for each of the five signal bands identified by the MDL computation.

and $\Lambda_2^s \sim 10^{U[\log_{10}(\gamma_{min}),\log_{10}(\gamma_{max})]}$ where the subscripts $_{min,max}$ denote the minimum and maximum of the range for a uniform distribution ($U$). For the shift variable $\Lambda$, this makes intuitive sense as the it can be varied from the noise floor to the highest expected signal value, uniformly on the $\log_{10}$ scale. Also, the $\Theta$ parameter allows for varied power efficiency in the signal bands.

The likelihood function for such a distribution is not mathematically tractable and therefore we compute the MLE of parameters for the uniform distributions independent of the Gamma distribution. This, of course, voids the claim of maximum likelihood on the parameters, but is a reasonable approach under the circumstance. And, as we will show,

this will give us desirable features in the synthetic PSD, such as varying power levels in the signal bands. The scale parameter $\beta$ is then a function of the two random variables as $\beta = \frac{\Lambda_2^s}{\Theta_2^s}$.

### 3.3.5 Use of the Markov model

In order to model the signal and noise bands and the transitions between signal and noise in the PSD, we use a a Markov process [118]. The most rudimentary such model is the two-state model in which the random sequence can assume two discrete values. For both **Model 1** and **Model 2** we define the two possible states with state vector $\underline{\delta} = \{s_0, s_1\}$, where $s_0 = 0$ represents the noise state and $s_1 = 1$, the signal state.

The transition matrix $\mathbf{P}$ is conveniently expressed in matrix form (for finite model order) with transition probabilities $Pr[\underline{\mathrm{X}}_{\mathrm{P}}(m) = s_i | \underline{\mathrm{X}}_{\mathrm{P}}(m-1) = s_j]$ with $i, j$ indicating the possible states and $\underline{\mathrm{X}}_{\mathrm{P}}(m)$ being the sequence at index $m$. In our case, this is a $2 \times 2$ transition matrix given by:

$$\mathbf{P} = \begin{bmatrix} Pr(s_0|s_0) & Pr(s_1|s_0) \\ Pr(s_0|s_1) & Pr(s_1|s_1) \end{bmatrix}. \tag{3.12}$$

Thus, we denote Markov sequence with transition matrix $\mathbf{P}$ and initial state $\underline{\delta}_{init}$ as $\underline{\mathrm{X}}_{\mathbf{P}} \sim \mathcal{M}(\underline{\delta}_{init}, \mathbf{P})$. Practically speaking, we define each probability as follows:

- $Pr(s_0|s_0)$, probability of transition from noise bin to adjacent noise bin
- $Pr(s_0|s_1)$, probability of transition from signal bin to adjacent noise bin
- $Pr(s_1|s_0)$, probability of transition from noise bin to adjacent signal bin
- $Pr(s_1|s_1)$, probability of transition from signal bin to adjacent signal bin

Then, to estimate the state transition matrix from measured data, with assumption of stationarity, we form a binary sequence using the MDL results to assign frequency bins to

states $s_0 = 0$ and $s_1 = 1$, representing noise and signal, respectively. We compute the estimated transition probabilities using the sequences while incrementing positively over frequency by counting each transition.

The random placement of RFI center frequencies and bandwidths allows liberal use of the Markov model that provides unique flexibility in generating synthetic RFI PSD.

### 3.3.6 Signal and Noise Modification to Markov model

Lastly, for **Model 1**, we modify the Markov sequence, $\underline{\mathrm{X}}_{\hat{\mathrm{P}}}$ with random variables $\hat{f}_1^n \sim G_{\alpha_1^n,\beta_1^n,\gamma_1^n}(x)$ and $\hat{f}_1^s \sim G_{\alpha_1^s,\beta_1^s,\gamma_1^s}(x)$ to develop the synthetic UHF PSD as:

$$\underline{\mathrm{PSD}}_1 = \begin{cases} (\underline{\mathrm{X}}_{\hat{\mathrm{P}}} + 1) \odot \underline{\hat{f}}_{-1}^{n}, & \text{if } \underline{\mathrm{X}}_{\hat{\mathrm{P}}} = 0, \text{for } \forall m \\ \underline{\mathrm{X}}_{\hat{\mathrm{P}}} \odot \underline{\hat{f}}_{-1}^{s}, & \text{otherwise} \end{cases} \tag{3.13}$$

where, $m = 1, \cdots, M$, $M$ is the sequence length, $m$ a frequency bin and $\hat{\mathbf{P}}$ is the estimated transition matrix.

Our equation for **Model 2** is similarly described as:

$$\underline{\mathrm{PSD}}_2 = \begin{cases} (\underline{\mathrm{X}}_{\hat{\mathrm{P}}} + 1) \odot \underline{\hat{f}}_{-2}^{n}, & \text{if } \underline{\mathrm{X}}_{\hat{\mathrm{P}}} = 0, \text{for } \forall m \\ \underline{\mathrm{X}}_{\hat{\mathrm{P}}} \odot \underline{\hat{f}}_{-2}^{s}, & \text{for each signal band} \end{cases} \tag{3.14}$$

where $\hat{f}_2^n \sim G_{\alpha_1^n,\beta_1^n,\gamma_1^n}(x)$ (same as **Model 1**) and $\hat{f}_2^s \sim G_{\Theta_1^s,\beta_1^s,\Lambda_1^s}(x)$ with $\Theta_2^s \sim U[\alpha_{min}, \alpha_{max}]$, $\Lambda_2^s \sim U[\log_{10}(\gamma_{min}), \log_{10}(\gamma_{max})]$ and $\beta = \frac{\Lambda_2^s}{\Theta_2^s}$. We point out that each signal band is an independent draw of the random variable allowing for different mean-amplitude and variance.

### 3.3.7 Measured Data and Technique Validation

Following the steps of the technique outlined in 3.3.2 and shown in figure 3.12, we examine the statistical properties of several measured data sets and verify similarity of the synthetic data to real-world RFI. We assume the collected data is prototypical and generalizable to other geographies.

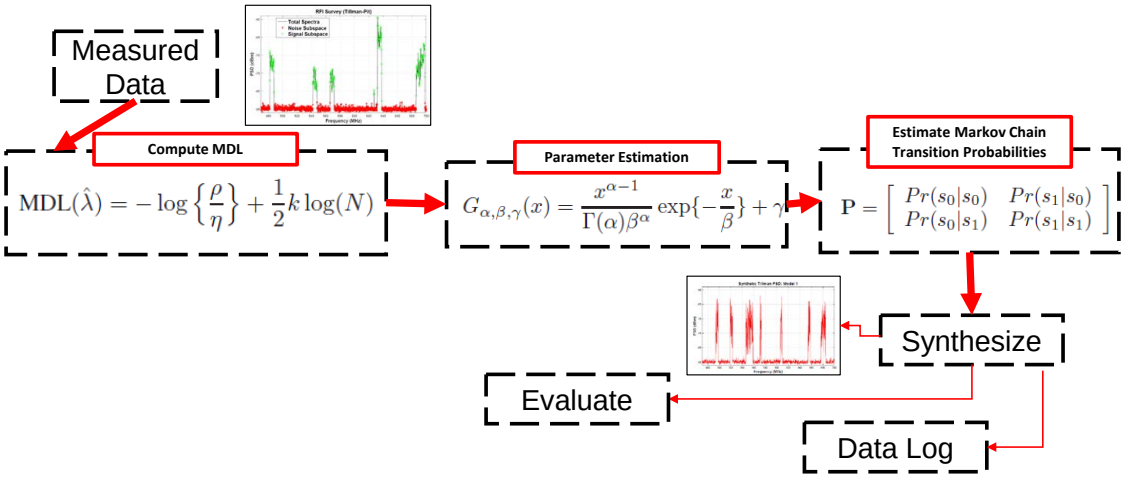


Figure 3.12: Synthetic data generation flow chart

The measured data, denoted the *Tillman-Pit* data, was collected using a spectral analyzer fed by pyramidal horn antennas atop a 50-foot mast with collection parameters denoted in Table 4.1. This data was collected with a directive antenna for each of the four cardinal directions (north, south, east, and west), giving four data sets to evaluate [2]. Figure 3.13 displays the spectrum survey for the east measurement set in dBm.

### 3.3.8 A Statistical Analysis

#### Rank of the Signal Subspace

Using the MDL in (3.10), we compute the signal subspace rank for the measured data, see Table 3.3 for results, with $N = 2000$, analogous to the spectrum being well estimated. It

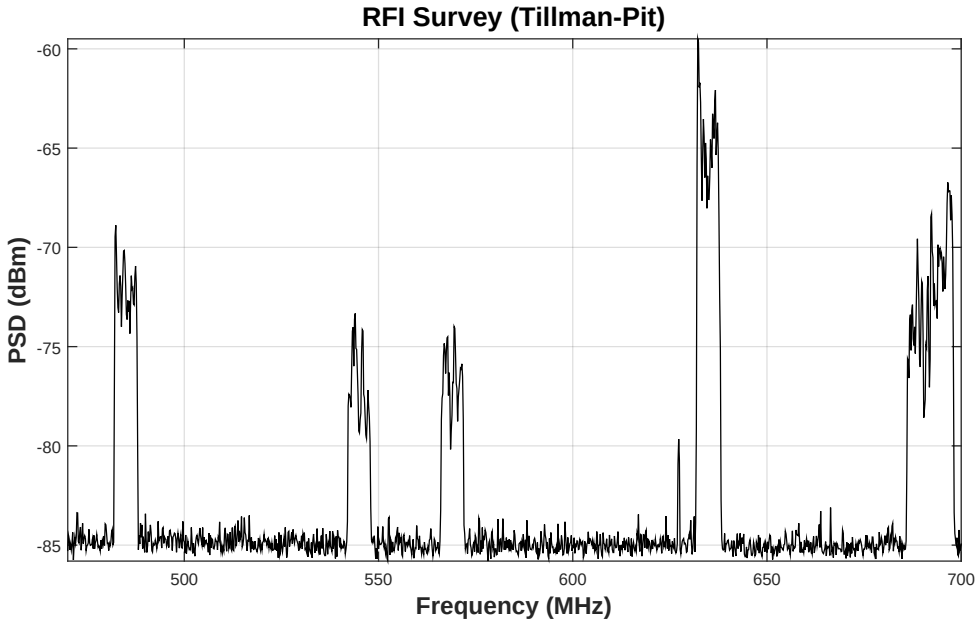


Figure 3.13: Power spectral density survey of *Tillman-Pit* (eastern directivity) in actual power (dBm) from $470$ MHz to $700$ MHz with collection parameters listed in Table 4.1.

is also worth pointing out that the *Tillman-Pit* spectrum data did not vary significantly for different directions [2] and this is reflected in the MDL. Figure 3.13 displays the spectrum survey for the east measurement set in dBm with the signal and noise subspaces, estimated using the MDL, highlighted.

### Signal and Noise ML Parameter Estimation

Following the flow chart in figure 3.13, we compute the dimension of the noise subspace by subtracting the MDL, for a particular measurement set, from the total dimension. After separating the signal and noise subspaces, we compute the maximum likelihood estimates for the shape, scale and shift parameters of the Gamma distribution described in (3.11).

For reproducibility, the $\alpha$, $\beta$, $\gamma$ quantities have been computed for both the noise and signal measurement sets and can be found in Table 3.4 for **Model 1** and Table 3.5 for **Model 2**.

Also, for comparison, we show in Figures 3.15 and 3.14 the computed CDF for the

Table 3.2: Tillman-Pit Collection Specifications

| **Parameter** | **Tillman-Pit** |
|---|---|
| Latitude | 39° 46' 11.9" |
| Longitude | −84° 7' 25.4" |
| Bandwidth | 230 MHz |
| Minimum Frequency | 470 MHz |
| Maximum Frequency | 700 GHz |
| Bin Width | 181.8 Khz |
| Samples | 1265 |

Table 3.3: Minimum Description Length

| **Data** | North | East | South | West |
|---|---|---|---|---|
| MDL | 201 | 204 | 206 | 219 |

*Tillman-Pit* east facing measurement set against the hypothesis for the signal and noise subspaces. The noise subspace is accurately modeled with the shifted Gamma distribution (confirmed with $\chi^2$-Test at the 1% significance level). However, the signal subspace comparison denotes error in the hypothesized distribution. We believe this is attributable to the limited data available to estimate the parameters and the simplistic process used to represent multiple signals.

Table 3.4: Computed MLE of $\alpha_1^{s,n}$, $\beta_1^{s,n}$, $\gamma_1^{s,n}$ parameters for available measurement sets, cardinal locations abbreviated (N, E, S, W) used in **Model 1**.

| **Data** | $\alpha_1^n$ | $\beta_1^n$ | $\gamma_1^n$ | $\alpha_1^s$ | $\beta_1^s$ | $\gamma_1^s$ |
|---|---|---|---|---|---|---|
| (N) | 3.700 | 1.85e-10 | 2.43e-9 | 0.765 | 6.84e-8 | 6.02e-9 |
| (E) | 3.108 | 1.96e-10 | 2.63e-9 | 0.674 | 1.45e-7 | 5.33e-9 |
| (S) | 3.308 | 2.17e-10 | 2.64e-9 | 0.783 | 1.63e-7 | 6.76e-9 |
| (W) | 2.599 | 2.73e-10 | 2.56e-9 | 0.623 | 6.46e-7 | 6.76e-9 |

Table 3.5: Computed MLE of $\Theta$, $\lambda$ parameters for available measurement sets, cardinal locations abbreviated (N, E, S, W) used in **Model 2**.

| **Data** | $\alpha^s_{min}$ | $\alpha^s_{max}$ | $\gamma^s_{min}$ | $\gamma^s_{max}$ |
|---|---|---|---|---|
| (N) | 1.767 | 9.253 | 1.22e-08 | 1.23e-07 |
| (E) | 1.563 | 8.589 | 0.32e-08 | 3.50e-07 |
| (S) | 1.111 | 9.650 | 2.08e-08 | 3.50e-07 |
| (W) | 0.404 | 11.05 | 2.56e-08 | 2.56e-07 |

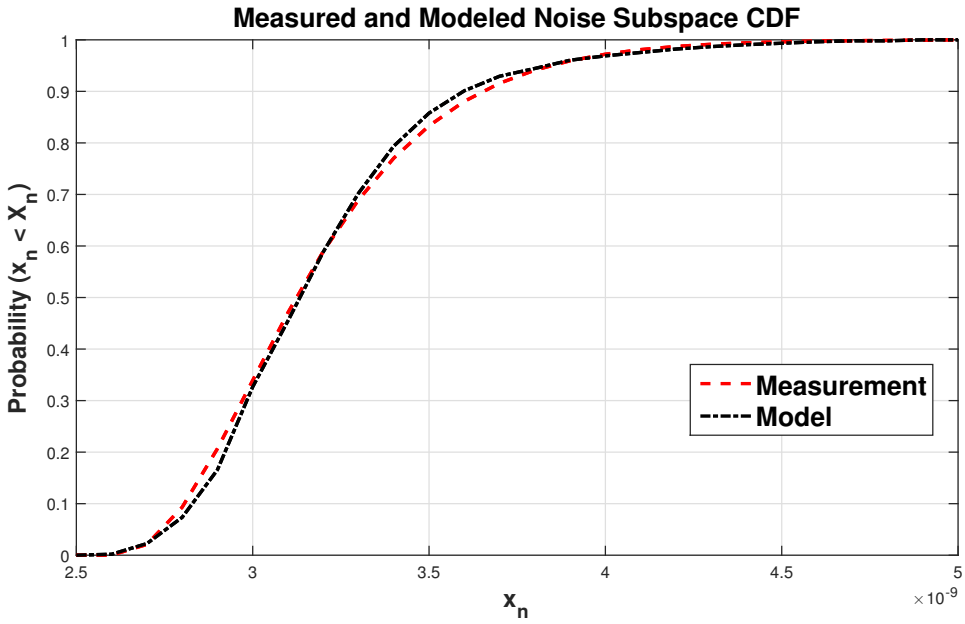


Figure 3.14: Noise subspace comparison between measurement and hypothesized CDF for the *Tillman-Pit* (east) collect.

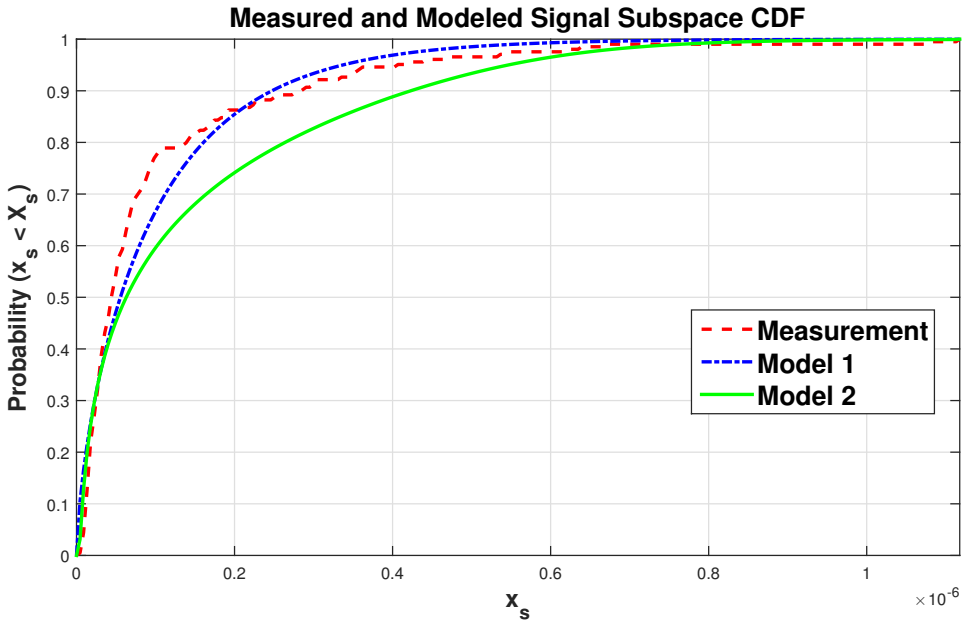


Figure 3.15: Signal subspace comparison between measurement and hypothesized (both **Model 1** and **Model 2**) CDF for the *Tillman-Pit* (east) collect.

#### Markov Transition Matrix Estimation

The estimated transition matrix for the *Tillman-Pit* (east) data gives the following (obtained by counting the number of each transition type for all the available data sets):

$$\hat{\mathbf{P}} = \begin{bmatrix} 0.9944 & 0.0056 \\ 0.0296 & 0.9704 \end{bmatrix}. \tag{3.15}$$

### 3.3.9 Synthetic RFI Example

Using the computed transition matrix and ML parameter estimates, we generate synthetic PSD's for both models using MATLAB [110]. The simulation results show that the proposed technique performs well and we explore the accuracy of the technique in (3.13) and (3.14) by generating example instantiations using the *Tillman-Pit* statistics and comparing to conventional models.

The synthetic PSD for **Model 1** (of same length and plotted against same frequencies listed in Table 4.1) is shown in Figure 3.16 with estimated transition matrix in (3.15)

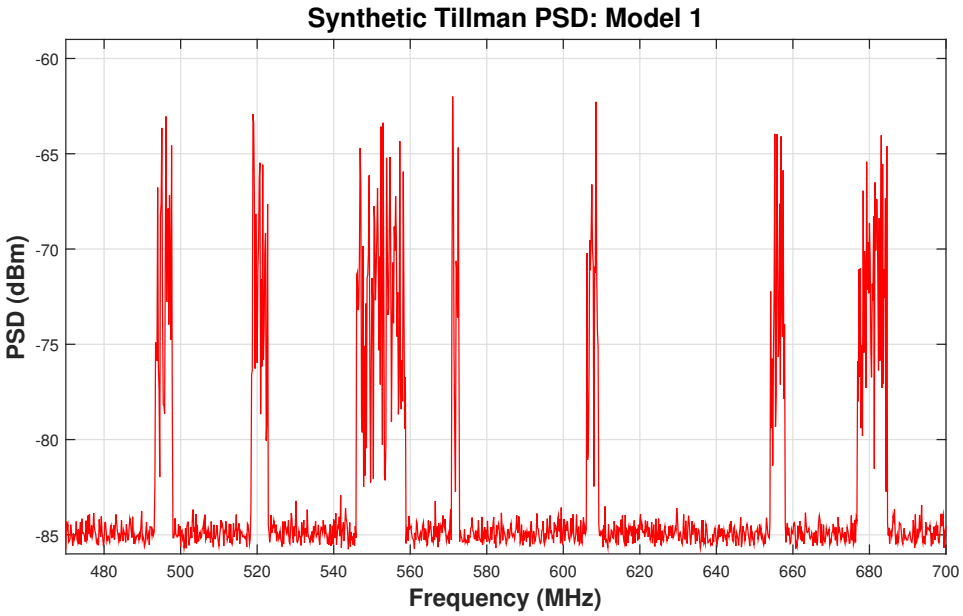


Figure 3.16: Example synthetic PSD for **Model 1** with the *Tillman-Pit* (east) data set parameters.

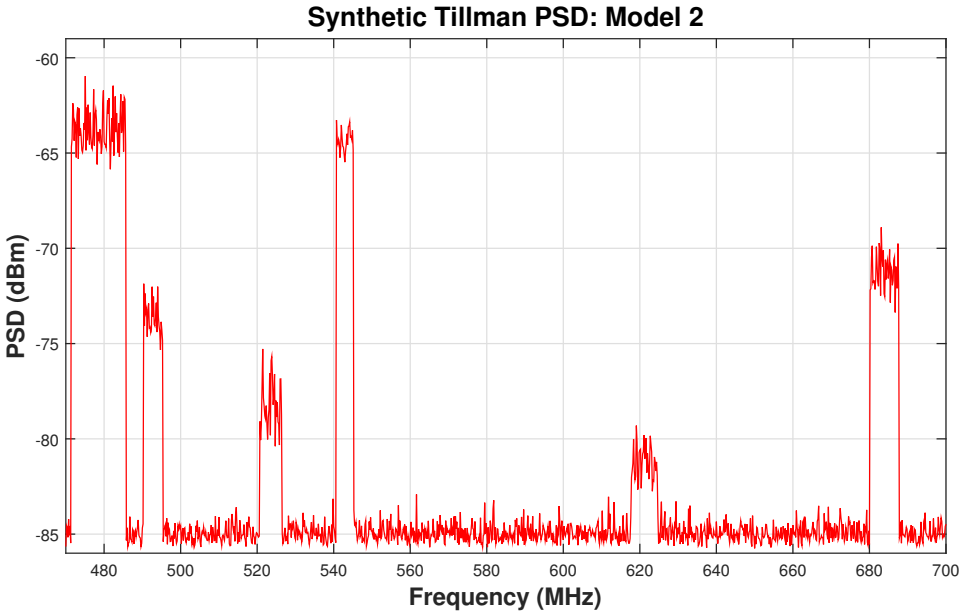


Figure 3.17: Example synthetic PSD for **Model 2** with the *Tillman-Pit* (east) data set parameters.

and Gamma distribution parameters derived from the *Tillman-Pit* (east) measurement data, listed in Table 3.4.

Generated from (3.13), this spectrum shows multiple desirable qualities such as; realistic noise floor, dynamic range, wide noise bands and multiple randomly placed signal bands. However, while we will show the statistical accuracy in the next section, it is evident that other features are not present. For example, the mean-amplitude for each signal band is constant and doesn't reflect actual variation present in the measured data sets. Additionally, this model has large signal band variance, equating to inefficient signal band power usage. This is also not reminiscent of the measured data sets.

To correct for the lack of realistic features in **Model 1**, we allowed for random variation of the shift and scale parameters in **Model 2**. An example spectrum is shown in Figure 3.17 and we observe the desired variation in the mean-amplitude for the signal bands (this could represent either power variation of the emitters in the scene or varied distances from the receiver) as well as more efficient usage of the signal band power. Other desirable features remain, like noise floor and dynamic range.

### 3.3.10 Goodness-of-Fit Analysis

To examine both models goodness-of-fit we look at three measures (1) $\chi^2$-Test (2) Trace of the inverse covariance matrix generated from each PSD model and (3) the Kullback-Leibler divergence.

#### $\chi^2$ Goodness-of-Fit Test

We compute the estimated CDF for both models with $10000$ MC trials. For **Model 1** we observed a p-value of $0.0104$ and, for **Model 2**, a p-value of $0.0118$. A p-value above $0.01$ for the $\chi^2$-Test denotes the test does not reject null at the $1\%$ significance level when compared against the *Tillman-Pit* (east) measured data set.

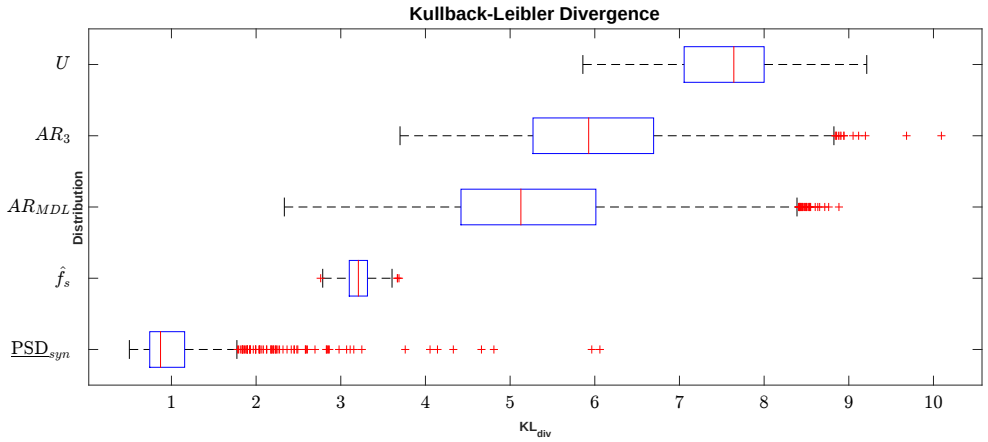


Figure 3.18: Box plot representing the KL divergence median (solid horizontal line), upper and lower quartile (box outline), extreme values (whiskers) and the outliers (+) for multiple distributions compared against *Tillman-Pit* (east) data. Closer to zero indicates higher similarity to measured data.

### Trace of Inverse Covariance

For the same $10000$ Monte Carlo trials used to compute the $\chi^2$-Test, we generate the covariance matrix associated with each PSD and compute the error in the Eigen-spectrum as $\textbf{Error} = \text{Tr}(\mathbf{R}^{-1}) - \text{Tr}(\hat{\mathbf{R}}^{-1})$ where $\mathbf{R}$ and $\hat{\mathbf{R}}$ are the *Tillman-Pit* (east) measured data and modeled covariance matrices, respectively.

In Figure 3.19 we show the PMF of the computed **Error** for both models. As expected, **Model 1** performs better, on average, than **Model 2** with the error distribution having a near zero mean ($-6.83e-07$). Additionally, we note the large negative tail for **Model 2**, suggesting the model can over value the Eigen-spectrum (equivalent to over estimating the power of the RFI). For algorithm design, this would give more conservative estimates of SINR performance.

### Entropic Measure

Lastly, the Kullback-Leibler divergence ($\text{KL}_{\text{div}}$), an information theoretic criteria, is used to observe the separability between the measurement distribution and the synthetic distri-

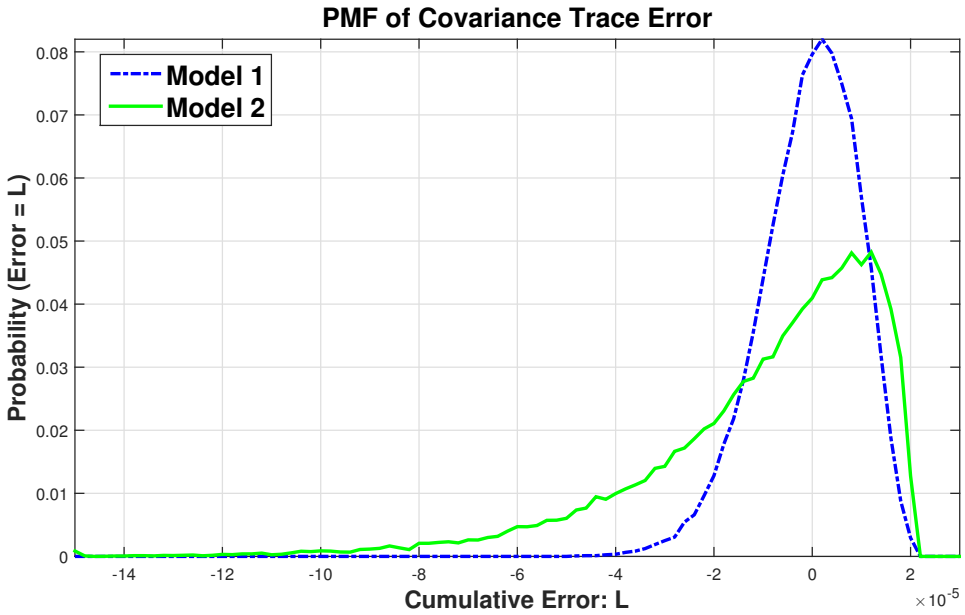


Figure 3.19: PMF of the Eigen-Spectrum error in the measured covariance and synthetic covariance generated from the PSD.

bution. The $\mathrm{KL}_{\mathrm{div}}$ is computed as:

$$\mathrm{KL}_{\mathrm{div}}(D|Q) = \sum_{i=1}^{W} D(i) \log \frac{D(i)}{Q(i)} \tag{3.16}$$

where $W$ is the number of data points in the discrete PMF, $D$ represents the measurement distribution and $Q$ the test distribution [119].

We display the technique's performance by providing, in Figure 3.18, a box plot comparison between the following test distributions; synthetic data (**Model 1** - $\underline{\mathrm{PSD}}_1$ and **Model 2** - $\underline{\mathrm{PSD}}_2$); **Model 1** signal only ($\hat{f}_s$); AR with model order 3 process ($\mathrm{AR}_3$); AR process with model order equal to the MDL ($\mathrm{AR}_{\mathrm{MDL}}$) and a uniform distribution ($U$). This was computed for $10000$ Monte Carlo trials where the average $\mathrm{KL}_{\mathrm{div}}$, for the different distributions, is displayed in Table 3.6. The AR model coefficients are estimated using Burg's method and the PSD is scaled to same dynamic range, relative to the measured data.

It is observed, in regards to the $\mathrm{KL}_{\mathrm{div}}$, that our technique out-performs the conventional models in representing the statistical properties of real-world RFI (where further from zero

Table 3.6: Average Kullback-Leibler Divergence

| **Test Distr.** | $\underline{\text{PSD}}_1$ | $\underline{\text{PSD}}_1$ | $\hat{f}_s$ | $\text{AR}_3$ | $\text{AR}_{\text{MDL}}$ | $U$ |
|---|---|---|---|---|---|---|
| $\text{E}\{\text{KL}_{\text{div}}\}$ | 1.046 | 2.726 | 3.208 | 5.338 | 5.994 | 7.756 |

indicates higher separability). Additionally, as expected, the higher model order AR does show improvement over the lower model order.

## 3.4 Chapter Summary

In this Chapter, we performed an examination of the three different data models used to represent PSD's, and their corresponding covariance matrices, that will be used to develop the SINR performance models when constraints are applied to the radar waveform. Additionally, we have derived and analyzed two new approaches to generating synthetic RFI for covariance matrix generation. This approach is based on a novel application of a two-state Markov Chain that approximates the random distribution of signal and noise bands and a statistical analysis of real-world data sets.

We were also able to show, from an information theoretic perspective, good improvement over the widely used low-order AR model and that our technique closely approximates real-world RFI, such as the *Tillman-Pit* data. Lastly, one of the major advantages of this technique is the simplicity in generating the synthetic RFI, requiring only the generation of three basic probability densities. The full MATLAB script for Model 2 is available in Appendix 9.1.

# Chapter 4

# Jointly Constrained Waveform Design SINR Analysis

This chapter begins our investigation into the trade-space between practical constraints and SINR performance in radar waveform design, an important topic in transmit-adaptive radar processing. For signal design, one must be concerned with the signal-to-noise and interference ratio gain, hardware needs for waveform synthesis (including bandwidth requirements, power constraints, etc.), and the shape of the ambiguity function when compared against a traditional non-adaptive signal (e.g. linear frequency modulated signal). We investigate the attendant performance degradation when constraints are imposed relating to the aforementioned issues[1]. We explore the effect of these constraints on the objective function performance as a function of signal length, interference complexity and constraint thresholds.

The optimal unconstrained waveform design solution for SINR is the Rayleigh solution or the eigenvector corresponding to the minimum eigenvalue of the noise and interference covariance matrix (for purposes of generality, a full rank covariance matrix is assumed) [76]. This is the SINR upper-bound. However, this waveform is unlikely to

[1]The work first published in A. M. Jones, B. Rigling, and M. Rangaswamy, "Eigen-space analysis of constrained adaptive radar waveform design," in *Radar Conference*. IEEE, May 2014.

exhibit low integrated sidelobes (ISL), low peak sidelobe ratio (PSLR), or near unity peak-to-average power ratio (PAPR) or constant modulus. We desire low integrated sidelobes to prevent masking of low SINR targets while low peak sidelobes reduces false alarms. The PAPR, where unity would be a constant modulus waveform, prevents a large power scaling due to the nonlinearity of the radar system's power amplifier and ensures efficient use of dynamic range. The impact of each of these constraints with respect to SINR performance is not completely understood, and this could be to the detriment of a cognitive/adaptive system requiring fast decisions (that is, on which waveform properties should be given emphasis) affecting signal design based on the mission/mode of operation.

Any waveform may be viewed as a linear combination of the eigenvectors of the interference and noise covariance matrix. Under the Rayleigh solution (i.e. the , the waveform is defined by a single eigenvector, but applying waveform constraints implies additional eigen-dimensions must be spanned. This is a key point in our analysis and can be problematic, for as the design leaks waveform energy into the higher noise and interference subspace, SINR will invariably degrade.

In [96], it is shown, with eigen-based waveform optimization, there exists a trade-off between SINR performance and the output response of the matched filter. Although they observe that as emphasis is placed on matched filter response it comes at the expense of SINR, quantifying this expense was not defined. Also pertinent to mention, in [13], the use of several least dominant eigenvectors to synthesize a waveform with desirable properties is investigated and the performance is benchmarked relative to a linear frequency modulated (LFM) waveform of the same bandwidth. Their results are evidence of the benefits, i.e. SINR gain, in adaptive constrained signal design. Other researchers have investigated optimal and sub-optimal designs with constraints as well as performance predictions for radar [3, 27, 101], though none explicitly define the expense of applying constraints, rather that the constraint itself is achieved.

In this Chapter, we develop the role of the eigen-basis when constraints are imposed

on the waveform design problem to maximize signal sub-space projection output SINR. We investigate the impact of constraints on the dimension of the clutter covariance matrix eigen-space used to represent the desired signal. As expected, when constraints are applied, a larger basis is required to meet the design needs. A similar approach is shown in [32] where the design is based on minimizing a least-squares metric against a waveform with desirable properties. In these results, we embark on observing this phenomenon with the ultimate goal of a developing performance prediction models.

The remainder of this Chapter is outlined as follows. In Section 4.1, we develop the signal model, discuss the constraints, and the waveform generation technique. In Section 4.2 we discuss the optimization problems to be solved to show the degradation in SINR performance as a function of the eigen-basis. Section 4.3 includes the results of Monte Carlo computer simulations. In Section 4.4, we state our observations and future work. Lastly, the appendix, containing the derivations and proofs of non-convexity are given in 9.2.

## 4.1 Preliminaries

To explicitly show how the waveform impacts SINR, we derive, with standard mono-static configuration assumptions, the quadratic form typically used in radar. In doing so, we define the transmit waveform $\underline{s} \in \mathbb{C}^{M\times 1}$, and denote the unprocessed received waveform by

$$\underline{y} = \underline{s} + \underline{n}, \tag{4.1}$$

where $\underline{n} \in \mathbb{C}^{M\times 1}$ is interference and additive noise. We match-filter the received waveform, representing the target as an impulse, giving

$$\underline{s}^H \underline{y} = \underline{s}^H \underline{s} + \underline{s}^H \underline{n}. \tag{4.2}$$

We can conservatively assume a known range and critically sampled on receive to give the discrete column vector representation. Using this formulation, we assume a power constrained transmit waveform, where, to enforce, we impose the constraint $\|\underline{\mathrm{s}}\|_2^2 = 1$ (choosing 1 for convenience). The SINR can then be calculated as

$$\text{SINR} = \frac{\underline{\mathrm{s}}^H \underline{\mathrm{s}}\underline{\mathrm{s}}^H \underline{\mathrm{s}}}{\mathrm{E}\{\underline{\mathrm{s}}^H \underline{\mathrm{n}}\underline{\mathrm{n}}^H \underline{\mathrm{s}}\}} = \frac{1}{\underline{\mathrm{s}}^H \mathbf{K} \underline{\mathrm{s}}}, \tag{4.3}$$

where $\mathbf{K} \in \mathbb{C}^{M \times M}$ is the interference and noise covariance matrix. For our analysis, the covariance is assumed known (unless otherwise stated). We highlight the SINR formulation in (4.3) is not the optimal SINR for joint transmit and receive filter design, studied extensively in [120], but for the matched filter on receive only. This is an intentional interpretation to investigate how the transmit waveform constraints affect the SINR.

Consequently, optimizations of the quadratic form, where the objective function is seen in the denominator of (4.3) where, for fixed energy, maximizing the SINR is equivalent to minimizing the denominator, gives

$$\min_{\underline{\mathrm{s}}} \underline{\mathrm{s}}^H \mathbf{K} \underline{\mathrm{s}}, \text{ s. t. } \|\underline{\mathrm{s}}\|_2^2 = 1, \tag{4.4}$$

an equation that frequently appears in radar waveform design applications. Again, $\underline{\mathrm{s}}$ is the waveform to be designed and $\mathbf{K}$ is Hermitian positive definite, and represents the interference and noise covariance matrix capturing the second-order statistical properties.

We note the objective function in (4.4) is and is easily solved (for arbitrary $\underline{\mathrm{s}}$) using the Lagrange method [121] where the optimum, in this case, is the aforementioned Rayleigh solution waveform design seen also in [122, 123]. However, this solution does not generally produce a desirable radar waveform, as the eigenvector offers no guarantees with respect to favorable ambiguity function properties or efficient use of transmit power. Thus, imposing additional constraints on the waveform construction is necessary to achieve a radar waveform suited for practice.

We investigate constraining the ISL, defined as the total energy of the sidelobes of the waveform's autocorrelation sequence (ACS) and computed as:

$$\mathrm{J_{isl}}(\underline{\mathrm{s}}) = \gamma \sum_{k=1}^{M-1} |\underline{\mathrm{s}}^H \mathbf{E_k} \underline{\mathrm{s}}|^2, \tag{4.5}$$

where $\mathbf{E}_k \in \mathbb{R}^{M\times M}$ is a zero matrix with 1's on the $k^{th}$ superdiagonal. A scaling factor (consistent throughout the analysis), $\gamma$ is used to increase the dynamic range of the cost function for simulation purposes in this Chapter only. In the appendix, **Proposition 1.** shows (4.5) to be nonconvex, thus only local optimality claims prevail. A related metric, the peak sidelobe ratio (PSLR), is defined as the peak sidelobe intensity normalized by the ACS peak,

$$\mathrm{J_{psl}}(\underline{\mathrm{s}}) = \frac{|\underline{\mathrm{r}}_{k'}|^2}{|\underline{\mathrm{r}}_0|^2}, \tag{4.6}$$

where $\underline{\mathrm{r}}_k = \sum_{n=1}^{M} \underline{\mathrm{s}}_n \underline{\mathrm{s}}^*_{n-k}$ and $k'$ is the lag of the peak sidelobe. While constraining PSLR directly requires M-1 inequality constraints, the $\mathrm{J_{isl}}$ is a single value. A relationship between (4.5) and (4.6) is discussed later.

Next, we investigate the cumulative modulus cost function, an atypical quantity used here to describe the total point-wise difference of each chip in the waveform from a normalized constant modulus waveform. The role of the fixed amplitude constraint was first introduced in [62] and explains the practical needs for radar operation near power saturation. A relationship can be made to the PAPR and is also discussed later. They are defined as:

$$\mathrm{J_{cm}}(\underline{\mathrm{s}}) = \sum_{l=1}^{M} \left[1 - \underline{\mathrm{s}}^H \mathbf{\Sigma}_l \underline{\mathrm{s}}\right]^2, \tag{4.7}$$

where $\mathbf{\Sigma}_l = \mathrm{diag}\{\underline{\mathrm{e}}_l\}$ and $\underline{\mathrm{e}}_l = [0, \cdots, 0, 1, 0, \cdots, 0]$ where 1 is on the $l^{th}$ entry and

$$\mathrm{J_{papr}}(\underline{\mathrm{s}}) = \frac{|\underline{\mathrm{s}}|^2_{\mathrm{peak}}}{\underline{\mathrm{s}}^2_{\mathrm{rms}}}, \tag{4.8}$$

where $|\underline{s}|_{\text{peak}}$ is the peak amplitude of the waveform and $\underline{s}_{\text{rms}}$ is the root mean square of the waveform. **Proposition 2**, in the appendix, we show in general, that (4.7) is non-convex. Upon further inspection, we simplify (4.7) to:

$$\mathrm{J}_{\text{cm}}(\underline{s}) = M - 2 + \|\underline{s}\|_4^4, \tag{4.9}$$

where $M - 2$ is constant relative to $\underline{s}$ and is removed. Multiplying by a scaling factor, $\gamma M$, to increase dynamic range for simulation purposes in this Chapter only, gives the final constraint as:

$$\mathrm{J}_{\text{cm}}(\underline{s}) = \gamma M \|\underline{s}\|_4^4. \tag{4.10}$$

Lastly, as a mechanism to explicitly observe the impact of constraints on the dimensionality of the waveform design space, we will express the designed waveform as a linear combination of an ordered subset of the eigenvectors of the interference and noise covariance matrix. For an eigen decomposition $\mathbf{K} = \mathbf{V}^H \mathbf{\Lambda} \mathbf{V}$ where $\mathbf{V} = [\underline{v}_1 \cdots \underline{v}_M]$ and $\mathbf{\Lambda} = \text{diag}\{\lambda_1 \cdots \lambda_M\}$ such that $\lambda_1 \leq \lambda_2 \leq \cdots \leq \lambda_M$. We endeavor to use the the smallest number of eigenvectors from the sub-dominant noise subspace to represent the signal. The waveform is then represented as

$$\underline{s} = \sum_{i=1}^{N} \alpha_i \underline{v}_i, \tag{4.11}$$

where $\alpha_i$ is the $i^{\text{th}}$ eigenvector weight, and $N \leq M$ eigenvectors comprise the support of $\underline{s}$[2].

## 4.2 Problem Formulation

In an original formulation, we discuss the role the eigen-basis of the noise and interference covariance matrix plays in constrained radar waveform design. We apply a finite energy,

[2]Formally, a discrete *Karhunen-Loève* expansion [28], we see this technique first employed for radar in [124], where the invention allows gradual modification of the waveform between competing properties: maximizing SINR and the pulse compression characteristics of the waveform.

sidelobe and modulus constraint on the waveform design and require the signal be an ordered subset of eigenvectors, as described in section 4.1. The problem formulation is thus

$$\begin{aligned} &\min_{\underline{\alpha}} \underline{s}^H \mathbf{K} \underline{s}, \text{ s. t. } \|\underline{s}\|_2^2 = 1, \\ &\mathrm{J}_{\mathrm{isl}}(\underline{s}) \leq \epsilon_{\mathrm{isl}}, \\ &\mathrm{J}_{\mathrm{cm}}(\underline{s}) \leq \epsilon_{\mathrm{cm}}, \end{aligned} \tag{4.12}$$

where the initial design satisfies all constraints. In practice the constraint thresholds ($\epsilon_{\mathrm{isl}}$ and $\epsilon_{\mathrm{cm}}$) for the problem in (4.12) are chosen to satisfy the needs of the system. However, in some cases, the thresholds could be too prohibitive given the degrees of freedom available in the design. As such, initialization of the problem to guarantee an initial design solution inside the feasible region is necessary.

### 4.2.1 Threshold Settings

The SINR optimization requires setting the constraint threshold(s) to achieve desirable performance. Therefore, it is important to relate the constraints to recognizable metrics. We relate $\mathrm{J}_{\mathrm{isl}}(\underline{s})$ to $\mathrm{J}_{\mathrm{psl}}(\underline{s})$ by setting $\epsilon_{\mathrm{isl}}$ in the following manner:

1. Select acceptable PSLR (dB),
2. Convert from log to linear scale,
3. Adjust for code length, and scaling $\gamma$, with the assumptions that mainlobe has width of 1 and exploit symmetry of ACS,

giving $\epsilon_{\mathrm{isl}} = \gamma 10^{\frac{x}{10}}(M-1)$ as the threshold, where $x$ is the chosen PSLR. This gives an upper-bound (worst case performance) on the average sidelobe level based on the length of the code. This threshold does not, however, guarantee a minimum PSLR. The chart shown in Figure 4.1 displays, for various average sidelobe levels, what $\epsilon_{\mathrm{isl}}$ should be chosen for

$M = 16$.

To relate the cumulative modulus threshold, $\epsilon_{\text{cm}}$, to the more common PAPR we suggest the following transformation:

1. Select acceptable PAPR (dB),
2. Convert from log to linear scale,
3. Multiply by scaling, $\gamma$,

giving the $\epsilon_{\text{cm}} = \gamma 10^{\frac{y}{10}}$ where $y$ is the desired PAPR, see Figure 4.1. In the appendix, **Proposition 3.** gives a proof that PAPR can serve as an upper-bound for the $\epsilon_{\text{cm}}$ threshold. This property guarantees a designer a worst case PAPR performance of the constrained waveform. In the following sections, we undertake development of a new algorithm and

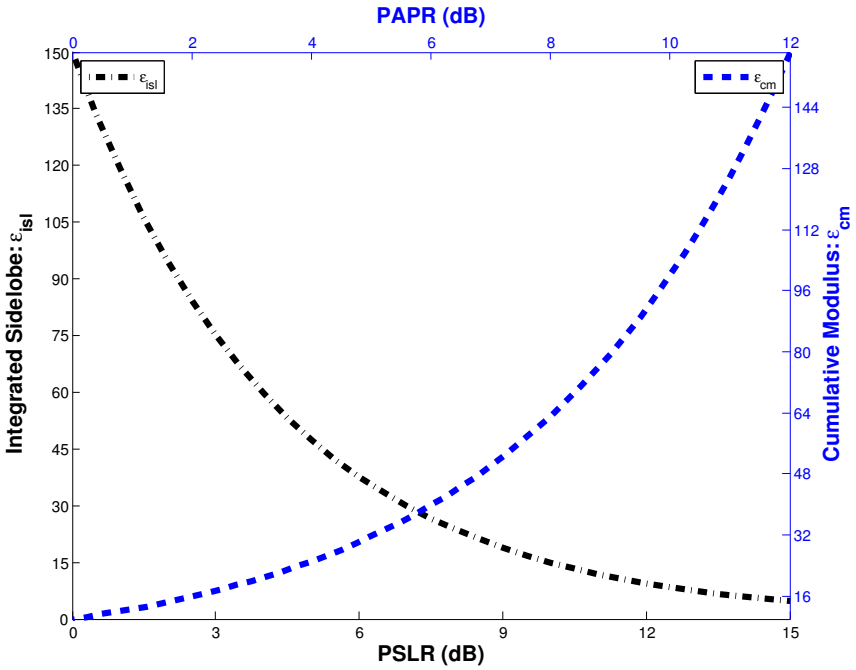


Figure 4.1: Average basis dimension for constrained waveforms of length 16 code over 5 Monte Carlo trials for each eigenvector and covariance matrix generated with AR-3 process.

perform initial Monte Carlo analysis to give new insights into the SINR performance impact when practical constraints are placed on the waveform design.

### 4.2.2 Basis Dimension Selection and Initialization

To solve the optimization problem, first a feasible solution must be found that satisfies the constraint thresholds. Therefore, appropriate initialization of (4.12) and selection of the basis size $N$, for given constraint thresholds, is an important aspect of the solution, for some threshold combinations may not be possible. While viewing the response of designs when either the ISL or CM constraint is applied is instructive, it is not as practical. Both constraints need consideration, and depending on the requirements, one may need more emphasis than the other. To investigate, a 2-D simplex technique[3] is used to view responses from various weights and basis dimension ($N$). The optimization is

$$\min_{\underline{\alpha}} \beta \mathrm{J}_{\mathrm{isl}}(\underline{\mathrm{s}}) + (1-\beta)\mathrm{J}_{\mathrm{cm}}(\underline{\mathrm{s}}) \text{ s. t. } \|\underline{\mathrm{s}}\|_2^2 = 1, \tag{4.13}$$

where $\beta \in [0,1]$. When $\beta = 0$, the emphasis is solely on the modulus, while a $\beta = 1$ constrains only the ISL. If the output signal of the minimization of (4.13) achieves the thresholds, $\epsilon_{\mathrm{isl}}$ and $\epsilon_{\mathrm{cm}}$, we pursue optimization of (4.12) and initialize with the design from (4.13). If the solution from (4.13) does not satisfy the constraint requirements of (4.12), the parameter, $\beta$, is incremented and/or the basis dimension, $N$, is increased until a feasible solution is found or all the dimensions have been exhausted. In the latter case, no possible solution is achievable and the constraints are too tight.

## 4.3 Numerical Solutions

No closed-form solution to (4.12) is possible due to the requirement the waveform be represented as a linear combination of eigenvectors. Therefore, we must pursue numerical analysis to obtain the solution. We use the MATLAB optimization toolbox [110] to compute the initialization (4.13) and the primary problem in (4.12).

[3]Due to the discrete values of $\beta$, the feasible dimension $N$ is considered the best approximation, not a guarantee of the minimum dimension.

Our experimental approach shows the effect of constraints on the dimension of the waveform basis and SINR degradation via computer simulations. The simulations investigate the combined constraints effect on the waveform basis with different emphasis given to each constraint and, for given constraint thresholds, how SINR performance degrades as the constraints are applied. Transmit and noise power are held constant (and unit-less) throughout, and we report the mean values derived from the MC trials. In section 4.3.2 we perform the simulations with a known covariance.

### 4.3.1 Simulation Process

1. Generate a random instantiation of the interference plus noise covariance matrix by modeling an order-$n$ AR process with random pole locations, thus giving a mix of narrow and wide-band interference instantiations. This model has been used previously to study adaptive waveform design strategies [3].

2. *Initialization:* Cycle through emphasis ($\beta$), dimension ($N$) and constraint thresholds ($\epsilon_{\text{isl}}$ and $\epsilon_{\text{cm}}$), first solving (4.13) to selection $N$. Begin with basis dimension of $1$ and increase until the constraints are satisfied (if possible), in (4.13).

3. If thresholds are reached, perform the constrained maximization for SINR performance with the limited basis, in (4.12).

4. Record SINR and basis dimension for each constraint threshold set.

This process is outlined in Figure 4.2.

### 4.3.2 Known Covariance Matrix Results

For the optimizations where the interference and noise covariance matrix is assumed known, the SINR was computed for the solutions of (4.12) and for the parameters in Table 4.1. We use the highly correlated covariance matrix model, described in section 3.2.1, with $P = 3$

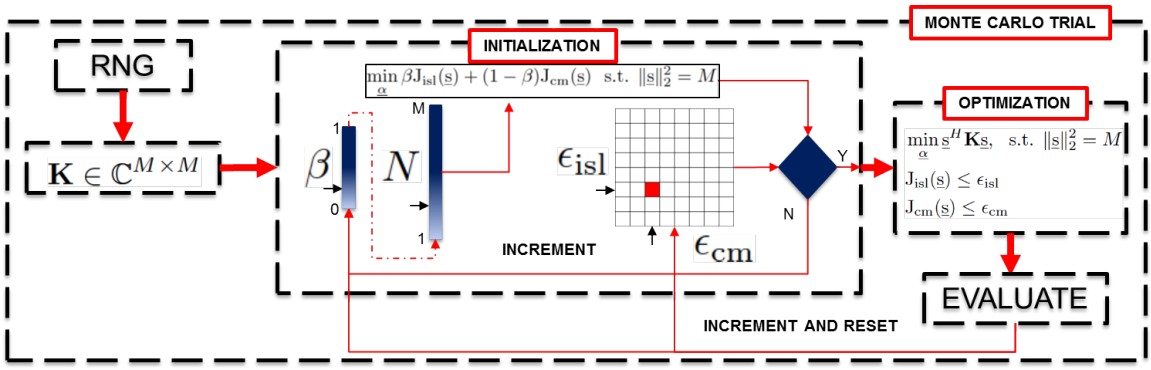


Figure 4.2: Simulation process for a single Monte Carlo trial of the jointly constrained waveform design SINR analysis.

to represent the noise and interference. The minimum basis dimension required to meet the constraints was also retained for further study.

In Figure 4.3, the mean SINR is reported for the grid of constraints ($\epsilon_{\mathrm{isl}}$ and $\epsilon_{\mathrm{cm}}$). On

Table 4.1: Parameters for SINR Degradation as Constraints are tightened

| Parameter | Value |
|---|---|
| Number MC Trials | 10 |
| Length Signal ($M$) | 16 |
| AR Model Order ($n$) | 3 |
| ISL Resolution ($\epsilon_{\mathrm{isl}}$) | 0.25 |
| CM Resolution ($\epsilon_{\mathrm{cm}}$) | 0.25 |
| Simplex Resolution ($\beta$) | 0.1 |
| Training Data Support | Known $K$ |
| Numeric Scaling ($\gamma$) | 10 |

the z-axis we view the average dependent variable, SINR in dB. The x-axis shows the values of the independent variable $\epsilon_{\mathrm{isl}}$ where $0.0$ represents no integrated sidelobes and $2M$ is the unconstrained result. On the y-axis, the second independent variable $\epsilon_{\mathrm{cm}}$ is incremented. Here, $\gamma$ represents constant modulus and $\gamma + M$ represents the unconstrained design. As the constraints are tightened on either axis we observe a monotonic decrease in the average SINR. This information could be used to help select constraints given the need to put the most energy on target.

Figure 4.4 reports the required minimum basis ($N$) as the constraints are tightened.

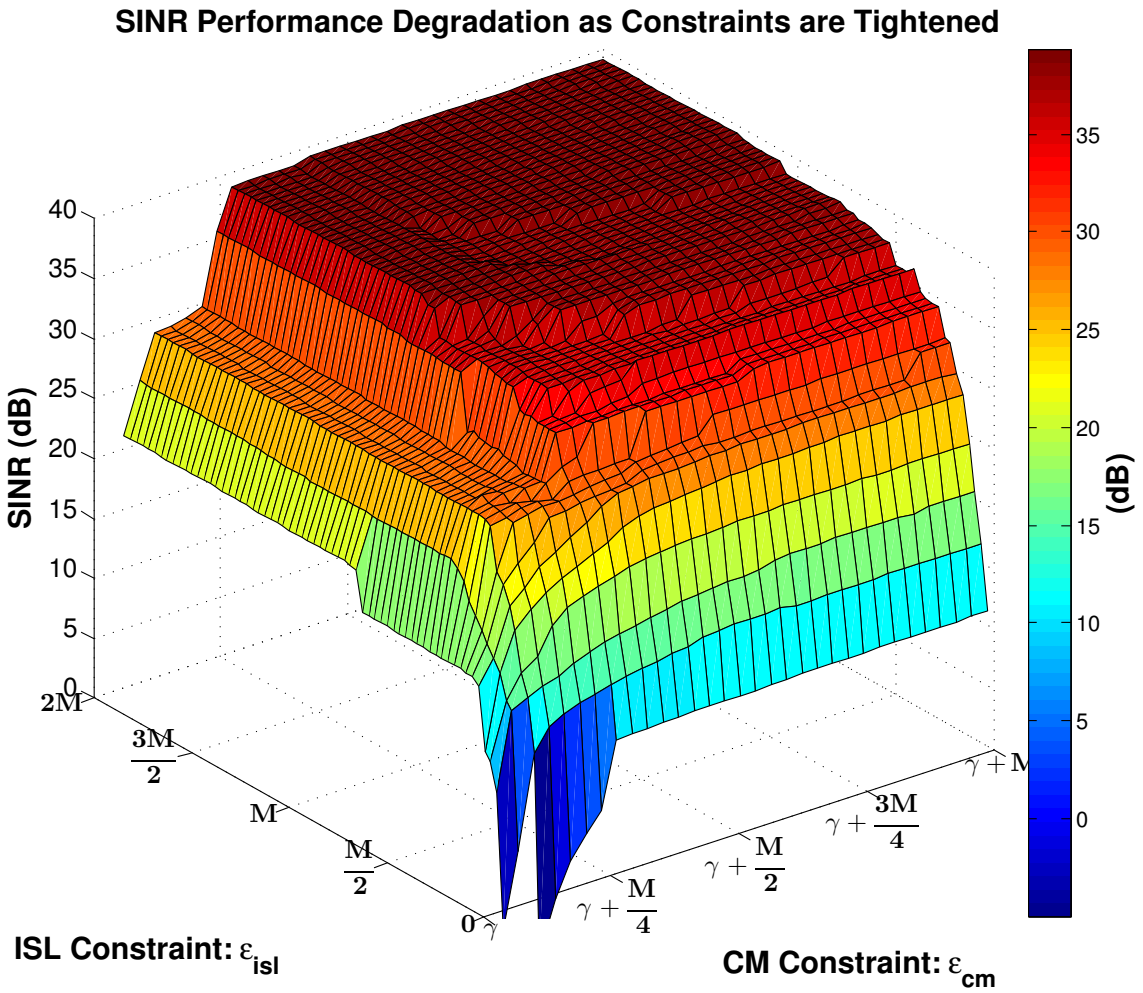


Figure 4.3: Average SINR degradation for constrained waveforms of length 16 code over 10 Monte Carlo trials for each eigenvector and AR process model order of 3.

Again, for the parameters in Table 4.1, the average minimum basis dimension is displayed for the grid of constraints. On the z-axis, the minimum basis dimension, on the x-axis the ISL threshold is varied and the y-axis varies the CM threshold. As expected, as we tighten the constraints, additional dimensions of the sub-dominant noise subspace must be spanned to achieve the design requirements. For a different perspective, the bird's eye views of figures 4.3 and 4.4 are shown in figures 4.5 and 4.6, respectively.

Also included are Figures 4.7 and 4.8 that show, respectively, the measure of spread in the distribution in the number of dimensions required for the CM and ISL constraints. It is interesting to note that for both constraints, a small subset of the noise subspace eigen-

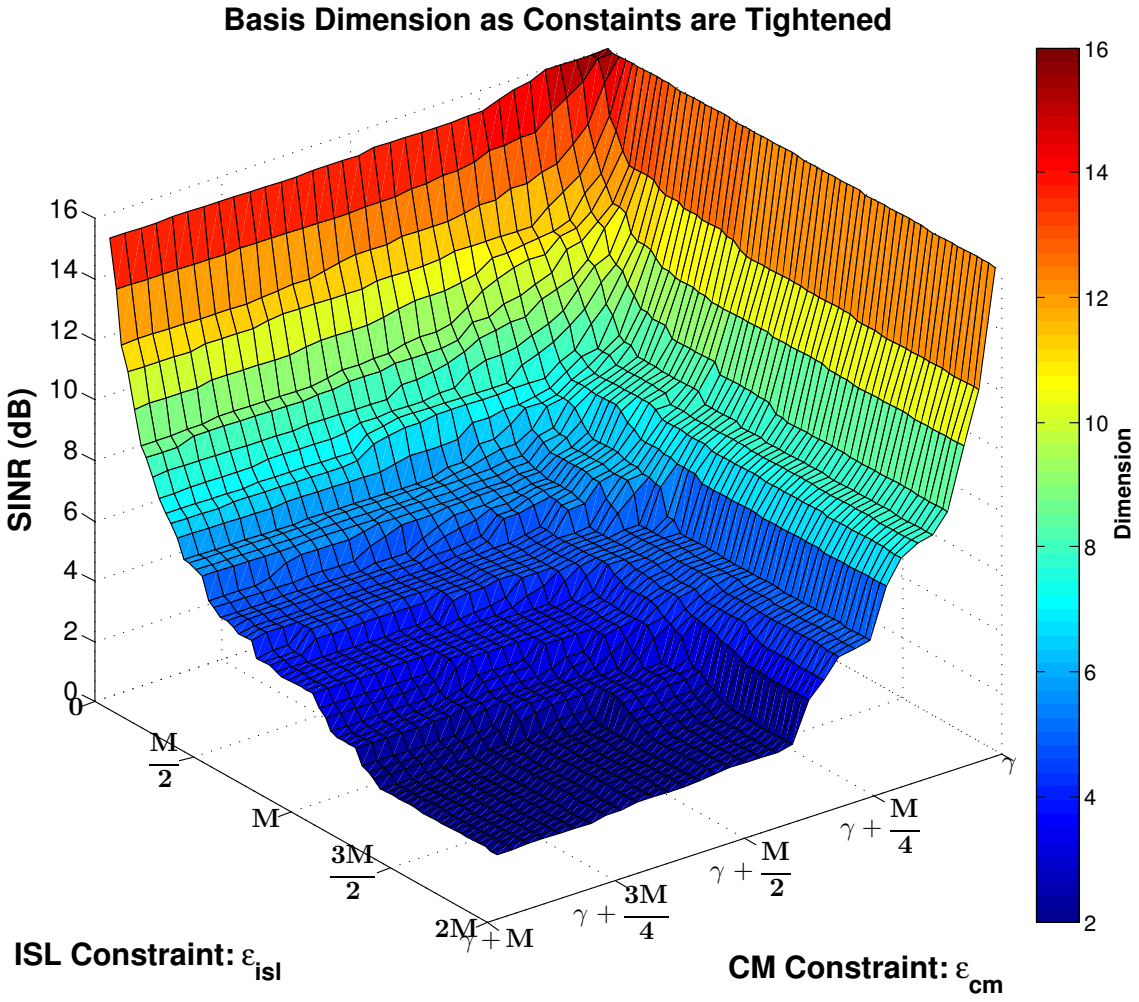


Figure 4.4: Average basis dimension for constrained waveforms of length 16 code over 10 Monte Carlo trials for each eigenvector and AR process model order of 3.

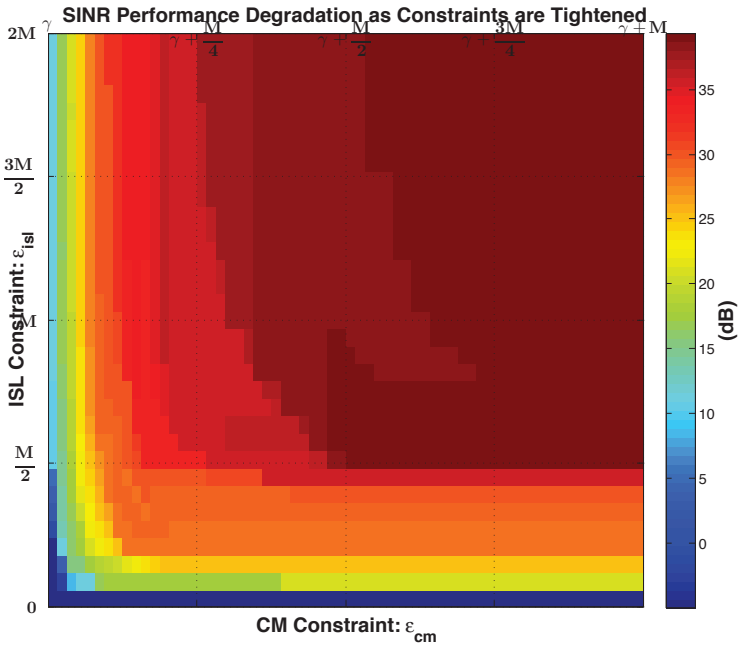


Figure 4.5: (Bird's Eye) Average SINR degradation for constrained waveforms of length 16 code over 10 Monte Carlo trials for each eigenvector and AR process model order of 3.

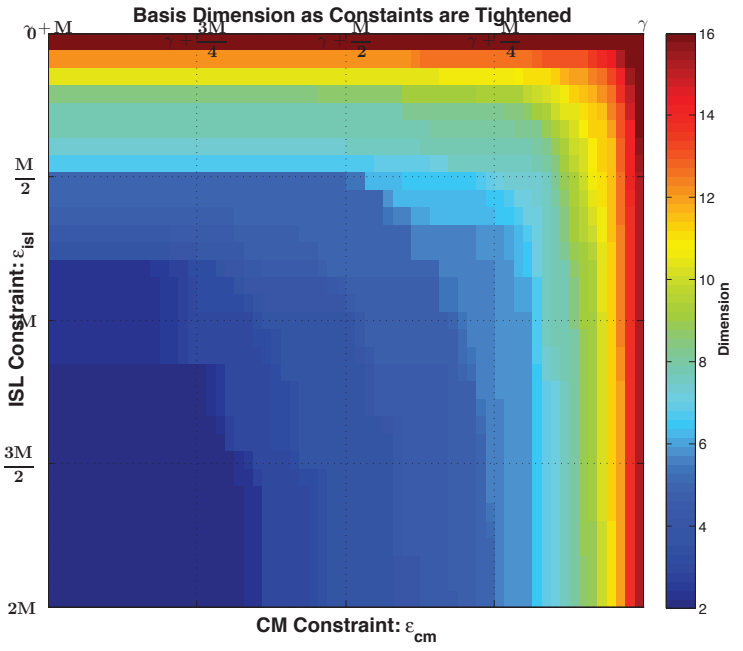


Figure 4.6: (Bird's Eye) Average basis dimension for constrained waveforms of length 16 code over 10 Monte Carlo trials for each eigenvector and AR process model order of 3.

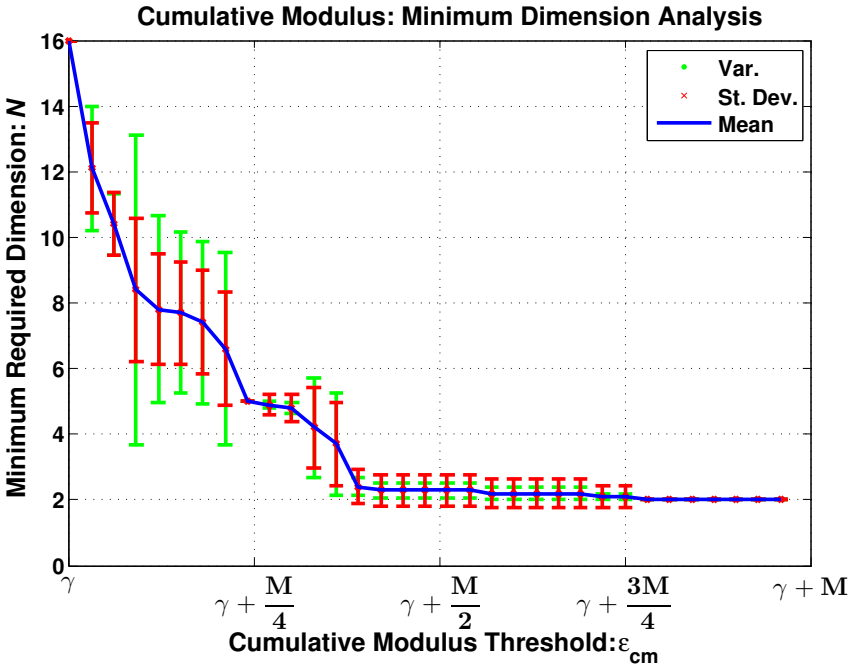


Figure 4.7: Eigen and power spectrum comparison for single instantiation of the clairvoyant and circulant approximation of covariance matrix. Average basis dimension CM constraint only for waveforms of length 16 code over 10 Monte Carlo trials for each eigenvector and AR process model order of 3. Error-bars with variance and standard deviation are included.

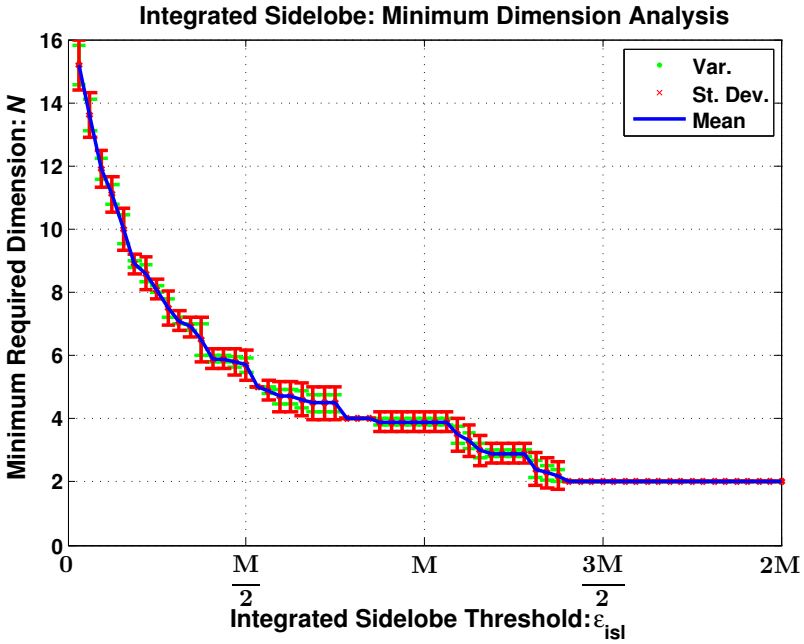


Figure 4.8: Eigen and power spectrum comparison for single instantiation of the clairvoyant and circulant approximation of covariance matrix. Average basis dimension ISL constraint only for waveforms of length 16 code over 10 Monte Carlo trials for each eigenvector and AR process model order of 3. Error-bars with variance and standard deviation are included.

vectors can achieve a large measure of favorable design characteristics.

## 4.4 Chapter Summary

In the previous sections, we devised a new algorithm for observing the SINR performance response for constrained radar waveform design. We have shown a non-linear relationship between the constraint threshold and the SINR performance degradation, from optimal.

Additionally, we have derived and implemented a new technique for waveform design that can be considered an implied SINR maximization by limited the basis dimension to the low noise subspace of the interference and noise covariance matrix. While not advisable to run in an adaptive scenario due to the computational complexity of the eigen-decomposition, it is highly instructive in giving intuition about the SINR performance degradation.

We developed and simulated a new optimization formulation that varies the emphasis between the cumulative modulus and the integrated sidelobes. We included a practical concern for numerical evaluation of the cost function with an added scaling term to ensure equal dynamic range of both terms in the cost function.

The new results showing the nonlinearity of the SINR degradation have impact for setting constraints thresholds in adaptive waveform design. For representative covariance matrices, this algorithm can identify the SINR consequence to constraints on the waveform design. Lastly, included in the Appendix, we have derived the proofs of non-convexity and show that PAPR is an upper bound for CM.

# Chapter 5

# Signal-to-Interference-Plus-Noise-Ratio Analysis for Modulus Constrained Radar Waveforms

To fully appreciate the benefits of arbitrary waveform design capability for transmit adaptive systems, the trade-space between constraints (employed to increase the measure of practicality for radar) and the usual performance driver (signal-to-interference-plus-noise ratio) needs to be better defined and understood. In this Chapter, we address this issue by developing performance models for radar waveform design with cumulative modulus and energy constraints[1]. Radar waveforms typically require a constant modulus (constant amplitude) transmit signal to efficiently exploit the available transmit power. However, recent hardware advances and the capability for arbitrary (phase and amplitude) designed waveforms have forced a re-examination of this assumption in order to quantify the impact of non-constant modulus designs. We develop performance models for the SINR as a function of the cumulative modulus for a random colored interference environment and validate the models against measured data.

[1]Preliminary results first published in [23] and final results in [29]

Typically, radar waveform design techniques focus on maximizing the SINR [13–15] while satisfying some practical constraint(s) quantified by a suitable measure (e.g., Doppler tolerance, peak side-lobe ratio (PSLR) and/or integrated side-lobe ratio (ISLR), bandwidth, energy, etc.). Success is claimed when the waveform achieves improved SINR, relative to the current best technique. However, what is ignored, or not fully understood, is the degradation in SINR, from optimal, when the constraint is allowed to be tightened or loosened. Designing waveforms and enforcing constraints without this understanding is a short-sighted approach for adaptive radar waveform design due to the nonlinear degradation of the SINR performance for practical constraints [16]. As such, it is important to develop relationships between waveform constraints and SINR performance. Adaptive systems can then use performance models to make intelligent, responsive selection of the transmit waveform based on the needs of the system [4, 19, 20, 125].

Constraints on waveform design are manifestations of the system and environmental considerations. For example, the peak-to-average power ratio (PAPR), where unity would be a constant modulus waveform, prevents a large power scaling due to the nonlinearity of a radar systems power amplifier and simplifies recognition of the target distortion on receive while also ensuring efficient use of dynamic range. Typically, a constant modulus waveform design is used to prevent this power loss. In this Chapter, we relax this requirement to investigate the effect on SINR of non-constant modulus waveform designs with finite energy.

In this innovative approach, it is our goal to devise straightforward performance models for achievable SINR as a function of the cumulative modulus constraint. Preliminary results pertaining to the impact of non-constant modulus waveforms on SINR performance were published in [16, 23].

The historical role of the amplitude constraint, first introduced in [62], explains the practical needs for radar operation near power saturation, including maximizing the average power output. Related literature exists for optimal waveform design including [54, 73, 74]

where clutter suppression or similarity constraints had been the design metric. Waveform design for PAPR constraints has been extensively investigated, including [64–66] where the designs allowed for additional, more practical concerns such as sidelobes and finite energy. Phase-only waveforms have been studied, and we refer the reader to the following and the references cited within [13, 18, 27, 32, 33, 41]. All of these designs leave at least half the available degrees-of-freedom (DOF) unchanged, that is, optimized for efficient use of power. This limits the overall capability of the waveform and inspires new formulations to consider perturbing the modulus to observe performance degradation and the available DOF for repurposing. Also, there remains a gap in the literature on the consequence to SINR that imposing these design restrictions imply. This work helps alleviate some of the uncertainty on SINR performance when constraints are applied on the waveform.

Finally, to effectuate the investigation and development of the performance models, a structured approach to observing the degradation is used. Motivated by the well-known optimal waveform design solution for SINR, the Rayleigh solution or the minimum eigenvector waveform, we implement a strategy where a sorted linear combination of the eigenvectors of the noise and interference covariance matrix comprises the waveform.

We formulate and solve multiple optimization problems that minimize the waveform deviation from a constant modulus design. We then analyze the SINR performance loss, from optimal, when modulus and energy constraints are applied to the waveform design. Furthermore, we develop innovative performance models for SINR and waveform cumulative modulus that can aid in the decision making process of what to transmit in an adaptive system by understanding the consequences of the constraints imposed on the waveform design. Lastly, we observe and report the performance response when compared against a leading waveform design technique with a PAPR constraint.

The chapter is organized as follows. In Section 6.1 we discuss fundamentals and concepts used to illustrate our work. Section 5.2 outlines the optimization problems to be solved. Section 5.3 discusses the cumulative modulus and SINR performance models, re-

spectively. In Section 5.4 we give empirical results derived from Monte Carlo computer simulations. Finally, we state the conclusions and other observations of this work in Section 5.5 with the derivations in the Appendix, 9.3.

## 5.1 Preliminaries

In this section, we detail the components for the waveform and the data representation, including waveform formulation, cost function, interference covariance matrix model, and the eigenvalue distribution and estimation technique used to compute the expected SINR.

As first outlined in Chapter 4, optimizations of the quadratic form

$$\min_{\underline{\mathrm{s}}} \underline{\mathrm{s}}^H \mathbf{K} \underline{\mathrm{s}}, \text{ s. t. } \|\underline{\mathrm{s}}\|_2^2 = 1, \tag{5.1}$$

frequently appear in radar waveform design application but note, imposing additional constraints on the waveform construction is necessary to achieve a radar waveform suited for practice.

### 5.1.1 Waveform Formulation Strategy

Again, for an eigen decomposition

$$\mathbf{K} = \mathbf{V}^H \mathbf{\Lambda} \mathbf{V}, \tag{5.2}$$

where $\mathbf{V} = [\underline{\mathrm{v}}_1 \cdots \underline{\mathrm{v}}_M]$ and $\mathbf{\Lambda} = \text{diag}\{\lambda_1 \cdots \lambda_M\}$ such that $\lambda_1 \leq \lambda_2 \leq \cdots \leq \lambda_M$, such that maximizing SINR implies use of the smallest number of eigenvectors from the subdominant noise subspace to represent the waveform. The waveform is thus represented as

$$\underline{\mathrm{s}} = \sum_{k=1}^{N} \alpha_k \underline{\mathrm{v}}_k, \tag{5.3}$$

where $\alpha_k \in \mathbb{C}^{1\times 1}$ is the $k^{\text{th}}$ eigenvector weight, and $N \leq M$ eigenvectors comprise the support of $\underline{s}$. While basis selection is non-unique, we intuitively grasp that as we apply constraints on the waveform design, we are forced to span into the higher eigen-dimensions. Quantifying the impact to SINR as a function of the constraints is the objective of this work.

### 5.1.2 Finite Energy Constraint and Cumulative Modulus Definition

As an obligatory requirement for practicality, a finite energy limit is placed on the waveform. This is the case in practice, and the squared $L_2$ norm ($\|\underline{s}\|_2^2 = 1$) constraint, imposes this restriction in our analysis. While the value can be chosen arbitrarily, we have set it equal to unity without loss of generality and for mathematical convenience. It is worth pointing out, for a constant modulus waveform, the energy constraint is redundant for fixed code length. However, when the modulus is varied, it is necessary to impose the energy constraint to readily observe consequence to SINR in the Monte Carlo analysis.

As fist seen in Chapter 4, the cumulative modulus, a new quantity, is used to describe the total point-wise difference of each sample in the waveform from a normalized peak amplitude, described mathematically as,

$$\text{CM}(\underline{s}) = \sum_{l=1}^{M} \left[1 - |\underline{s}_l|^2\right]^2, \tag{5.4}$$

$$= M - 2\|\underline{s}\|_2^2 + \sum_{l=1}^{M} |\underline{s}_l|^4, \tag{5.5}$$

where, for $\|\underline{s}\|_2^2 = 1$, this quantity can be simplified to

$$\text{CM}(\underline{s}) = M - 2 + \|\underline{s}\|_4^4. \tag{5.6}$$

We recognize $M-2$ is a nonnegative constant for waveform lengths $M \geq 2$ that can be omitted to give a simplified function,

$$\mathrm{J_{cm}}(\underline{\mathrm{s}}) = \|\underline{\mathrm{s}}\|_4^4. \tag{5.7}$$

Instructively, we claim minimization of the $\|\underline{\mathrm{s}}\|_4^4$ is analogous to minimizing the dissipated or wasted energy in a constant supply voltage system. That is, as the design approaches a constant modulus waveform (i.e. PAPR$= 1$), the system can operate closer to saturation, thus more efficient use of the finite energy supply. It is evident that the $\|\cdot\|_4^4$ is an alternative formulation to the more well-known PAPR constraint for waveform design. We also note, with the $\|\underline{\mathrm{s}}\|_2^2 = 1$ imposition, the problem is evidently non-convex. Therefore, we investigate (in the following section) a convex relaxation, for comparison.

We also observe an additional alternate formulation of the objective with a slight modification to (5.4), given as:

$$\bar{\mathrm{CM}}(\underline{\mathrm{s}}) = \sum_{l=1}^{M} \left[1 - |\underline{\mathrm{s}}_l|\right]^2, \tag{5.8}$$

$$= M - 2\sum_{l=1}^{M} |\underline{\mathrm{s}}_l| + \|\underline{\mathrm{s}}\|_2^2, \tag{5.9}$$

$$= M + 1 - 2\sum_{l=1}^{M} |\underline{\mathrm{s}}_l|, \tag{5.10}$$

where, after simplification and the assumption $\|\underline{\mathrm{s}}\|_2^2 = 1$, the objective would be maximization on the $\mathrm{L}_1$ norm ($\|\underline{\mathrm{s}}\|_1$) [126]. We give this as a possible new alternate definition but only perform analysis using the objective in (5.7) to avoid confusion.

### 5.1.3 SINR Expression as Function of Eigenvalues

The SINR of the output of a matched filter, with fixed energy constraint ($\|\underline{s}\|_2^2 = 1$), can be expressed as a linear combination of weighted eigenvalues,

$$\text{SINR} = \frac{1}{\underline{s}^H \mathbf{K} \underline{s}}, \tag{5.11}$$

$$= \frac{1}{(\mathbf{V}\underline{\alpha})^H \mathbf{V}\mathbf{\Lambda}\mathbf{V}^H(\mathbf{V}\underline{\alpha})}, \tag{5.12}$$

$$= \frac{1}{\underline{\alpha}^H \mathbf{\Lambda}\underline{\alpha}}, \tag{5.13}$$

$$= \frac{1}{\sum_{k=1}^{N\leq M} |\underline{\alpha}_k|^2 \underline{\lambda}_k}. \tag{5.14}$$

For deterministic eigen-values, it becomes, then, a matter of the weights to compute SINR, where, for example, the "best" SINR corresponds to $\underline{\alpha}_1 = 1$ and all others as zero (i.e., the Rayleigh solution). The "worst" performance would be inclusion of only the $N^{\text{th}}$ eigenvalue while an average would put an equal weight on each of the $N$ values. Evidence of these observations are shown in the simulations.

## 5.2 CM Optimization Problems

In this section, we bring together the definitions of the waveform, objective function and the covariance representation in a straightforward optimization problem (and its convex relaxation) to minimize the CM with a finite energy constraint. Additionally, instead of explicitly maximizing for SINR, we use the technique described in 5.1.1 to degrade SINR and allow the objective function to focus on the cumulative modulus in (5.7). We represent this as

$$\min_{\underline{\alpha}} \|\underline{s}\|_4^4, \text{ s. t. } \|\underline{s}\|_2^2 = 1, \ \underline{s} = \sum_{k=1}^{N} \alpha_k \underline{v}_k \tag{5.15}$$

where for arbitrary $\underline{s}$ the optimal solution is obvious, any constant modulus waveform. However, the imposition that the waveform be comprised of an ordered subset of eigenvec-

tors of the interference and noise covariance matrix muddles the solution. We point out, due to selection of the reduced dimension basis for the waveform, it is expected that, on average, a constant modulus design may not exist for all subsets.

The optimization problem in (5.15) is evidently non-convex and therefore, the solution may be highly dependent on the initialization and no guarantee of global optimality may be made. Thus, we formulate, solve, and analyze the following convex relaxation of (5.15) and give insights into the differences between the two:

$$\begin{aligned} \min_{\mathbf{A}} \ & \text{vec}^H(\mathbf{A}) \Big[ \sum_{i=1}^{M} \text{vec}(\hat{\mathbf{V}}_i) \text{vec}^H(\hat{\mathbf{V}}_i) \Big] \text{vec}(\mathbf{A}) \\ \text{s.t.} \ & \ \text{vec}^H(\mathbf{I}\text{dim}(\mathbf{A})) \text{vec}(\mathbf{A}) = 1 \end{aligned} \tag{5.16}$$

where $\mathbf{A} = \underline{\alpha}\underline{\alpha}^H$, $\mathbf{I}$ is the identify matrix, $\hat{\mathbf{V}}_i = \underline{v}_i^H \underline{v}_i$ and $\dim(\mathbf{A}) = M$. The matrix $\mathbf{A}$ is necessarily positive semi-definite in order for (5.16) to be convex. The solution to (5.16) will, most likely, yield a higher than rank-1 $\mathbf{A}$ matrix (hence the relaxation). Thus, to compute the waveform that permits analysis of the SINR and cumulative modulus, we extract the best rank-1 eigen-weights ($\underline{\alpha}_{\text{relax}}$) solution as defined by having the lowest cumulative modulus waveform. We accomplish by performing an eigen-decomposition on the $\mathbf{A}$ matrix and computing an exhaustive search of all possible waveforms with the prescribed eigen-basis of the interference and noise covariance matrix $\mathbf{K}_{\text{MP}}$. This solution is then used as part of the average for the relaxed formulation. The full derivation of the relaxation can be found in the Appendix.

One could certainly perform waveform design using these algorithms (although not advised due to computational burden of the eigen-decomposition), we, instead, use this as a systematic approach to develop performance models for waveforms with a cumulative modulus restriction. These models, then, could become a surrogate for waveform design algorithms when knowledge of performance is required.

## 5.3 Eigen-Basis Analysis Relating SINR & CM

The objective of the chapter is to understand and model the the outcome to (5.15) and the corresponding SINR for a given basis dimension (N). We are challenged by the fact that obtaining a closed-form representation for $\|\underline{s}\|_4^4$ in terms of specific eigenvectors $\underline{v}$ corresponding to a single instantiation of noise and interference is mathematically intractable, as it calls for obtaining unique solutions to coupled cubic equations. Thus, the expected value cannot be found analytically and we are forced to develop an empirical model that represents the correspondence.

Our approach involves first computing the CM model as a function of $N$. Next, we continue by developing the SINR model as a function $N$. Finally, we relate SINR and CM in section 5.3.3. This connection allows interchangeability between SINR requirements and CM thresholds settings.

### 5.3.1 Cumulative Modulus Performance Model

This section develops the model for the cumulative modulus as a function of the dimension of the eigen-basis. Models, such as exponential, inverse power and circular have been explored, but not with the same success as the Lamẽ curves (discussed next), and thus are not depicted.

The Lamẽ curve is perhaps more familiarly known as a generalized super-ellipse of the form:

$$\left|\frac{x - X_c}{a}\right|^p + \left|\frac{y - Yc}{b}\right|^q = 1, \tag{5.17}$$

where $a$, $b$ are the minor and major axis (or semi-diameters), respectively, $p$, $q$ are parameters to shape the ellipse, ($X_c$, $Y_c$) denotes the ellipse center location. Note, for a curve located at the origin and equal normalized axes, when the powers ($p$, $q$) are set to 2, (5.17) reduces to the unit circle.

We seek to fit (5.17) to the expected cumulative modulus (E$\{\|\underline{s}\|_4^4\}$, the average so-

lution to (5.15)) for a given eigen-basis dimension (N). We use a least-squares estimation of the parameters $p, q$ of the Lamẽ curve from the resulting solution of (5.15). We then define parameters $x$, $y$ to represent the number of eigenvectors used in the design and the cumulative modulus quantity, respectively. Solving for $y$ in terms of $x$ gives the cumulative modulus as a function of the eigen-basis dimension. The canonical form of the model of cumulative modulus as a function of basis dimension is [127];

$$y(x) = b\sqrt[q]{1 - \frac{(x - X_c)^p}{a^p}} + Y_c. \tag{5.18}$$

We set $a = \frac{1}{M}$ (minor axis). This is explained by noting the minimal solution will yield a result of $\|\underline{s}^*\|_4^4 = \frac{1}{M}$ (i.e. constant modulus) and for $N = 1$, or the worst performing waveform design, we achieve $\mathrm{E}\{\|\underline{s}_1\|_4^4\} = \frac{2}{M}$ (coincidentally, this is also the expected value of the 4th-moment of a complex Gaussian random vector with variance $\frac{1}{M}$) giving a dynamic range of $\frac{1}{M}$. The major axis $b$ is the number of eigenvectors required to achieve the optimal. Given the design parameters have $2M$ complex degrees of freedom and the modulus, or amplitude, describes only half the waveform (the other half being the phase), we would expect to use only half our degrees of freedom to achieve constant modulus. Therefore, only $b = \frac{M}{2}$ basis vectors would be required. This description is depicted in Figure 5.1.

Substituting in (5.18), our parameters, the performance model for cumulative modulus as a function of basis dimension is

$$\mathrm{CM} \cong \frac{2}{M} - \frac{1}{M}\sqrt[q]{1 - \frac{(\frac{M}{2} - N)^p}{(\frac{M}{2} - 1)^p}}, \tag{5.19}$$

$N$ valid from 1 to $\frac{M}{2}$. Or conversely, the dimension of the basis required when given a modulus constraint

$$\mathrm{N} \cong \frac{M}{2} - \sqrt[p]{1 - (2 - M\mathrm{CM})^q}(\frac{M}{2} - 1). \tag{5.20}$$

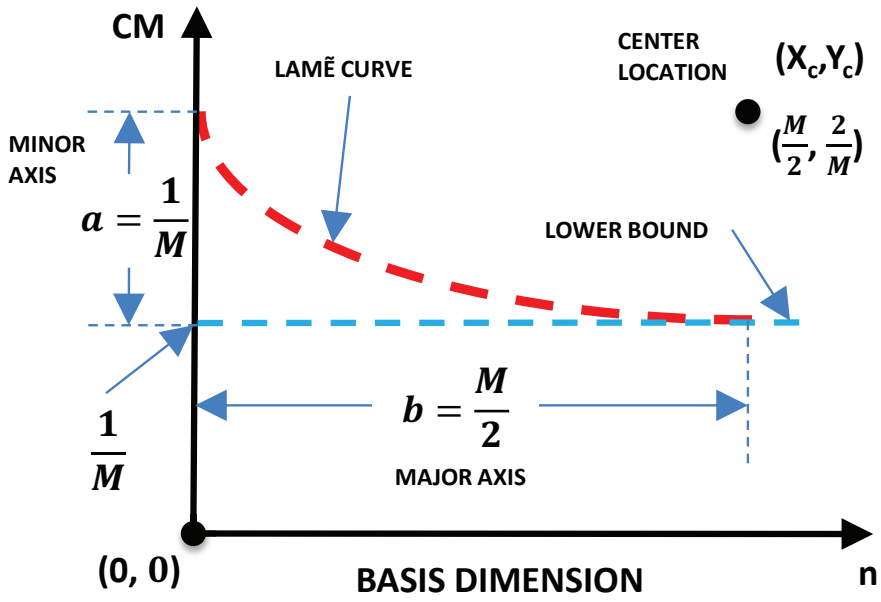


Figure 5.1: Description of waveform length dependent parameters of the Lamẽ model for expected cumulative modulus as a function of the basis dimension $N$.

These models provide quick but rough insights into the behavior of the objective function in (5.15).

### 5.3.2 SINR Performance Model

Next, we pursue development of a performance model for SINR degradation as the waveform basis is expanded for the MP covariance matrix definition. As outlined in Section 5.1.3, the SINR, for fixed energy, is $\frac{1}{\sum_{k=1}^{N\leq M} |\underline{\alpha}_k|^2 \underline{\lambda}_k}$. Since the MP asymptotic distribution allows computation of an eigen-spectrum for a large matrix, whose column dimension corresponds to waveform length, we consider the eigenvalues, $\underline{\lambda}_k$ to be deterministic, and have modeled for the optimal weights $\underline{\alpha}^*$.

We define the magnitude function of the weights vector by a power law model, $|\bar{\underline{\alpha}}_N(k)| = \frac{1}{\sqrt{k}}$. Power law models are used extensively in physics, biology and other sciences and are attractive in this context due to its simplicity [128].

These approximations allow us to write the $\text{SINR}_{\text{MP}}$ as:

$$\text{SINR}_{\text{MP}} \cong \frac{1}{\sum_{k=1}^{N \leq M} \left|\underline{\bar{\alpha}}_N(k)\right|^2 \underline{\mathcal{Z}}(k)}, \tag{5.21}$$

where $\underline{\mathcal{Z}}(k)$ is the expected eigen-value vector with distribution described in (3.2). This formulation gives a simple representation of the consequences to SINR as the constraint tightens and forces a larger basis dimension [16].

### 5.3.3 SINR as function of CM

Connecting the CM model in (5.19) and the SINR model in (5.21) facilitates development of a performance model for SINR as a function of the cumulative modulus constraint. Using the approximation for the number of eigenvectors needed to meet a CM constraint, seen in (5.20), we can connect the two models. This is computed as:

$$\text{SINR}_{\text{MP}}(\text{CM}) \cong \frac{1}{\sum_{k=1}^{\lfloor N \rfloor(\text{CM})} \left|\underline{\bar{\alpha}}_N(k)\right| \underline{\mathcal{Z}}(k)}, \tag{5.22}$$

where $\lfloor \text{N} \rfloor(\text{CM})$ is a function of the desired cumulative modulus as seen in (5.20). This model can be employed to advise the waveform designer on the rough consequence to SINR when applying an cumulative modulus constraint on the waveform design.

## 5.4 Numerical Illustrations

To validate the CM and SINR models, we use computer simulations to show the effect of the waveform basis dimension on the modulus and SINR, from optimal. The covariance matrix is assumed known in the optimization routines and the eigen-spectra are approximated with the MP distribution. We note, the MP model is the pessimistic assumption on the covariance statistics. That is, if more information is available on the structure of the covariance, you would necessarily incorporate into the analysis. We also hold transmit and

Table 5.1: Lamẽ Model Parameters

| Length | $\mathrm{p}_{MP}$ | $\mathrm{q}_{MP}$ |
|---|---|---|
| 8 | 2.2409 | 1.8794 |
| 16 | 2.4470 | 2.1247 |
| 32 | 2.7647 | 2.1067 |
| 64 | 2.6494 | 2.1065 |

noise power constant (and unit-less) throughout, and we report the mean values derived from the MC trials.

The MATLAB software package, including the Optimization Toolbox, [110] and CVX (a package for specifying and solving convex programs) [129, 130] was used to generate the data, figures and perform the optimization routines. Algorithm 1 describes the process used to generate the numerical results for (5.15). In Table 5.1, we list values obtained for a variety of waveform lengths and it is reasonable to assume that the theory scales for larger length waveforms that are computationally prohibitive for large Monte Carlo analysis.

For our purposes, it is important to determine the degradation of SINR from optimal as we include additional eigenvectors to minimize CM. It is appropriate to initialize with the optimal waveform (eigenvector associated with minimum eigenvalue) and place no emphasis on other eigenvectors (e.g. $\underline{\alpha} = [1\ \underline{0}^{N-1\times 1}]$), where $N$ is the number of eigenvectors used in the design.

As evidenced by considerable Monte Carlo analysis, (see Table 5.1) the model parameters are largely waveform length agnostic for the MP data model. We, therefore, only display results for the $M = 64$ length waveform.

### 5.4.1 Simulation Results with MP Covariance Matrix Models

We numerically solve for (5.15) and (5.16) and compare the results against the models in (5.19) and (5.21), respectively. The solution reported for the optimization in (5.16) is the rank$-1$ solution of $\mathbf{A}$ that gives the lowest resulting $\mathrm{L}_4$ norm of the designed waveform.

**Algorithm 1** Modulus and SINR Performance Simulation Pseudo-Code for (5.15)

**for all** $k = 1$:MC (Monte Carlo trials) **do**
  **procedure** GENERATE SAMPLE COVARIANCE($M$)
    RawData = Cov{randn($M$) + $i$randn($M$)}
    $\mathbf{K}_{\text{mp}}$ = Normalize{RawData}
  **end procedure**
  **procedure** EIGENDECOMPOSITION(Data)
    $[\mathbf{V}, \mathbf{\Lambda}]$ = eig{Data} ($\mathbf{K} = \mathbf{V}^H \mathbf{\Lambda} \mathbf{V}$)
  **end procedure**
  **for all** $k = 1 : \frac{M}{2}$ (half Eigenvectors) **do**
    Initialize: $\underline{\alpha}$
    Split the complex coefficient: $\underline{\alpha} = [\text{Re}(\underline{\alpha}); \text{Im}(\underline{\alpha})]$
    Perform Optimization in (5.15)
    Unsplit the complex: coefficient $\underline{\alpha}^*$
    Compute waveform: $\underline{\text{s}} = \mathbf{V}\underline{\alpha}^*$
    Compute Modulus: $\|\underline{\text{s}}\|_4^4$
    Compute SINR: $\frac{1}{\underline{\text{s}}^H \mathbf{K} \underline{\text{s}}}$
    Data Log
  **end for**
**end for**
Least-Square Regression Analysis
Compute CM Model
Compute SINR Model
Connect SINR to CM constraint

This is the best case case scenario for this formulation. In Figure 5.2, the expectation of $\|\cdot\|_4^4$ as a function of the basis dimension ($N$) is reported for $M = 64$ and MC $= 100$. The lower-bound is, of course, a constant modulus waveform, and for our energy constraint would give $\|\cdot\|_4^4 = \frac{1}{M}$. The data and Lamẽ model (overlaid), and shown only for the first half of the basis ($\frac{M}{2}$) as the average modulus achieves the lower-bound when using half the DOF. For completeness, the maximum and minimum computed modulus is reported, we see the dynamic range converges as the basis dimension increases.

We see in Figure 5.2, the relaxed optimization problem of (5.16) behaves predictably. As the basis dimension increases, we initially observe improvement in the $\mathrm{L}_4$ norm of the rank$-1$ solution waveform. However, as the optimization achieves the minimal value, i.e. $\|\cdot\|_4^4 = \frac{1}{M}$ (not shown, but occurs $\approx$ at $10$ basis vectors in our example, on average) it begins to spread the weights out evenly over the basis of $\mathbf{A}$, thus, the best rank$-1$ solution has less influence on the final waveform design in regards to the $\mathrm{L}_4$ norm. Consequently, we observe the rank$-1$ solution reverting back to the unconstrained value.

In Figure 5.3, the normalized average SINR degradation, from optimal, is shown. The exponential model in (5.21) is overlaid and showing good results for a highly simplified model when compared against the solution of (5.15).

Using (5.19) and (5.21) in conjunction allow for SINR performance given a modulus constraint on the waveform design. Or, given the basis dimension of the low-noise subspace (i.e. avoiding the spectrum associated with clutter and interference) one could estimate modulus performance and SINR degradation.

### 5.4.2 Simulation of the SINR as a function of CM

More important than the performance models that predict SINR as a function of the eigen-basis is connecting the eigen-basis models of the SINR and CM results in a unified model that gives the consequence to SINR as a function of the CM. We are able to perform computer simulations to solve (5.15) and subsequently compute the output SINR for a given

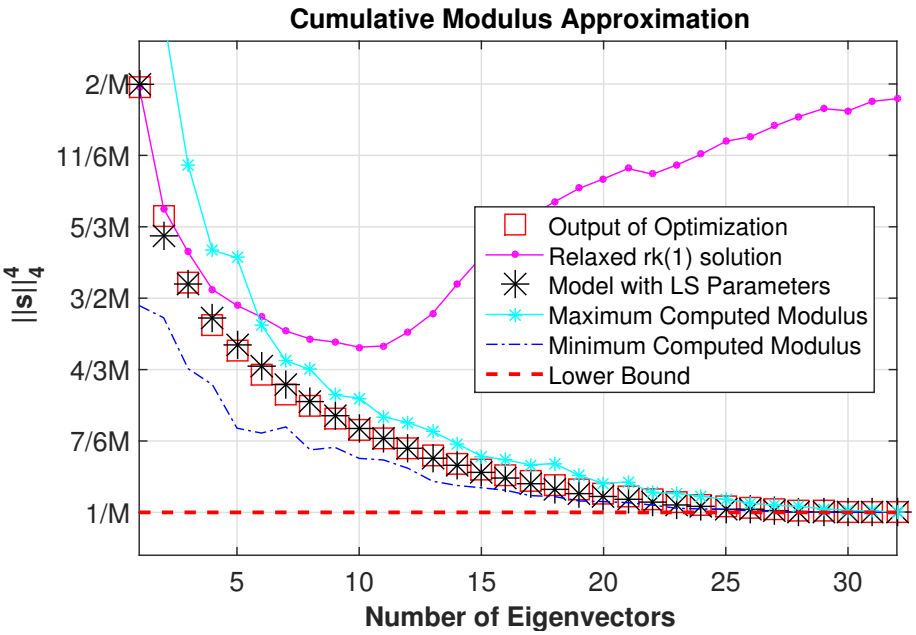


Figure 5.2: Expected cumulative modulus with model comparison and minimum and maximum outputs.

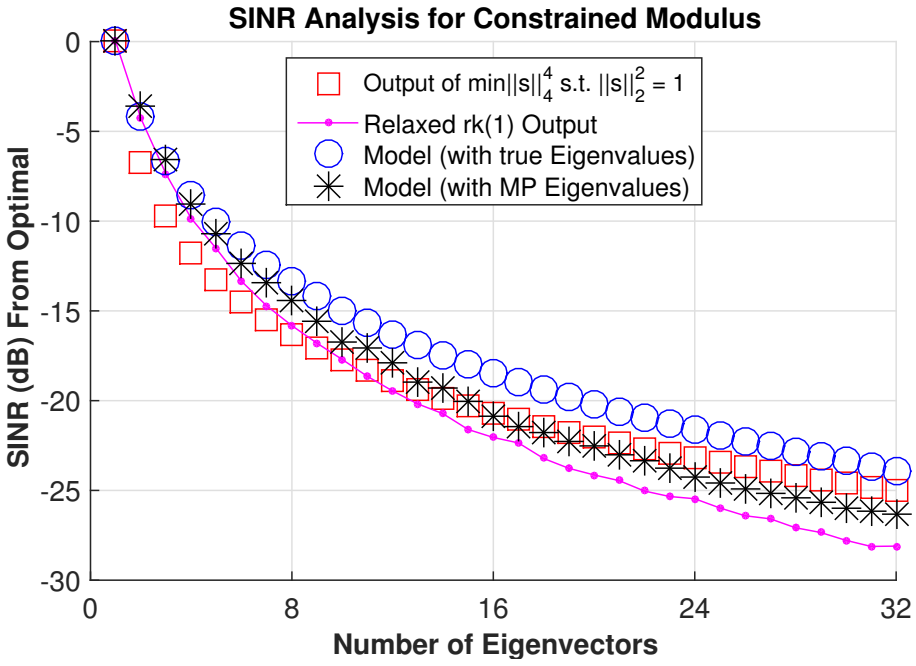


Figure 5.3: Expected signal-to-interference-and-noise ratio with model comparison.

eigen-basis dimension. We can then associate the results, for a given eigen-basis dimension, and compare against the model in (5.22), with results shown in Figure 5.4. For comparison, we also compute and display the rank$-1$ solution waveform for the optimization in (9.45).

We observe that the model predicts the outcome, within several dB, of SINR for a

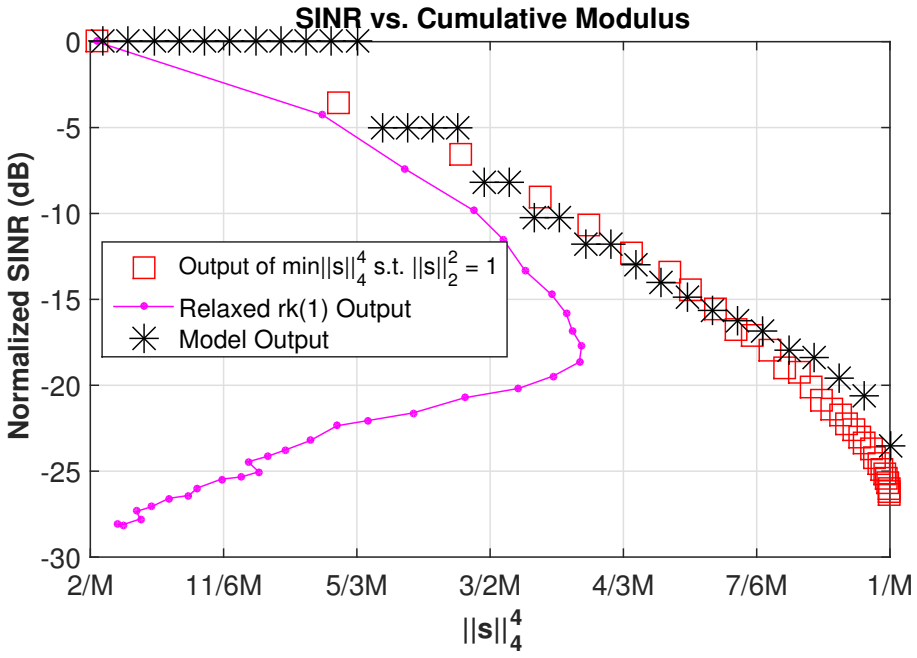


Figure 5.4: SINR vs. CM model comparison against the resulting output SINR from (5.15).

given CM constraint value in (5.15). As noted earlier, the discrete *Karhunen-Loève* waveform generation technique is not optimized for SINR but uses the reduced basis dimension to investigate the SINR performance. Also, the model does not reconcile for waveform designs that more gradually degrade SINR and are not restricted to an integer numbers of eigen-basis dimensions. Hence, we observe the quantization in SINR levels as the model truncates to the dimension of the eigen-basis. While the convexity property of (5.16) does guarantee global optimality, the rank$-1$ relaxation, in this case, gives severely misleading results and suggests that certain CM levels are not possible and confounds the relationship between SINR and CM.

### 5.4.3 Simulation of Model vs. Leading Technique

In [63], several techniques are discussed for designing waveforms that maximize SINR while applying PAPR and finite energy constraints for known and unknown normalized Doppler cases. Here, we intend to compare our performance prediction model in (5.22) to a similar problem for the known Doppler case in [63]. We begin to formulate our similar problem by first stating:

$$\min_{\underline{\mathrm{S}}} \ \underline{\mathrm{s}}^H \mathbf{K}_{\mathrm{MP}} \underline{\mathrm{S}}, \text{ s. t. PAPR} \leq \epsilon, \|\underline{\mathrm{s}}\|_2^2 = 1, \tag{5.23}$$

where $\epsilon$ is the highest acceptable PAPR. We understand that minimizing PAPR is analogous to minimizing the wasted energy in a fixed voltage environment and, thus, a comparable problem employing the CM constraint can be stated in the following manner,

$$\min_{\underline{\mathrm{S}}} \underline{\mathrm{s}}^H \mathbf{K}_{\mathrm{MP}} \underline{\mathrm{S}}, \text{ s. t. CM} \leq \epsilon_{\mathrm{cm}}, \|\underline{\mathrm{s}}\|_2^2 = 1, \tag{5.24}$$

where $\epsilon_{\mathrm{cm}}$ is allowed to vary from $\frac{2}{M}$ (unconstrained CM) to $\frac{1}{M}$ (constant modulus or fully constrained CM).

We numerically perform Monte Carlo analysis to solve (5.24) for multiple instantiations of the interference and noise covariance matrix $\mathbf{K}_{\mathrm{MP}}$. Although, here, we place no imposition that the waveform be comprised of a subset of the eigen-basis thus allowing to search over the entire vector space. In Figure 5.5, we compare the results of the analysis of (5.24) and compare against the model in (5.22). The strong relationship between trends in Figure (7) validates the approach to use and eigen-decomposition technique to formulate the SINR/CM relationship model. The model provides estimation of the degradation to SINR, to within a few dB, when the modulus is constrained.

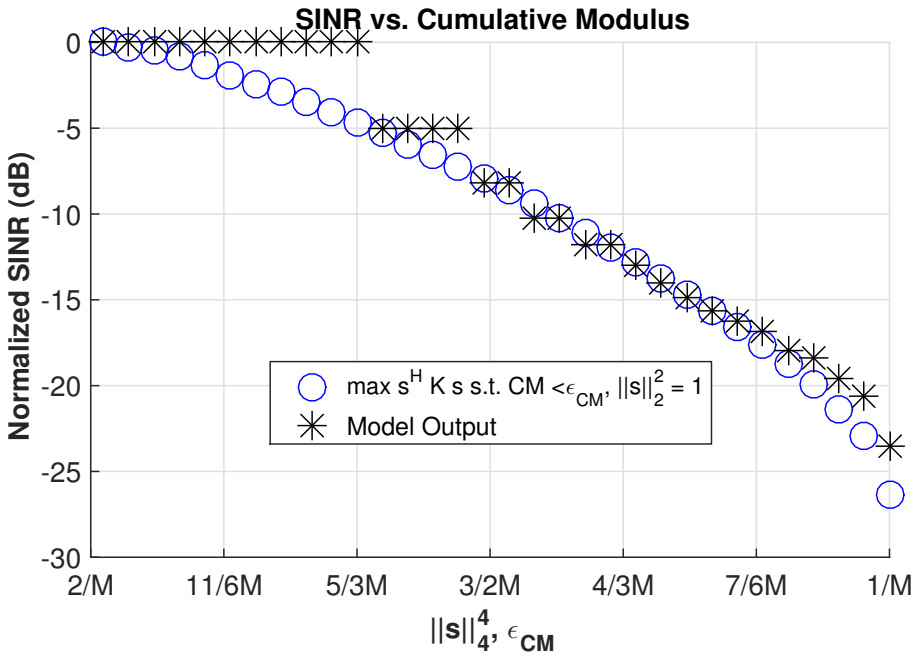


Figure 5.5: Simulation results for the cumulative and SINR models with MP interference model. Simulation parameters include $M = 64$ and 100 Monte Carlo trials. Model CM vs SINR and the Output of optimization.

## 5.5 Chapter Summary

As was the intent, we have devised a novel technique to develop performance models for constrained radar waveforms. Additionally, we have investigated, developed and analyzed empirical models for a balanced class of interference (MP). This had led to several new performance models that accurately approximate the outcome in (5.24) as seen in the literature.

As fully adaptive radar systems become more prevalent, the ability to estimate transmit performance and make decisions quickly and accurately increases in importance. This work showcases some of the challenges inherent with performance estimation (i.e. analytical intractability's, data model inaccuracies), but also shows straightforward equations can be used to represent high dimensional problems.

It is important to note that the waveform design can obtain a low cumulative modulus (near unity) with a very limited basis, on average, implying that use of the smaller

basis could limit the search space when performing the optimization, thus saving computation time. It is also important for the waveform designer to consider the nonlinearity of the SINR when selecting the constraint level. For example, relaxing the constant modulus requirement might enable additional degrees of freedom to minimize the waveform range side-lobes.

The models developed give a first-order approximation of the eigen-basis dimension (i.e. the approximate minimum number of eigenvectors) required to achieve a certain waveform cumulative modulus and the corollary SINR degradation, from optimal. Understanding these performance trades enables a more efficient decision making process for an adaptive system.

# Chapter 6

# Subspace Approach to Performance Analysis for Range-Sidelobe Suppressed Waveforms

Another important concern in constrained radar waveform design is understanding the consequence on SINR performance when sidelobe constraints are required[1]. In this Chapter, we derive new analytical models for the expected integrated sidelobe as a function of the dimension of the eigen-basis. We approach understanding the consequence of the ISL constraint from the perspective of the constraint rather than SINR to provide new insights into the behavior of the constraint on SINR. We then examine the performance for two unique interference and noise scenarios and connect the ISL to SINR forming simple performance models. Finally, we give Monte Carlo simulation analysis and compare our approach to a leading waveform design technique from the perspective of SINR maximization and conclude the proposed approach can provide comparable performance prediction with additional insights into the relationship between constraint and SINR[2].

[1]Portions of this work initially featured in; A.M.Jones, B.D.Rigling, and M.Rangaswamy,*Performance models for sidelobe constrained signal design with eigen-basis formulation*, in Proceedings of the 2015 IEEE Radar Conference, May 2015

[2]Portions of this work are under review with the IET Journal of Radar, Sonar and Navigation

As a signal design criteria, the integrated sidelobe has been studied in great depth [3, 30–34] and we note its important role in multiple radar functions, including reducing the number of false alarms, improving multiple target resolution and efficient spreading of the energy contained within the signal. The literature mentions many design methodologies for limiting sidelobe levels, including; periodic autocorrelation function technique possessing a zero sidelobes attribute [37], and similarly a cyclic technique, PeCAN [14, 34] or a competing technique Signal Waveform's Optimal Under Restriction Design for Active Sensing (SWORD) [15], among others. However, the progressive consequence to SINR as the design drives down the sidelobes has not been studied.

The motivation for this work is to gain a greater understanding of how constraints affect SINR performance in order to improve the decision making process of an adaptive system. For example, when the number of design degrees of freedom are finite, one might sacrifice peak-to-average-power for ISL performance in a high SINR environment to resolve near-in targets. Conversely, the most efficient use of power might be necessary, limiting the degrees of freedom for ISL performance.

This Chapter gives insight into the behavior of the trade-space between the competing signal traits of SINR and ISL levels for two subspace perspectives and develops performance models [131] to aid in the selection process of what to transmit. Others have investigated performance models for similar metrics, integrated sidelobe ratio (ISLR) and peak-sidelobe ratio but limited the data models of noise and interference modeled to Bernoulli distributions [35, 36].

The remained of the Chapter is organized as follows. We develop the signal model and define preliminaries in section 6.1. This includes formulation of new optimization problems that are ISL centric rather than the typical SINR centric formulations found in the literature. Also, we define an interference and noise covariance matrix model, validated with measured data, to evaluate performance in a manner that provides a convenient closed-form expression for the expected eigen-values. Next, in section 6.2, we derive an analytical

expression for the expected ISL as a function of the waveform parameters. Following in section 6.3, we develop the corresponding SINR model. We validate the theoretical models via simulation in section 6.4 and compare our novel approach to the leading SINR centric ISL optimization problem. The conclusions and additional insights are given in the chapter summary 6.5.

## 6.1 Preliminaries and Problem Formulation

As a quick review, to elucidate the difference between SINR centric and ISL centric optimization problems, and inspire our approach to developing performance models, we consider the signal model first outlined in Chapter 4.

Then, for the ISL centric optimization problem, we begin with the auto-correlation sequence $\underline{\mathrm{r}}_m = \sum_{q=1}^{M} \underline{\mathrm{s}}_m \underline{\mathrm{s}}^*_{m-q}$, where $m$ is the lag. We then define the integrated sidelobe as

$$\mathrm{J_{ISL}} = \sum_{m=1}^{M-1} \left| \sum_{q=1}^{M} \underline{\mathrm{s}}_m \underline{\mathrm{s}}^*_{m-q} \right|^2 \tag{6.1}$$

$\underline{\mathrm{s}} \in \mathbb{C}^{M\times 1}$ where we exploit symmetry and assume a main lobe width of $1$, a reasonable simplification in most cases. We compact this notation using $\mathbf{E}_m \in \mathbb{R}^{M\times M}$, a zero-matrix with $1$'s on the $m^{\text{th}}$ upper super-diagonal. For example, when $m = 1$, we have the following

$$\mathbf{E}_1 = \begin{bmatrix} 0 & 1 & 0 & \cdots & 0 \\ 0 & 0 & 1 & \cdots & 0 \\ \vdots & \vdots & \vdots & \ddots & \vdots \\ 0 & 0 & 0 & \cdots & 1 \\ 0 & 0 & 0 & \cdots & 0 \end{bmatrix} \tag{6.2}$$

giving $J_{ISL} = \sum_{m=1}^{M-1} |\underline{s}^H \mathbf{E_m} \underline{s}|^2$. Also, to provide an implicit maximization of SINR, we express the designed waveform as a linear combination of an ordered subset of the eigenvectors of the interference and noise covariance matrix (K). For an Eigenvector decomposition

$$\mathbf{K} = \mathbf{V}^H \mathbf{\Lambda} \mathbf{V} \tag{6.3}$$

where $\mathbf{V} = [\underline{v}_1 \cdots \underline{v}_M]$ and $\mathbf{\Lambda} = \text{diag}\{\lambda_1 \cdots \lambda_M\}$ such that $\lambda_1 \leq \lambda_2 \leq \cdots \leq \lambda_M$, maximizing SINR implies use of the smallest number of eigenvectors from the sub-dominant subspace to represent the signal. This approach is intended to provide an intuitive investigation of the SINR degradation, not to be an efficient waveform design technique. The waveform is thus represented as an eigenvector reconstruction of the form

$$\underline{s} = \sum_{n=1}^{N} \alpha_n \underline{v}_n \tag{6.4}$$

where $\alpha_n \in \mathbb{C}^{1\times 1}$ is the $n^{\text{th}}$ eigenvector weight, and $N \leq M$ eigenvectors comprise the support of $\underline{s}$. Formally, a discrete *Karhunen-Loève* expansion [28], we see this technique first employed for radar in [5,124] (described as the Generalized Matched Subspace Projection approach), where the invention allows gradual modification of the waveform between competing properties: maximizing SINR and the pulse compression characteristics of the waveform. SINR is then defined as:

$$\begin{aligned} \text{SINR} &= \frac{1}{\underline{s}^H \mathbf{K} \underline{s}} && (6.5)\\ &= \frac{1}{(\mathbf{V}\underline{\alpha})^H \mathbf{V} \mathbf{\Lambda} \mathbf{V}^H (\mathbf{V}\underline{\alpha})} && (6.6)\\ &= \frac{1}{\underline{\alpha}^H \mathbf{\Lambda} \underline{\alpha}} && (6.7)\\ &= \frac{1}{\sum_{n=1}^{N\leq M} |\underline{\alpha}_n|^2 \lambda_n}. && (6.8) \end{aligned}$$

Using (6.2) and (6.4) allows us to succinctly form an optimization problem to mini-

mize sidelobes subject to a finite energy constraint and eigen-basis dimension restriction as

$$\min_{\underline{\alpha}} \sum_{m=1}^{M-1} |\underline{\mathrm{s}}^H \mathbf{E_m} \underline{\mathrm{s}}|^2, \text{ s. t. } \|\underline{\mathrm{s}}\|_2^2 = 1 \tag{6.9}$$

$$\underline{\mathrm{s}} = \sum_{n=1}^{N} \underline{\alpha}_n \underline{\mathbf{v}}_n \tag{6.10}$$

which we define as the ISL centric approach. We note, (6.9) does not explicitly maximize for SINR, which can instead be maximized by choosing a minimal $N$. As shown in the Appendix, the objective function is non-convex (hence, no guarantee of optimality). Also, in the Appendix is a convex relation formulation (with analysis) which provides motivation for use of the non-convex optimization problem.

For the SINR centric approach, where the objective function is seen in the denominator of (6.5), we maximize the SINR while applying the additional ISL constraint, denoted $\epsilon_{\text{ISL}}$. The SINR centric design approach is defined as

$$\min_{\underline{\mathrm{s}}} \underline{\mathrm{s}}^H \mathbf{K} \underline{\mathrm{s}}, \text{ s. t. } \|\underline{\mathrm{s}}\|_2^2 = 1 \tag{6.11}$$

$$\mathrm{J_{ISL}} \leq \epsilon_{\text{ISL}} \tag{6.12}$$

without the restriction on the waveform that it be composed of an ordered subset of the eigenvectors of the interference and noise covariance matrix. It is well known that the unconstrained objective function in (6.11) is easily solved (for arbitrary $\underline{\mathrm{s}}$) using the Lagrange method [121] where the optimum is the minimum eigenvector solution waveform seen also in [122, 123]. A major focus of this Chapter is to develop performance models and understand the outcome of (6.11), (considered the leading SINR centric approach) as the ISL constraint is tightened. We will compare the results from each approach in (6.9) and (6.11), respectively in section 6.4.

Finally, to model the impact of ISL on SINR performance, we discuss a random inter-

ference environment having general utility that is useful in the situation where no a priori information about the interference and noise is available. We compare the eigen-spectrum of the model to measured data and show the model is appropriate for this type of analysis.

The covariance data representation is an asymptotic result reported in random matrix theory literature [104] denoted as Marčenko-Pastur (MP), and defined

$$\mathbf{K}_{\text{MP}} = \frac{1}{M}\mathbf{Z}\mathbf{Z}^H \tag{6.13}$$

where elements $\mathbf{Z}_{ij}$ are $\mathbb{CN}(0, \sigma\mathbf{I})$ [132]. Please refer to Chapter 3 for in-depth discussions on data models.

## 6.2 Expected Integrated Sidelobe Performance Model for Gaussian Eigen-vector Model

In this section, we derive an expectation model for ISL as a function of the basis dimension ($N$) of the waveform design, detailed in (6.4). It is our goal to develop and analyze the SINR performance as the waveform ISL is suppressed. However, since no claims on the distribution of the elements in eigenvectors for either covariance matrix model can be made, that we are aware of, we will assume a Gaussian model (i.e. the waveform itself can be represented as a random variable) and derive an expected value of ISL, defined in (6.1), under these pretenses. We do so as a function of the signal length (M), eigen-basis dimension (N), and the weights vector ($\underline{\alpha}$). This gives us a model for the output of the optimization in (6.9) and helps in obtaining a model for SINR as a function of the ISL constraint in the sections to follow.

Starting with the definition of ISL in (6.9), the expected ISL can be derived as

$$\mathrm{E}\{\mathrm{ISL}\}(M,N,\mathrm{V},\underline{\alpha}) = \mathrm{E}\Big\{\sum_{m=1}^{M-1}|\underline{\mathrm{s}}^H\mathbf{E}_m\underline{\mathrm{s}}|^2\Big\} \tag{6.14}$$

$$= \mathrm{E}\Big\{\sum_{m=1}^{M-1}(\underline{\mathrm{s}}^H\mathbf{E}_m\underline{\mathrm{s}})(\underline{\mathrm{s}}^H\mathbf{E}_m^t\underline{\mathrm{s}})\Big\} \tag{6.15}$$

$$= \mathrm{E}\Bigg\{\sum_{m=1}^{M-1}\Big(\sum_{i=1}^{N}\underline{\alpha}_i^H\underline{\mathrm{v}}_i^H\mathbf{E}_m\sum_{j=1}^{N}\underline{\alpha}_j\underline{\mathrm{v}}_j\Big)\Big(\sum_{k=1}^{N}\underline{\alpha}_k^H\underline{\mathrm{v}}_k^H\mathbf{E}_m^t\sum_{l=1}^{N}\underline{\alpha}_l\underline{\mathrm{v}}_l\Big)\Bigg\} \tag{6.16}$$

$$= \sum_{i=1}^{N}\sum_{j=1}^{N}\sum_{k=1}^{N}\sum_{l=1}^{N}\underline{\alpha}_i^H\underline{\alpha}_j\underline{\alpha}_k^H\underline{\alpha}_l\sum_{m=1}^{M-1}\mathrm{E}\Big\{\underline{\mathrm{v}}_i^H\mathbf{E}_m\underline{\mathrm{v}}_j\underline{\mathrm{v}}_k^H\mathbf{E}_m^t\underline{\mathrm{v}}_l\Big\} \tag{6.17}$$

where, to evaluate the expectation, we describe the elements ($p$) of each eigen-vector ($\underline{\mathrm{v}}$) as a random variable $v_{p,i} \sim \mathbb{CN}(0, \frac{1}{M})\forall\ p,(i,j,k,l)$ whose entries are independent and identically distributed. We note $\mathrm{E}\big\{\underline{\mathrm{v}}_i^H\mathbf{E}_m\underline{\mathrm{v}}_j\underline{\mathrm{v}}_k^H\mathbf{E}_m^t\underline{\mathrm{v}}_l\big\}$ is the partial ACS of a complex Gaussian sequence. Using dummy variables, $a$, $b$, $c$, $d \sim \mathbb{CN}(0, \frac{1}{M})$, we see three unique terms develop from the evaluation of $\mathrm{E}\big\{\underline{\mathrm{v}}_i^H\mathbf{E}_m\underline{\mathrm{v}}_j\underline{\mathrm{v}}_k^H\mathbf{E}_m^t\underline{\mathrm{v}}_l\big\}$, pairs of squares (eg. $\mathrm{E}\{a^2\}\mathrm{E}\{b^2\}$), single square (eg. $\mathrm{E}\{a\}\mathrm{E}\{b^2\}\mathrm{E}\{c\}$) or quartic (e.g. $\mathrm{E}\{a\}\mathrm{E}\{b\}\mathrm{E}\{c\}\mathrm{E}\{d\}$). The single square and quartic terms evaluate to zero leaving only the pairs of squares terms. It is straightforward, but tedious and thus not shown, to show that $(M-m)$ number of pairs of squared terms exists and only when $i=j=k=l$, otherwise all other terms average to zero. Thus, $\mathrm{E}\{a^2\}\mathrm{E}\{b^2\} = \sigma^4$ giving

$$\mathrm{E}\big\{\underline{\mathrm{v}}_i^H\mathbf{E}_m\underline{\mathrm{v}}_j\underline{\mathrm{v}}_k^H\mathbf{E}_m^t\underline{\mathrm{v}}_l\big\} = \sigma^4(M-m). \tag{6.18}$$

Then, $\sum_{m=1}^{M-1} \mathrm{E}\Big\{\underline{\mathrm{v}}_i^H \mathbf{E}_m \underline{\mathrm{v}}_j \underline{\mathrm{v}}_k^H \mathbf{E}_m^t \underline{\mathrm{v}}_l\Big\} = \sigma^4 \sum_{m=1}^{M-1}(M-m)$, where $\sum_{m=1}^{M-1}(M-m) = \frac{M^2}{2} - \frac{M}{2}$. This implies

$$\sigma^4 \sum_{m=1}^{M-1}(M-m) = \frac{1}{M^2}\big(\frac{M^2}{2} - \frac{M}{2}\big) \tag{6.19}$$

$$= \frac{1}{2} - \frac{1}{2M}, \tag{6.20}$$

which approaches $\frac{1}{2}$ for large $M$ (reasonably defined as $M \geq 32$) and $\sigma = \frac{1}{\sqrt{M}}$. Thus, we conveniently write,

$$\mathrm{E}\{\mathrm{ISL}\}(M, N, \underline{\alpha}) = \frac{1}{2}\sum_{i=1}^{N} |\underline{\alpha}_i|^4 - \frac{|\underline{\alpha}_i|}{M}. \tag{6.21}$$

where $\|\underline{\alpha}\|_2^2 = 1$. It becomes, then, a matter of the weight selection to predict ISL performance as a function of the eigen-basis dimension. We approach the modeling of the weights from an intuitive perspective, which is by designing the PSD to be as flat as possible for a given Eigen-basis dimension. The eigenvalues are an approximation of the PSD [114], thus to flatten the PSD, the reciprocal of the Marcenko-Pastur distributed eigen-values is appropriate for the weighting.

Shown in Figure 6.1 is the MP eigen-spectrum as well as sample eigen-spectrum from $25$ random instantiations for $M = 256$. Additionally, we compare the eigen-spectrum of the MP model against measured data of the same size covariance. The measured data is interference and noise data collected with system parameters listed in Table 6.1 for an air-to-ground radar operating at X-band. The standardized eigen-values on a log scale are shown against the theoretical model. We will use the eigen-value models to develop the performance models and validate against the measured data set.

The inverse weights model is then

$$\underline{\alpha}_{inverse} = \frac{1}{\hat{\underline{\lambda}}}. \tag{6.22}$$

Table 6.1: Interference and Noise Measurement Specifications

| Parameter | Value |
|---|---|
| Bandwidth | 1 GHz |
| Minimum Frequency | 9.2 GHz |
| Maximum Frequency | 10.2 MHz |
| Pulses | 256 |
| Fast-time Samples | 256 |
| Sample Rate | 3 GHz |
| Number Channels | 1 |

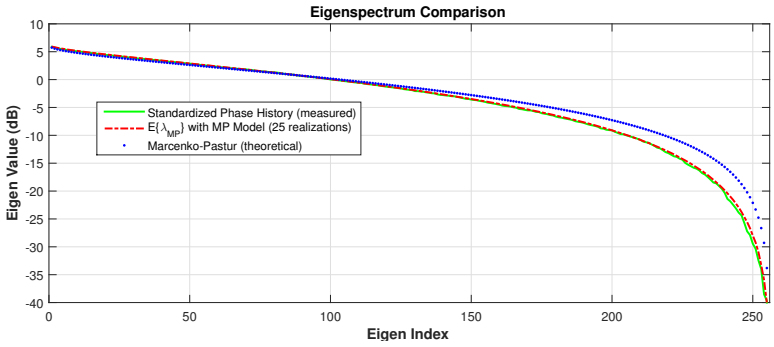


Figure 6.1: Eigen-spectrum comparison of theoretical Marčenko-Pastur (3.2), sample covariance eigen-spectrums generated from 25 random instantiations of (6.13), and eigen-spectrum of measured data with collection specifics in Table 6.1 for $M = 256$, for comparison.

where $\hat{\underline{\lambda}}$ are the $N$ sorted eigen-values of the interference and noise covariance matrix. The expected ISL becomes

$$\mathrm{E}\{\mathrm{ISL}\}(M, N, \hat{\underline{\lambda}}) = \frac{1}{2}\sum_{i=1}^{N} \frac{1}{|\hat{\underline{\lambda}}_i|^4} - \frac{1}{M|\hat{\underline{\lambda}}_i|}. \tag{6.23}$$

where $\|\hat{\underline{\lambda}}\|_2^2 = 1$. For $M = 64$ we have simulated the $\mathrm{E}\{\mathrm{ISL}\}$ and is shown in Figure 6.2.

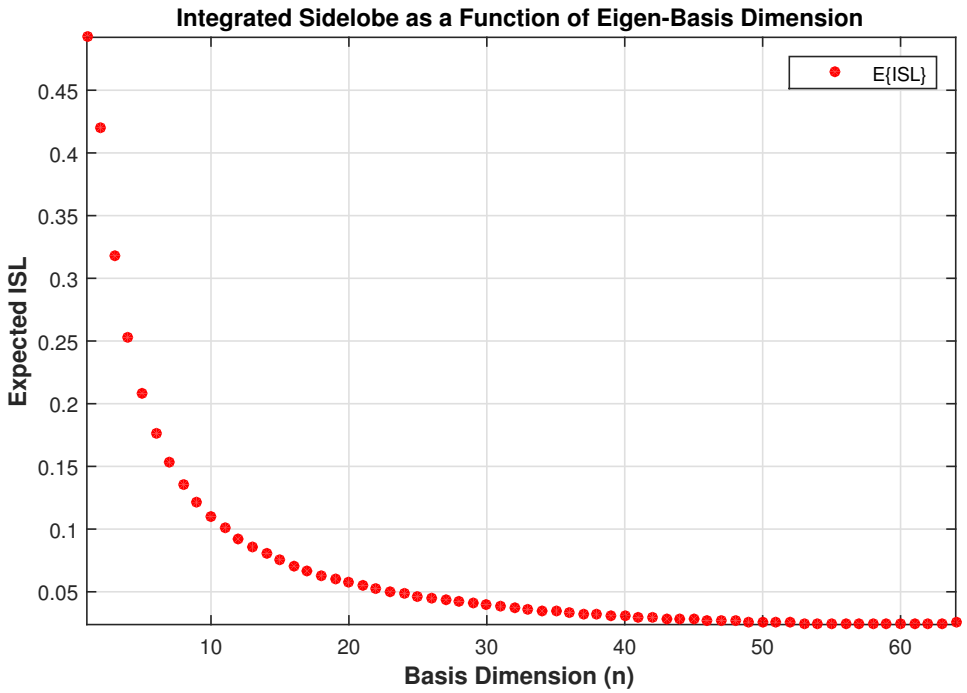


Figure 6.2: Performance model of the expected integrated sidelobe as a function of the basis dimension of the waveform as described in (6.23) when the MP distributed eigenvalues are employed.

## 6.3 Expected SINR Performance Model

The SINR model as a function of the eigen-basis dimension used to comprise the support of the waveform follows in a straightforward manner. For deterministic eigen-values, it becomes, then, a matter of the weights to compute SINR, where for example, the "best" SINR corresponds to $\underline{\alpha}_1 = 1$ and all others as zero (i.e., the Rayleigh solution). The "worst" performance would be inclusion of only the $N^{\text{th}}$ eigenvalue while an "average" would put an equal weight on each of the $N$ values. Thus, using (6.5), we know SINR $= \frac{1}{\sum_{n=1}^{N\leq M} |\underline{\alpha}_n|^2 \lambda_n}$ and for our interference and noise covariance model in (6.13), whose eigen-values are MP

distributed, we let $\underline{\alpha} = \underline{\alpha}_{inverse}$ and are able to write the SINR model as

$$\mathrm{E}\{\mathrm{SINR}\}(N, \hat{\underline{\lambda}}, \underline{\alpha}_{inverse}) = \frac{1}{\sum_{n=1}^{N} |\underline{\alpha}_{inverse,n}|^2 \hat{\underline{\lambda}}_n} \tag{6.24}$$

$$= \frac{1}{\sum_{n=1}^{N} \frac{1}{\hat{\underline{\lambda}}_n}} \tag{6.25}$$

where for $M = 64$ we have plotted the curve defined in (6.24) in figure 6.3. This intuitive representation suggests, that for the ISL constraint and the inverse weights vector ($\underline{\alpha}_{inverse}$), that SINR is linearly dependent on the number of basis-vectors (for large $M$ this is analogous to the bandwidth or number of frequencies used in the waveform design).

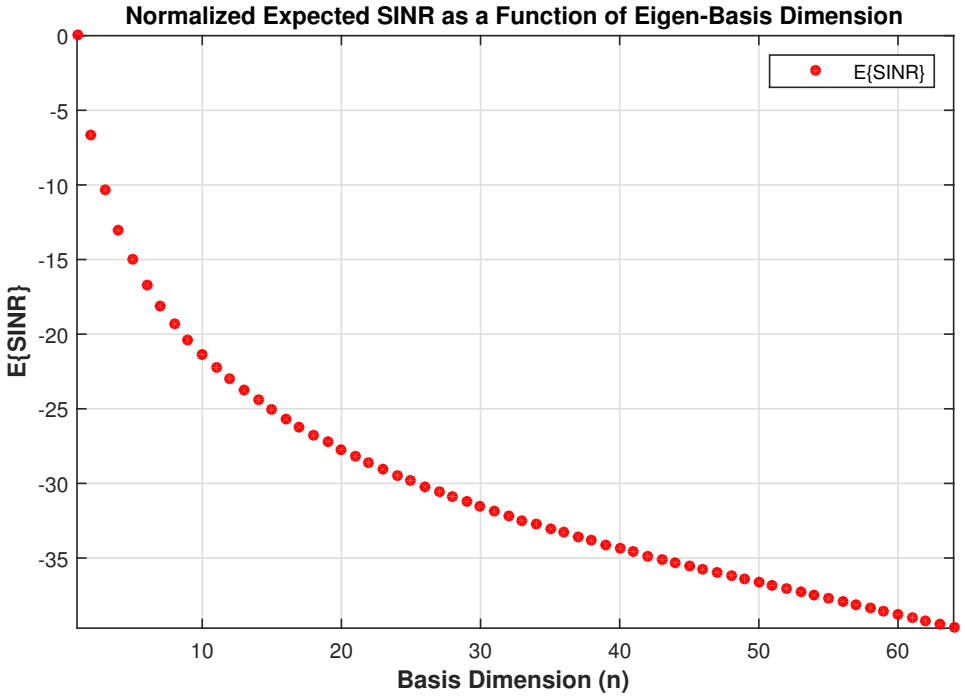


Figure 6.3: Performance model of the expected SINR as a function of the basis dimension of the waveform as described in (6.24) when the MP distributed eigenvalues are employed.

## 6.4 Simulation Results and Comparison to Measured Data

In this section, we use Monte Carlo simulation analysis and measured data to validate the performance models developed in sections 6.2 and 6.3. For $M = 64$ length waveform and the interference and noise covariance matrix model defined in (6.13), we perform 25 Monte Carlo simulations using different realizations of $\mathbf{K}_{\text{MP}}$ and solve the optimization in (6.9) incrementing through the entire eigen-basis dimension. We also use the covariance matrix estimated from measured data (described in section 6.1 and table 6.1) also for $M = 64$ length signal and incremented through the entire eigen-basis dimension. The results are compared to the models in (6.23) and (6.25) for the computed ISL and SINR as a function of the eigen-basis dimension for both the Monte Carlo analysis and measured data. The results are shown, in Figures 6.4 and 6.5, respectively. The simulation algorithm is shown in Algorithm 1.

In Figure 6.4, we show the performance model as a function of the eigen-basis to be a good representation for both the Monte Carlo simulation trials and the measured data set, suggesting the Gaussian model for the eigen-vectors to be reasonable. Additionally, we observe the limitation in the model for large basis dimension when the signal length is finite, that is, we see the model diverge from the solution to (6.9). However, as the signal length increases, the model will drive the expected ISL closer to zero sidelobe level, reducing this error.

We compare the SINR model to the Monte Carlo trials and measured data set in Figure 6.5. We observe remarkable accuracy in our ability to predict SINR degradation as a function of the eigen-basis used in the support of $\underline{s}$. This confirms the expectation that, for the ISL constraint, the primary driver to reduce sidelobe levels is simply the inclusion of additional frequencies (or in this case, a larger basis dimension).

Lastly, we complete the performance model analysis by connecting the ISL model in (6.23) to the SINR model in (6.24). We also compare the outcome of the optimization in (6.11) and for the SINR centric approach when the measured data is used to estimate the

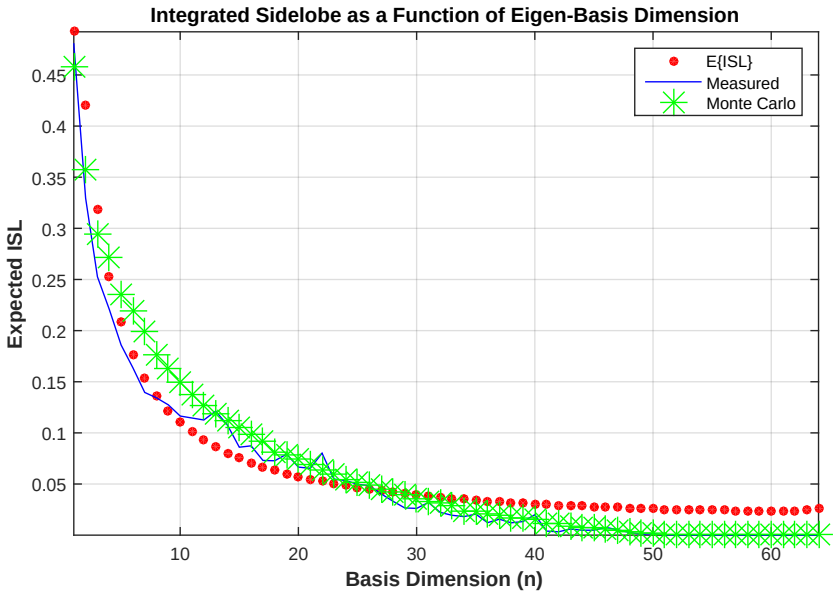


Figure 6.4: Comparison of ISL model in (6.23) as a function of the eigen-basis dimension to the outcome of (6.9) when Monte Carlo simulation trials (with covariance $\mathbf{K}_{\text{MP}}$) and the covariance from measured data set are used.

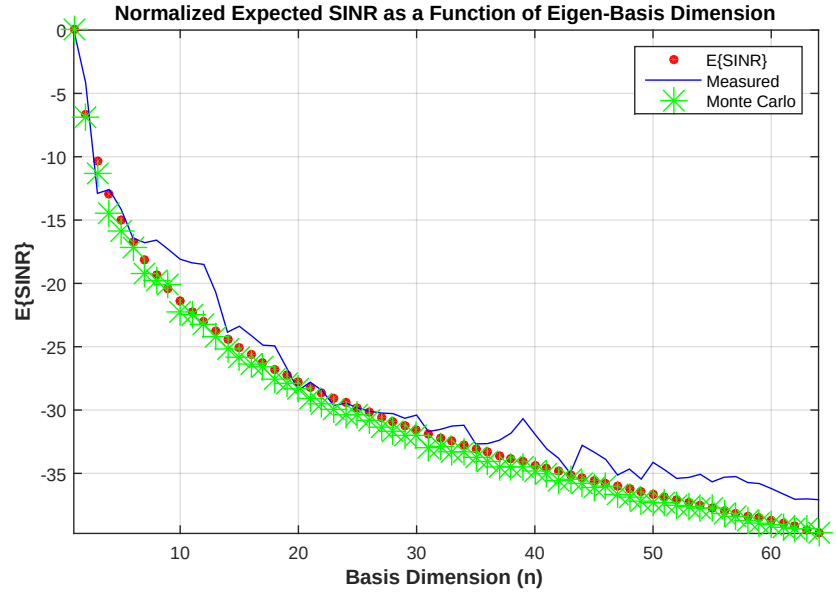


Figure 6.5: Comparison of SINR model in (6.24) as a function of the eigen-basis dimension to the outcome of (6.9) when Monte Carlo simulation trials (with covariance $\mathbf{K}_{\text{MP}}$) and the covariance from measured data set are used.

**Algorithm 2** ISL and SINR Performance Simulation Pseudo-Code

**for all** $k = 1$:MC (Monte Carlo trials) **do**
  **procedure** GENERATE SAMPLE COVARIANCE($M$)
    RawData = Cov{randn($M$) + $i$randn($M$)}
    $\mathbf{K}_{\text{MP}}$ = Normalise{RawData}
  **end procedure**
  **procedure** EIGENDECOMPOSITION(Data)
    $[\mathbf{V}, \mathbf{\Lambda}]$ = eig{Data$_{MP}$} ($\mathbf{K}_{\text{MP}} = \mathbf{V}^H \mathbf{\Lambda} \mathbf{V}$)
  **end procedure**
  **for all** $k = 1 : M$ (all basis vectors) **do**
    Initialise: $\underline{\alpha}$
    Perform Optimisation in (6.9)
    Compute waveform: $\underline{\mathrm{s}} = \mathbf{V}\underline{\alpha}^*$
    Compute ISL: $\mathrm{J}_{\text{ISL}} = \sum_{m=1}^{M-1} |\underline{\mathrm{s}}^H \mathbf{E}_{\mathbf{m}} \underline{\mathrm{s}}|^2$
    Compute SINR: $\frac{1}{\underline{\mathrm{S}}^H \mathbf{K} \underline{\mathrm{S}}}$
    Data Log
  **end for**
**end for**

covariance. In Figure 6.7, we show the model is able to predict, within a reasonable error, the SINR degradation as a function of the ISL.

Lastly, we complete the performance model analysis by connecting the ISL model in (6.23) to the SINR model in (6.24). We also compare the outcome of the optimization in (6.11) and for the SINR centric approach when the measured data is used to estimate the covariance. In figure 6.7 we show the model is able to predict, within a reasonable number of db, the SINR degradation as a function of the ISL.

## 6.5 Chapter Summary

The transmit signal ISL level affects many of a radar systems core functions and the ability to understand how it affects the SINR will drive an adaptive system to place the DOF where they are most valuable. For example, in resolving targets vs. improving signal strength. In this Chapter, we have developed two novel performance models, expected ISL and expected SINR, both as a function of the eigen-basis dimension used to comprise the support

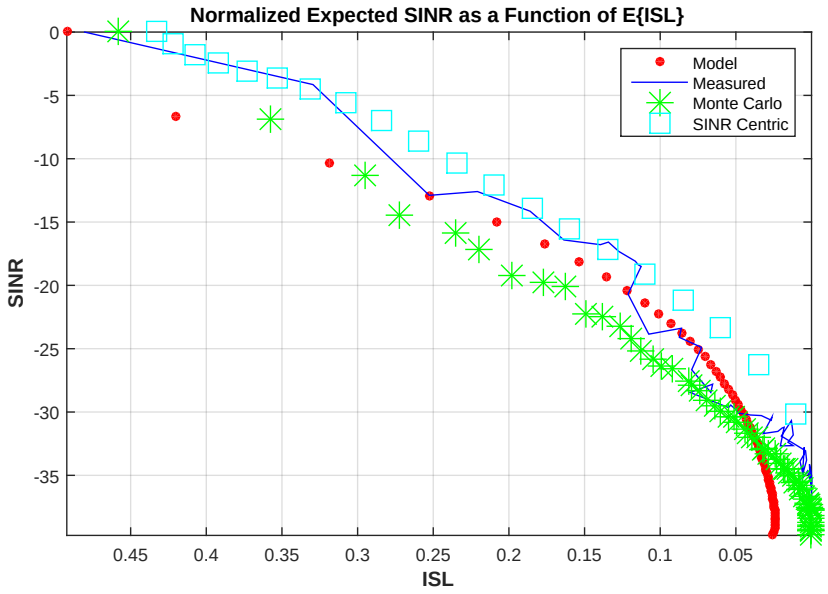


Figure 6.6: Normalized SINR degradation, relative to optimal, as a function of the ISL constraint on the waveform design.

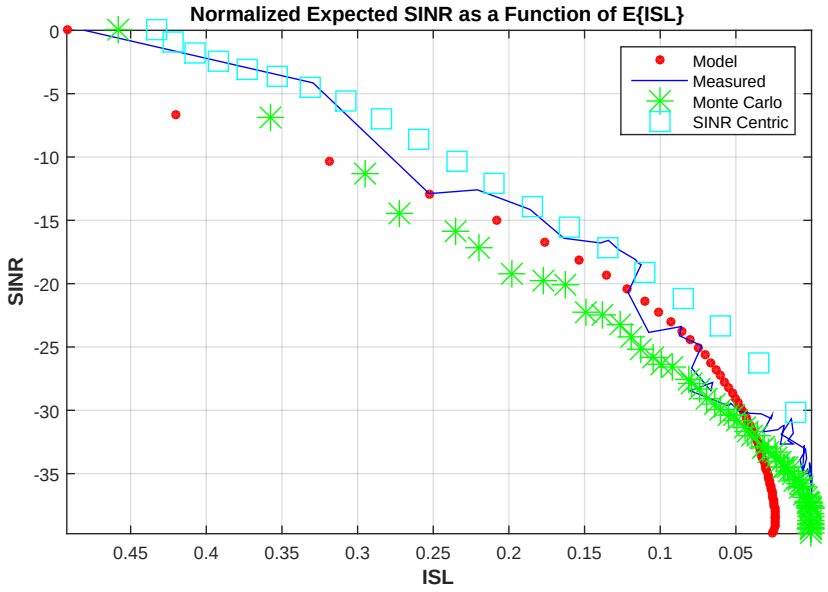


Figure 6.7: Normalised SINR degradation, relative to optimal, as a function of the ISL constraint on the waveform design.

of $\underline{s}$. The models perform well and allow a rough expectation to the SINR degradation as a function of the ISL constraint in radar waveform design.

Performance prediction models could potentially become a surrogate for computational expensive waveform design algorithms in an adaptive radar scenario. Future work calls for higher-order development of performance models for waveform design.

# Chapter 7

# Future Work

We briefly discuss four possible directions for future work. In section 7.1, we encourage additional data models be developed. Section 7.2 briefly mentions how one could incorporate additional constraints on the waveform. In this dissertation, we deliberately observed the response from the transmit waveform only; however, in a truly adaptive system one must consider the receiver design as well. This is motivated in section 7.3. Lastly, we prompt additional practicality by incorporating measured data in section 7.4.

## 7.1 Data Model Development

In this dissertation, we developed a new approach to generate synthetic data that has been analyzed and validated against measured data. Future work will necessarily involve the development of additional synthetic data models that accurately portray the signal types and phenomenology for all RF bands of interest and locations. It is conceivable to take a similar approach but also incorporate additional features. This may complicate the modeling but give further improved realism.

In figure 7.1, we suggest a possible beginning to the next version of synthetic data generation at the UHF band. This is the constructive approach to forming realistic interference and noise covariance matrices to then analyze the impact to SINR performance in

adaptive radar waveform design.

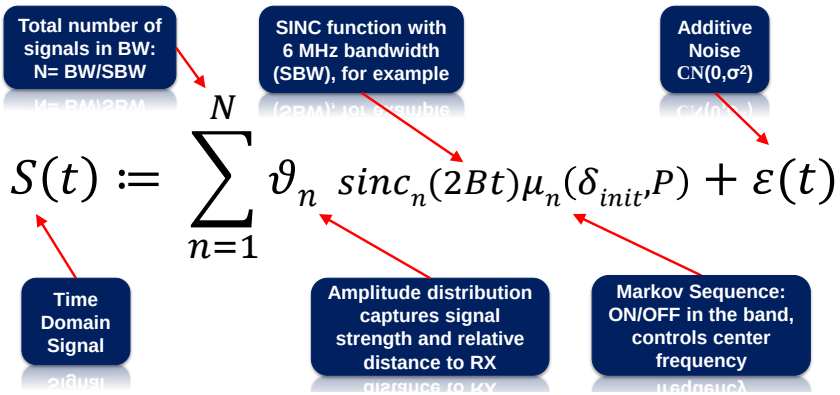


Figure 7.1: Potential constructive approach to generation of synthetic PSD realizations

## 7.2 SINR Analysis for Additional Constraints

One might also study the consequence to SINR, as we have, for additional practical constraints or concerns. For example, a similarity constraint against a waveform with desirable properties. In this case SINR generally improves as the similarity is relaxed (instead of degrades as investigated in this dissertation). The question then becomes, how much SINR retrieval ifs possible while achieving a suitable similarity. Second, some have mentioned Doppler tolerant waveforms as a possible design metric to overcome DSP complications in simple system architectures. Here, requiring waveform to possess these characteristics with, invariable degrade SINR. It is possible then, to answer, what is the cost of the Doppler tolerance characteristic.

## 7.3 SINR Analysis for Joint Transmit / Receive Filter Design

Adaptive radar implies closing the loop on the radar cycle via joint TX/RX adaptation. While this dissertation intentionally focused on the transmit aspect to better understand the role the constraints play in the SINR degradation. It is an obvious next step to fold in the receive filter with constraints such as the Capon constraint. The logical questions is, what is the SINR cost of additional constraints on the receive filter? And, can they be modeled or prediction to aid in the decision making process of an adaptive radar?

## 7.4 Validation Through Experimentation

While the synthetic model developed in this dissertation was derived from measured data, one should undertake additional experimentation to validate the performance model algorithms. This might include set-up of laboratory experiments with arbitrary waveform design control with matched filter receiver and known colored interference environment where the SINR can be captured as the constraint is varied.

## 7.5 Metric Definition

As mentioned previously, comparison of the synthetic PSD models was a challenge. We showed a strong statistical similarity for **Model 1.** to the measured data, but clearly observed that is was a poor physical representation. However, **Model 2.** was clearly similar in its physical attributes, but the measures used, (Kullback-Leibler, Chi-Square Test and the trace of the covariance) showed worse performance, statistically speaking, than Model 1. One could an envision development of a metric (or process) that can capture the salient features of the desirable PSD and thus a mechanism to compare one synthetic PSD generation technique to another as compared to measured data.

# Chapter 8

# Closing Remarks

In this chapter, we provide a summary of the unique contributions and our final thoughts on research in this area.

First, we defined and developed new interference and noise data models. We use the low model AR data model to give a comparison to what is currently in the literature. We then extended to radar a familiar result in the RMT literature on the asymptotic CDF of the eigenvalues for a certain type of covariance matrix. Finally, we developed an easy-to-compute practical model for the interference and noise PSD for the UHF band in North America. This allows generation of realistic covariance matrices and thus once can make insightful decision on the impact constraints have on SINR.

Next, we developed the role of the eigen-basis dimension required to achieve practical constraint thresholds for radar waveforms. We defined new, simplified expressions for the waveform cumulative modulus and range sidelobes. Next, we developed an original initialization scheme to select the approximate minimum basis dimension required to achieve practical constraint thresholds. This initial design was then employed in a constrained maximization of the SINR. This work illustrated the nonlinearity of the SINR performance to the constraint thresholds and gave a new algorithm for others to investigate the performance for different interference classes.

We then focused our attention on development of innovative performance models for the CM as a function of the eigen-basis. We defined and motivated a novel, straight forward model via a Lamẽ curve and used a least-squares regression technique to compute the curve parameters for a given length and interference class. Following, we developed a innovative performance prediction model for the SINR as a function of the CM constraint. We formulated the model using approximate eigen-values and a power law model on the weights of the eigen-values and compared the results for three unique interference classes.

Lastly, we used a subspace approach to develop performance prediction models for range-sidelobe suppressed waveforms. In this work, we developed two novel models. One for each, the ISL as a function of the basis-dimension of the waveform and SINR as a function of the basis-dimension of the waveform. We showed, for a particular covariance model the non-linear degradation and develop accurate performance prediction models to use as surrogates for waveform design. We validated the models with Monte Carlo computer simulations and through measured data.

Of the many important observations, the most significant would have to be the non-linear relationship to SINR as we apply the constraints. We observed for both the cumulative modulus and the ISL that achieving a high degree of either constraint, came at significant cost to the SINR performance. This suggests that perhaps waveform designers may be better suited to relax very stringent sidelobe or modulus requirements for the benefit of SINR.

Performance prediction for adaptive radar waveform design, using the subspace approach to investigate the impact to SINR as the constraints are tightened, has been shown to provide new insights to enable smarter decision making for an adaptive radar. It is clear that adaptation will become mandatory for future fielded radar systems and understanding these consequences, and predicting them in certain scenarios, will provide a tactical advantage over static, or non-knowledge aided processing schemes.

# Chapter 9

# Appendices

## 9.1 Appendices from Chapter 3

Synthetic RFI Generation Technique

```
function [PSD] = ...
    Synthetic_UHF_RFI(M,alpha_n,beta_n,gamma_n,P,S_init,a,b,min_mu,max_mu)
% [PSD] = ...
    Synthetic_UHF_RFI(M,alpha_n,beta_n,gamma_n,P,S_init,a,b,min_mu,max_mu)
% returns a vector of randomly distributed values using the gamma
% distribution and a Markov sequence of length M.
%
% ver 1.0, 5/01/2016
% Code POC: Aaron M Jones, AFRL / RYAP aaron.jones.41@us.af.mil
%
% Example using Model 2 from RadarCon 2016 Paper:
%
%   [PSD] = Synthetic_UHF_RFI(1266,3.1075,1.9617e-10,2.6278e-09, ...
%   [0.9944 0.0056; 0.0296 0.9704],[0.5 0.5], 1.5634 , 8.5887, ...
%   2.2151e-08, 3.5018e-07);
%   figure(1); plot(10*log10(PSD)); axis('tight');
```

```
15 %   title('\bfSynthetic RFI');xlabel('Frequency Bin');ylabel('PSD ...
       (dBm)');
16 %
17 % INPUT Definitions:
18 % M =       = length of sequence
19 % alpha_n   = noise distribution shape parameter
20 % beta_n    = noise distribution scale parameter
21 % gamma_n   = noise distribution shift parameter (dBm)
22 % P         = Markov sequence transition matrix (2 state only)
23 % S_init    = initial state vector
24 % a         = minimum signal distribution shape parameter
25 % b         = maximum signal distribtuion shape parameter
26 % min_mu    = minimum of signal amplitude range
27 % max_mu    = maximum of signal amplitude range
28 %
29 % OUTPUT Definitions:
30 % PSD       = output power spectral density (dBm/frequency bin)
31 %
32 % If you are you using this script in research work to be published,
33 % please include explicit mention of our work in your publication.
34 %
35 % We suggest language such as this:
36 %
37 % "To model the interference and noise in problem (12), we used the
38 % computationally efficient method described in [1]."
39 %
40 % with the following corresponding entry in your bibliography:
41 %
42 % [2] Aaron Jones and Brian Rigling and Muralidhar Rangaswamy. ...
       "Generation
43 %   of Synthetic UHF RFI in Urban North American Environments", ...
       IEEE Radar
44 %   Conference, Philadelphia, PA, May 2016.
```

```
45
46 % References:
47 % [1] H. Zhou, B. Wen, and W. S, Dense radio frequency interference
48 %   suppression in hf radars,  IEEE Signal Processing Letters, ...
     vol. 12,
49 %   pp. 361364, May 2005.
50 % [2] G. Scalzi, Afrl sensors directorate rf range measurement ...
     capabilities.
51 %   Presentation, October 2014.
52 % [3] S. Frost, Markov chain spectrum representations for ...
     sidelobe prediction.
53 %   Personal Correspondence, 2015.
54 % [4] L. Patton, S. Frost, and B. Rigling, Efficient design of ...
     radar waveforms
55 %   for optimised detection in coloured noise,  IET Radar, Sonar and
56 %   Navigation, vol. 6, no. 1, pp. 2229, 2012.
57 % [5] L. Patton and B. D. Rigling, Autocorrelation constraints ...
     in radar
58 %   waveform optimization for detection,  IEEE Trans. Aerospace and
59 %   Electronic Systems, vol. 48, pp. 951968, April 2012.
60 % [6] J. Li, J. Guerci, and L. Xu, Signal waveforms optimal ...
     under restriction
61 %   design for active sensing,  in Sensor Array and Multichannel ...
     Processing,
62 %   2006. Fourth IEEE Workshop on, pp. 382386, 2006.
63 % [7] J. Proakis, Digital Communications. McGraw-Hill, 3rd ed., ...
     March 1994.
64 % [8] M. Wax and Kailath, Detection of signals by information ...
     theoretic
65 %   criteria,  IEEE Transactions Acoust. Speech Signal ...
     Processing, vol. 33,
66 %   pp. 387392, April 1985.
67 % [9] T. K. Moon and W. C. Stirling, Mathematical methods and ...
```

```
      algorithms
68 %   for signal processing, vol. 1. New York: Prentice Hall, 2000.
69 % [10] D. Messerschmitt, Autocorrelation matrix eigenvalues and ...
      the power
70 %   spectrum,  Tech. Rep. UCB/EECS-2006-90, EECS Department, ...
      University
71 %   of California, Berkeley, June 2006.
72 % [11] K. Sunggon, J. Lee, and D. Sung,  A shifted gamma distribution
73 %   model for long-range dependent internet traffic,  IEEE ...
      Communications
74 %   Letters, vol. 7, pp. 124126, March 2003.
75 % [12] K. S. Shanmugan and A. M. Breipohl, Random Signals: Detection,
76 %   Estimation and Data Analysis. New York: John Wiley and Sons, ...
      1 ed.,
77 %   1988.
78 % [13] MATLAB, Version 7.14.0.739 (2013b). The MathWorks Inc., 2012.
79 % [14] T. Cover and J. Thomas, Elements of Information Theory. ...
      Wiley, 2nd ed.,
80 %   200.
81
82 %  Copyright 2016, Aaron M. Jones, Brian D. Rigling, Murali ...
      Rangaswamy
83
84 % test
85 if nargin < 1
86    disp('Running RadarCon 2016 Example');
87
88    M = 1266; alpha_n = 3.1075; beta_n = 1.9617e-10; gamma_n = ...
         2.6278e-09;
89    P = [0.9944 0.0056; 0.0296 0.9704]; S_init =- [0.5 0.5];  a = ...
         1.5634;
90    b = 8.5887; min_mu = 2.2151e-08;  max_mu =3.5018e-07;
91
```

```
92  end
93
94  %%  preallcoate
95  x                   = zeros(1,M);
96  xx                  = zeros(1,M);
97  PSD                 = 0.*ones(1,M);
98  signal_dist_total   = [];
99  length_band         = zeros(M,1);
100
101 %% initialize
102 x(1)                = rando(S_init); %  initial state of markov ...
        sequence
103 amp                 = 10.^(log10(min_mu) + ...
        (log10(max_mu)-log10(min_mu)) * rand(1,1)); % amplitude of ...
        first signal band
104 total_bands         = 0; % signal band counter (# of signal bands)
105 trigger             = 0; % flag
106 idx_xx              = 0; % index counter
107 signal_dist         = 0; % signal distribution
108
109 %% set output of initial state
110 if(x(1) == 1);  xx(1)           = 0;   end % noise state
111
112 if(x(1) == 2); % signal state
113     xx(1)           = amp;
114     total_bands     = 1;
115     length_band(1)  = 1;
116 end;
117
118 %% generate Markov sequence with different signal band amplitudes
119 for i=1:M-1
120
121     x(i+1)          = rando(P(x(i),:)); % equation
```

```
122
123     % set signal band amplitude
124     if(x(i) == 1 && x(i+1) == 2 && trigger == 0)
125         amp          = 10.^(log10(min_mu) + ...
                (log10(max_mu)-log10(min_mu)) * rand(1,1));
126         xx(i+1)      = amp;
127         trigger      = 1;
128         total_bands = total_bands + 1;
129         length_band(total_bands) = length_band(total_bands) + 1;
130     end
131
132     % if same band - keep amplitude same
133     if(x(i) == 2 && x(i+1) == 2);
134         xx(i+1) = amp;
135         length_band(total_bands) = length_band(total_bands) + 1;
136     end
137
138     % if noise
139     if(x(i+1) == 1), xx(i+ 1) = 0; end
140
141     % reset trigger
142     if(x(i) == 2 && x(i+1) == 1); trigger = 0; end
143 end
144
145 % find noise/signal values
146 noise_idx   = x == 1;
147 signal_idx  = find(x == 2);
148
149 % generate noise dist - gamma with shape, scale and shift ...
      (equation 3)
150 noise_dist = gamrnd(alpha_n,beta_n, [1,length(find(x ==1))]) + ...
      gamma_n;
151
```

```
% only use right number of bands
length_band = length_band(1:total_bands);

for k = 1:total_bands

    % take only the signal indexes
    xxx = xx(signal_idx);

    alpha1 = a + (b-a).*rand(1,1);

    mean = xxx(idx_xx+1);

    beta1 = mean/alpha1; % beta is depedent on the uniform alpha ...
        and uniform (in dB) mean

    signal_dist =   gamrnd(alpha1,beta1, [1,length_band(k)]) ;

    % set PSD of the signal index(s) for each band to the values ...
        of the rv
    PSD(signal_idx(idx_xx+1:idx_xx +length_band(k))) = ...
        xxx(idx_xx+1:idx_xx +length_band(k)) + signal_dist; % mean ...
        + distribution

    signal_dist_total = [signal_dist_total ...
        PSD(signal_idx(idx_xx+1:idx_xx +length_band(k)))];

    % increment to the next band
    idx_xx = sum(length_band(1:k));
end

% generate the synthetic PSD
PSD(noise_idx) = noise_dist;

```

```
%% markov random sequence
function [index] = rando(p)

u = rand; i = 1;
s = p(1);

while ((u > s) && (i < length(p)))
    i=i+1; s=s+p(i);
end

index=i;
```

## 9.2 Appendices from Chapter 4

**Proposition 1.** *The constraint function in (4.5) is non-convex with respect to* $\underline{s}$.

*Proof:* The definition of convexity cannot be applied directly to $\mathrm{J_{isl}}(\underline{\mathrm{s}})$ as $\underline{\mathrm{s}}$ is complex. We perform the transformation $\underline{\mathrm{s}} = \mathbf{V}\bar{\underline{\mathrm{s}}}$, where $\bar{\underline{\mathrm{s}}} \in \mathbb{R}^{2M\times 1} = [\mathrm{Re}\{\underline{\mathrm{s}}\}^T, \mathrm{Im}\{\underline{\mathrm{s}}\}^T]^T$ and $\mathbf{V} = [\mathbf{I}^{M\times M}, \jmath\mathbf{I}^{M\times M}] \in \mathbb{C}^{M\times 2M}$. With this transformation, we define an equivalent $\mathrm{J_{isl}}(\bar{\underline{\mathrm{s}}})$ : $\mathbb{R}^{2M} \rightarrow \mathbb{R}^M$ to apply the definition, in [121], of convexity. We must show:

$$f(\theta\bar{\underline{\mathrm{s}}}_1 + (1+\theta)\bar{\underline{\mathrm{s}}}_2) \leq \theta f(\bar{\underline{\mathrm{s}}}_1) + (1-\theta) f(\bar{\underline{\mathrm{s}}}_2), \tag{9.1}$$

where $0 \leq \theta < 1$, $f(\bar{\underline{\mathrm{s}}}) = (\bar{\underline{\mathrm{s}}}^T\mathbf{P}\bar{\underline{\mathrm{s}}})(\bar{\underline{\mathrm{s}}}^T\mathbf{Q}\bar{\underline{\mathrm{s}}})$, and $\bar{\underline{\mathrm{s}}}_1, \bar{\underline{\mathrm{s}}}_2$ are arbitrary signals. The matrices $\mathbf{P}$ and $\mathbf{Q}$ are used to simplify notation and are defined as: $\mathbf{P} = \mathbf{V}^H\mathbf{E}_k\mathbf{V}$ and $\mathbf{Q} = \mathbf{V}^H\mathbf{E}_k^T\mathbf{V}$ and $k$ designates a specific lag in the ACS.

We expand using basic algebra (these steps omitted) and again compress the notation by defining: $A = \bar{\underline{\mathrm{s}}}_1^T\mathbf{P}\bar{\underline{\mathrm{s}}}_1$, $B = \bar{\underline{\mathrm{s}}}_1^T\mathbf{Q}\bar{\underline{\mathrm{s}}}_1$, $C = \bar{\underline{\mathrm{s}}}_2^T\mathbf{P}\bar{\underline{\mathrm{s}}}_2$, $D = \bar{\underline{\mathrm{s}}}_2^T\mathbf{Q}\bar{\underline{\mathrm{s}}}_2$, $E = \bar{\underline{\mathrm{s}}}_2^T\mathbf{P}\bar{\underline{\mathrm{s}}}_2$, $F = \bar{\underline{\mathrm{s}}}_2^T\mathbf{P}\bar{\underline{\mathrm{s}}}_1$,

$G = \bar{\underline{s}}_1^T \mathbf{Q} \bar{\underline{s}}_2$, $H = \bar{\underline{s}}_2^T \mathbf{Q} \bar{\underline{s}}_1$. Combining like terms to the left-hand side we can write (9.1) as:

$$(\theta^2 + \theta + 1)AB+ \tag{9.2}$$

$$\theta^2(AG + AH + EB + FB)+ \tag{9.3}$$

$$\theta(1-\theta)(AD + EG + EH + FG + FH + CB)+ \tag{9.4}$$

$$(1-\theta)^2(ED + FD + CG + CH)+ \tag{9.5}$$

$$+ (-\theta^2 + 3\theta - 3)CD \leq 0. \tag{9.6}$$

By simple counter example we let $\bar{\underline{s}}_1 = [1,1]^T$, $\bar{\underline{s}}_2 = [1,1]^T$, $\theta = 0.5$, summing the contribution from lags $1, M-1$ gives the LHS $= 3.5 \not\leq 0$. ■

**Proposition 2** *The constraint function in (5.7) is non-convex with respect to* $\underline{s}$.

*Proof:* Proof by counter example. Expanding (5.7) we have

$$\mathrm{J}_{\mathrm{cm}}(\underline{\mathrm{s}}) = \sum_{l=1}^{M} \left[1 - \underline{\mathrm{s}}^H \mathbf{\Sigma}_l \underline{\mathrm{s}}\right]^2, \tag{9.7}$$

$$= M - 2\|\underline{\mathrm{s}}\|_2^2 + \sum_{l=1}^{M} (\underline{\mathrm{s}}^H \mathbf{\Sigma}_l \underline{\mathrm{s}})^2, \tag{9.8}$$

$$= M - 2 + \|\underline{\mathrm{s}}\|_4^4. \tag{9.9}$$

Where, for real $\underline{\mathrm{s}}$ and $M = 2$, (9.7) becomes

$$\mathrm{J}_{\mathrm{cm}}(\underline{\mathrm{s}}) = M - 2\big(\sqrt{s_1^2 + s_2^2}\big)^2 + \big((s_1^4 + s_2^4)^{1/4}\big)^4, \tag{9.10}$$

$$= 2 - 2\big(s_1^2 + s_2^2\big) + s_1^4 + s_2^4. \tag{9.11}$$

Where, W.L.O.G., the first and second derivatives:

$$\frac{\partial \mathrm{J_{cm}}}{\partial s_1} = -4s_1 + 4s_1^3, \tag{9.12}$$

$$\frac{\partial^2 \mathrm{J_{cm}}}{\partial s_1^2} = -4 + 12s_1^2. \tag{9.13}$$

Thus, for (9.13) to positive, a sufficient condition, $s_1 > \sqrt{\frac{4}{12}}$. Choose $s_1$ and $s_2 < \sqrt{\frac{4}{12}}$, as a counter example. Therefore, non-convex. ■

**Proposition 3.** *PAPR can serve as an upper bound for the constraint threshold $\epsilon_{cm}$.*

*Proof:* From the result in (9.7) is it evident that the dynamic range is $M-2 \rightarrow M-1$. Removing the constant, $M-2$, to normalize, gives the threshold $\epsilon_{\mathrm{cm}}$. Now, we are given $\mathrm{PAPR}(\underline{\mathrm{s}}) = \frac{|\underline{\mathrm{s}}|^2_{\mathrm{peak}}}{\underline{\mathrm{s}}^2_{\mathrm{rms}}}$ and $\epsilon_{\mathrm{cm}}(\underline{\mathrm{s}}) = \|\underline{\mathrm{s}}\|_4^4$ and need to show $\mathrm{PAPR}(\underline{\mathrm{s}}) \geq \epsilon_{\mathrm{cm}}(\underline{\mathrm{s}})\ \forall\ \underline{\mathrm{s}}$ subject to $\|\underline{\mathrm{s}}\|_2^2 = 1$. To begin, we write

$$\mathrm{PAPR}(\underline{\mathrm{s}}) = \frac{|\underline{\mathrm{s}}|^2_{\mathrm{peak}}}{\underline{\mathrm{s}}^2_{\mathrm{rms}}}, \tag{9.14}$$

$$= \frac{|\underline{\mathrm{s}}|^2_{\mathrm{peak}}}{\frac{1}{M}\|\underline{\mathrm{s}}\|_2^2}, \tag{9.15}$$

$$= M|\underline{\mathrm{s}}|^2_{\mathrm{peak}}. \tag{9.16}$$

$$\tag{9.17}$$

Thus, we must show

$$M|\underline{\mathrm{s}}|^2_{\mathrm{peak}} \geq \|\underline{\mathrm{s}}\|_4^4, \tag{9.18}$$

We know the lower-bound on $|\underline{\mathrm{s}}|^2_{\mathrm{peak}}$ is $\frac{1}{M}$, while the upper-bound on $\|\underline{\mathrm{s}}\|_4^4$ is 1. It is obvious, then, $1 \geq 1$. Therefore, we have shown, $\forall\ \underline{\mathrm{s}}$ subject to $\|\underline{\mathrm{s}}\|_2^2 = 1$, that $\mathrm{PAPR}(\underline{\mathrm{s}}) \geq \epsilon_{\mathrm{cm}}(\underline{\mathrm{s}})$. ■

## 9.3 Appendices from Chapter 5

We derive a convex relaxation for the optimization problem in (6.9) by a change of variables and removal of the implicit rank$-1$ constraint on the $\underline{\alpha}\underline{\alpha}^H$ matrix.

We consider first, the objective function:

$$\begin{aligned}\|\underline{\mathrm{s}}\|_4^4 &= \sum_{i=1}^{M} |\sum_{l=1}^{N} \alpha_l v_{i,l}|^4 \\ &= \sum_{i=1}^{M} \big(|\sum_{l=1}^{N} \alpha_l v_{i,l}|^2\big)^2 \\ &= \sum_{i=1}^{M} \big(|\underline{\alpha}^H \underline{v}_i^H|^2\big)^2 \\ &= \sum_{i=1}^{M} \big(\underline{\alpha}^H \underline{v}_i^H \underline{v}_i \underline{\alpha}\big)^2\end{aligned} \tag{9.19}$$

where $v_{i,l}$ is $i^{\text{th}}$ element of the $l^{\text{th}}$ eigenvector.

Letting $\mathbf{A} = \underline{\alpha}\underline{\alpha}^H$ and $\hat{\mathbf{V}}_i = \underline{v}_i^H \underline{v}_i$ then, we know

$$\begin{aligned}\text{tr}(\hat{\mathbf{V}}_i \mathbf{A}) &= \text{vec}^H(\hat{\mathbf{V}}_i)\text{vec}(\mathbf{A}) \\ &= \text{vec}^H(\mathbf{A})\text{vec}(\hat{\mathbf{V}}_i)\end{aligned} \tag{9.20}$$

for $\forall\ \hat{\mathbf{V}}_i, \mathbf{A} \in \mathcal{H}$. This gives

$$\begin{aligned}\|\underline{\mathrm{s}}\|_4^4 &= \sum_{i=1}^{M} \Big(\text{vec}^H(\hat{\mathbf{V}}_i)\text{vec}(\mathbf{A})\Big)^2 \\ &= \text{vec}^H(\mathbf{A})\Big[\sum_{i=1}^{M} \text{vec}(\hat{\mathbf{V}}_i)\text{vec}^H(\hat{\mathbf{V}}_i)\Big]\text{vec}(\mathbf{A}).\end{aligned} \tag{9.21}$$

A quadratic objective, known to be convex for positive semi-definite $\sum_{i=1}^{M} \text{vec}(\hat{\mathbf{V}}_i)\text{vec}^H(\hat{\mathbf{V}}_i)$.

Now the constraint. It is clear $\|\underline{\mathrm{s}}\|_2^2 = 1$ is proportional to $\|\underline{\alpha}\|_2^2 = 1$. So, we can write

the constraint as

$$\begin{aligned} \|\underline{\alpha}\|_2^2 &= \text{tr}(\underline{\alpha}\underline{\alpha}^H) \\ &= \text{tr}(\mathbf{A}) \\ &= \text{tr}(\mathbf{I}\mathbf{A}) \\ &= \text{vec}^H(\mathbf{I}\text{dim}(\mathbf{A}))\text{vec}(\mathbf{A}) = 1. \end{aligned} \tag{9.22}$$

Where in (6.9), the rank of $\mathbf{A}$ is implicitly constrained to 1. Without this constraint, we have an affine equality constraint in $\mathbf{A}$, giving a convex formulation in (9.45). The matrix $\mathbf{A}$ is necessarily positive semi-definite in order for (9.45) to be convex.

## 9.4 Appendices From Chapter 6

### 9.4.1 Gradient of ISL objective function

Given the cost function in (6.9) we compute the gradient vector. To facilitate the derivative operation we write (6.9) as a function of real variables using the following transformations

$$\mathbb{R}\{\underline{\text{s}}^H\mathbf{E}_\mathbf{m}\underline{\text{s}}\} = \begin{bmatrix} \underline{\text{s}}_r^t & \underline{\text{s}}_i^t \end{bmatrix} \begin{bmatrix} \mathbf{E}_{\mathbf{m}r} & -\mathbf{E}_{\mathbf{m}i} \\ \mathbf{E}_{\mathbf{m}i} & \mathbf{E}_{\mathbf{m}r} \end{bmatrix} \begin{bmatrix} \underline{\text{s}}_r \\ \underline{\text{s}}_i \end{bmatrix} \tag{9.23}$$

and

$$\mathbb{I}\{\underline{\text{s}}^H\mathbf{E}_\mathbf{m}\underline{\text{s}}\} = \begin{bmatrix} \underline{\text{s}}_r^t & \underline{\text{s}}_i^t \end{bmatrix} \begin{bmatrix} \mathbf{E}_{\mathbf{m}r} & \mathbf{E}_{\mathbf{m}i} \\ \mathbf{E}_{\mathbf{m}i} & -\mathbf{E}_{\mathbf{m}r} \end{bmatrix} \begin{bmatrix} \underline{\text{s}}_i \\ \underline{\text{s}}_r \end{bmatrix} \tag{9.24}$$

where subscripts $(\cdot)_r$ and $(\cdot)_i$ denote the real and imaginary components [133]. After simplification, this allows us to write the argument in the summation of (6.9) as

$$|\underline{\text{s}}^H\mathbf{E}_\mathbf{m}\underline{\text{s}}|^2 = (\underline{\text{s}}^H\mathbf{E}_\mathbf{m}\underline{\text{s}})(\underline{\text{s}}^H\mathbf{E}_\mathbf{m}\underline{\text{s}})^H \tag{9.25}$$

$$= \mathbb{R}\{\underline{\text{s}}^H\mathbf{E}_\mathbf{m}\underline{\text{s}}\}^2 + \mathbb{I}\{\underline{\text{s}}^H\mathbf{E}_\mathbf{m}\underline{\text{s}}\}^2 \tag{9.26}$$

$$= (\underline{\text{y}}^t\mathbf{B}_1\underline{\text{y}})^2 + (\underline{\text{y}}^t\mathbf{B}_2\underline{\text{y}})^2 \tag{9.27}$$

where $\underline{\mathrm{y}} = \begin{bmatrix} \underline{\mathrm{s}}_r^t \\ \underline{\mathrm{s}}_i^t \end{bmatrix}$, $\mathbf{B}_1 = \begin{bmatrix} \mathbf{E}_{\mathbf{m}r} & -\mathbf{E}_{\mathbf{m}i} \\ \mathbf{E}_{\mathbf{m}i} & \mathbf{E}_{\mathbf{m}r} \end{bmatrix}$ and $\mathbf{B}_2 = \begin{bmatrix} \mathbf{E}_{\mathbf{m}r} & \mathbf{E}_{\mathbf{m}i} \\ \mathbf{E}_{\mathbf{m}i} & -\mathbf{E}_{\mathbf{m}r} \end{bmatrix}$. The gradient vector is computed with multiple applications of the chain rule. The complete gradient is then given as

$$\nabla_{\underline{\mathrm{y}}} \mathrm{J}_{\mathrm{ISL}}(\underline{\mathrm{y}}) = 2 \sum_{m=1}^{M-1} (\underline{\mathrm{y}}^t \mathbf{B}_{1,m} \underline{\mathrm{y}})(\mathbf{B}_{1,m} + \mathbf{B}_{1,m}^t)\underline{\mathrm{y}} + (\underline{\mathrm{y}}^t \mathbf{B}_{2,m} \underline{\mathrm{y}})(\mathbf{B}_{2,m} + \mathbf{B}_{2,m}^t)\underline{\mathrm{y}}. \tag{9.28}$$

### 9.4.2 Hessian of ISL objective function

The Hessian is computed using the above gradient and applying multiple applications of the chain rule. We define the Hessian as

$$\mathcal{H}_{\underline{\mathrm{y}}} \mathrm{J}_{\mathrm{ISL}}(\underline{\mathrm{y}}) = \frac{\partial^2 \mathrm{J}_{\mathrm{ISL}(\underline{\mathrm{y}})}}{\partial \underline{\mathrm{y}} \partial \underline{\mathrm{y}}^t} \tag{9.29}$$

$$= \frac{\partial}{\partial \underline{\mathrm{y}}} \Big( \frac{\partial \mathrm{J}_{\mathrm{ISL}}}{\partial \underline{\mathrm{y}}} \Big)^t \tag{9.30}$$

$$= \frac{\partial}{\partial \underline{\mathrm{y}}} \big( \nabla_{\underline{\mathrm{y}}} \mathrm{J}_{\mathrm{ISL}(\underline{\mathrm{y}})} \big)^t. \tag{9.31}$$

Using the same definitions as above to simplify, we compute the complete Hessian as

$$\mathcal{H}_{\underline{\mathrm{y}}} \mathrm{J}_{\mathrm{ISL}}(\underline{\mathrm{y}}) = 2 \sum_{m=1}^{M-1} \Big[ \underline{\mathrm{y}}^t \mathbf{B}_{1,m} \underline{\mathrm{y}} (\mathbf{B}_{1,m} + \mathbf{B}_{1,m}^t) + (\mathbf{B}_{1,m} + \mathbf{B}_{1,m}^t) \underline{\mathrm{y}} \underline{\mathrm{y}}^t (\mathbf{B}_{1,m} + \mathbf{B}_{1,m}^t) \tag{9.32}$$

$$+ \underline{\mathrm{y}}^t \mathbf{B}_{2,m} \underline{\mathrm{y}} (\mathbf{B}_{2,m} + \mathbf{B}_{2,m}^t) + (\mathbf{B}_{2,m} + \mathbf{B}_{1,m}^t) \underline{\mathrm{y}} \underline{\mathrm{y}}^t (\mathbf{B}_{2,m} + \mathbf{B}_{2,m}^t) \Big]. \tag{9.33}$$

Of course, the Hessian can be further simplified for symmetric $\mathbf{B}_{1,2}$, allowing for ease of computation of the determinant.

### 9.4.3 Convex Relaxation of (6.9)

We derive a formulation for a convex relaxation of (6.9) that guarantees global optimality in the solution but sacrifices the rank-1 constraint on the $\underline{\alpha\alpha}^H = \mathbf{\Delta}$ matrix. The relaxation

is derived as follows:

$$\mathrm{J_{ISL}} = \sum_{m=1}^{M-1} (\underline{\mathrm{s}}^H \mathbf{E}_m \underline{\mathrm{s}})(\underline{\mathrm{s}}^H \mathbf{E}_m^{\mathrm{t}} \underline{\mathrm{s}}) \tag{9.34}$$

$$= \sum_{m=1}^{M-1} (\underline{\alpha}^H \mathbf{V}^H \mathbf{E}_m \mathbf{V} \underline{\alpha})(\underline{\alpha}^H \mathbf{V}^H \mathbf{E}_m^t \mathbf{V} \underline{\alpha}) \tag{9.35}$$

$$= \sum_{m=1}^{M-1} \boldsymbol{\Delta} \mathbf{V}^H \mathbf{E}_m \mathbf{V} \boldsymbol{\Delta} \mathbf{V}^H \mathbf{E}_m^t \mathbf{V} \tag{9.36}$$

$$= \sum_{m=1}^{M-1} \mathrm{tr}\{\boldsymbol{\Delta} \mathbf{V}^H \mathbf{E}_m \mathbf{V} \boldsymbol{\Delta} \mathbf{V}^H \mathbf{E}_m^t \mathbf{V}\} \tag{9.37}$$

where we know $\mathrm{tr}(\mathbf{ABCD}) = \mathrm{vec}^H(\mathbf{A}^H)\mathrm{vec}(\mathbf{D}^t \otimes \mathbf{B})\mathrm{vec}(\mathbf{C})$, [134] and therefore can write

$$\mathrm{J_{ISL}} = \sum_{m=1}^{M-1} \mathrm{vec}(\boldsymbol{\Delta})(\mathbf{V}^t \mathbf{E}_m \mathbf{V}^* \otimes \mathbf{V} \mathbf{E}_m \mathbf{V})\mathrm{vec}(\boldsymbol{\Delta}) \tag{9.38}$$

$$= \sum_{m=1}^{M-1} \mathrm{vec}^H(\boldsymbol{\Delta})\big[\mathbf{V}^* \otimes \mathbf{V}\mathbf{E}_m \otimes \mathbf{E}_m \mathbf{V}^* \otimes \mathbf{V}\big]\mathrm{vec}(\boldsymbol{\Delta}) \tag{9.39}$$

$$= \mathrm{vec}^H(\boldsymbol{\Delta})\big[\mathbf{V}^* \otimes \mathbf{V} \sum_{m=1}^{M-1} \Big(\mathbf{E}_m \otimes \mathbf{E}_m\Big) \mathbf{V}^* \otimes \mathbf{V}\big]\mathrm{vec}(\boldsymbol{\Delta}) \tag{9.40}$$

where the matrix $\Big[\mathbf{V}^* \otimes \mathbf{V} \sum_{m=1}^{M-1} \big(\mathbf{E}_m \otimes \mathbf{E}_m\big) \mathbf{V}^* \otimes \mathbf{V}\Big] = \beta$ is not guaranteed to be hermitian, therefore we take the Hermitian component $\frac{1}{2}(\beta^H + \beta) = \boldsymbol{\Gamma}$ for the analysis.

Additionally, it is clear $\|\underline{\mathrm{s}}\|_2^2 = 1$ is proportional to $\|\underline{\alpha}\|_2^2 = 1$. So, we can write the constraint as

$$\|\underline{\alpha}\|_2^2 = \mathrm{tr}(\underline{\alpha}\underline{\alpha}^H) \tag{9.41}$$

$$= \mathrm{tr}(\boldsymbol{\Delta}) \tag{9.42}$$

$$= \mathrm{tr}(\mathbf{I}\boldsymbol{\Delta}) \tag{9.43}$$

$$= \mathrm{vec}^H(\mathbf{I}\mathrm{dim}(\boldsymbol{\Delta}))\mathrm{vec}(\boldsymbol{\Delta}) = 1 \tag{9.44}$$

Where in (6.9), the rank of $\mathbf{\Delta}$ is implicitly constrained to 1 and $\dim(\mathbf{\Delta}) = M$. Without this constraint, we have an affine equality constraint in $\mathbf{\Delta}$. The matrix $\mathbf{A}$ is necessarily positive semi-definite.

The relaxed optimization is then defined as

$$\min_{\mathbf{\Delta}} \text{vec}^H(\mathbf{\Delta})\mathbf{\Gamma}\ \text{vec}(\mathbf{\Delta}) \tag{9.45}$$

$$\text{s.t.}\ \ \text{vec}^H(\mathbf{I}\text{dim}(\mathbf{\Delta}))\text{vec}(\mathbf{\Delta}) = 1 \tag{9.46}$$

The solution to (9.45) will, most likely, yield a higher than rank-1 $\mathbf{\Delta}$ matrix (hence the relaxation). Therefore, the recovery procedure to synthesise a waveform using the rank-1 weights vector is to find the best rank-1 eigen-weights ($\underline{\alpha}_{\text{relax}}$) solution as defined by having the lowest ISL waveform. We accomplish by performing an eigen-decomposition on the $\mathbf{\Delta}$ matrix and computing an exhaustive search of all possible waveforms with the prescribed eigen-basis of the interference and noise covariance matrix $\mathbf{K}$.

For $M = 24$ and for a total of 25 Monte Carlo trials we have computed the lowest ISL rank-1 solution waveform and display the results in figure 9.1 and 9.2 for the ISL and SINR as a function of the Eigen-basis dimension, respectively. Notice, as expected, the lower dimension basis solution improves the sidelobe levels, however, as the basis-dimension increases, the solution is broad over the $\mathbf{\Delta}$ matrix and therefore the lowest ISL rank-1 solution is not as effective. The SINR, however, degrades as if the ISL is being improved. This analysis motivates use of the non-convex formulation in (6.9) and the performance models developed.

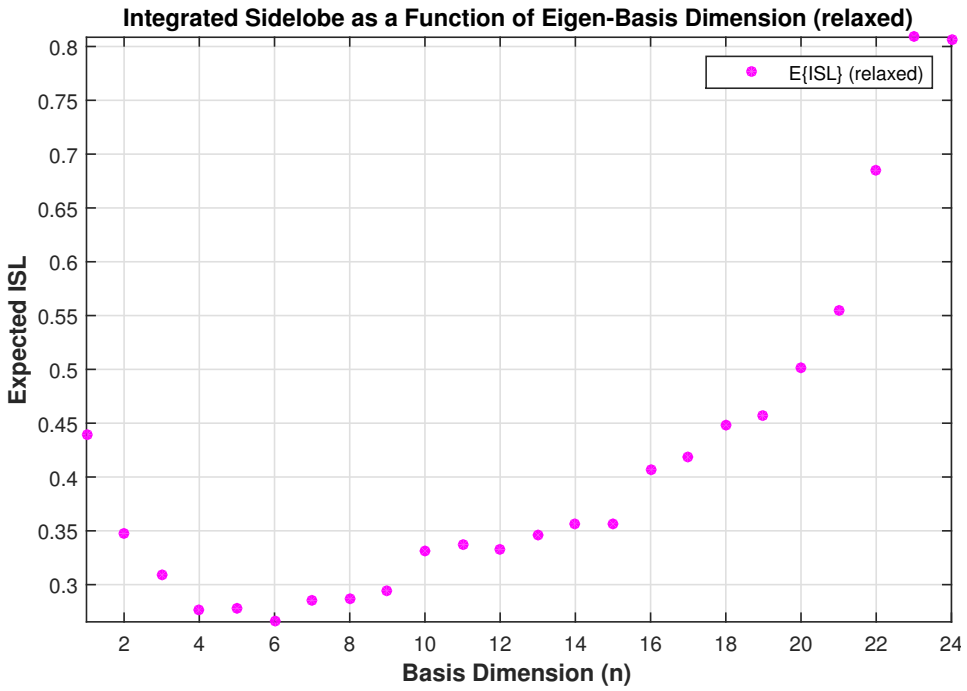


Figure 9.1: Output ISL of (9.45) with the lowest ISL rank-1 solution as a function of the Eigen-basis dimension.

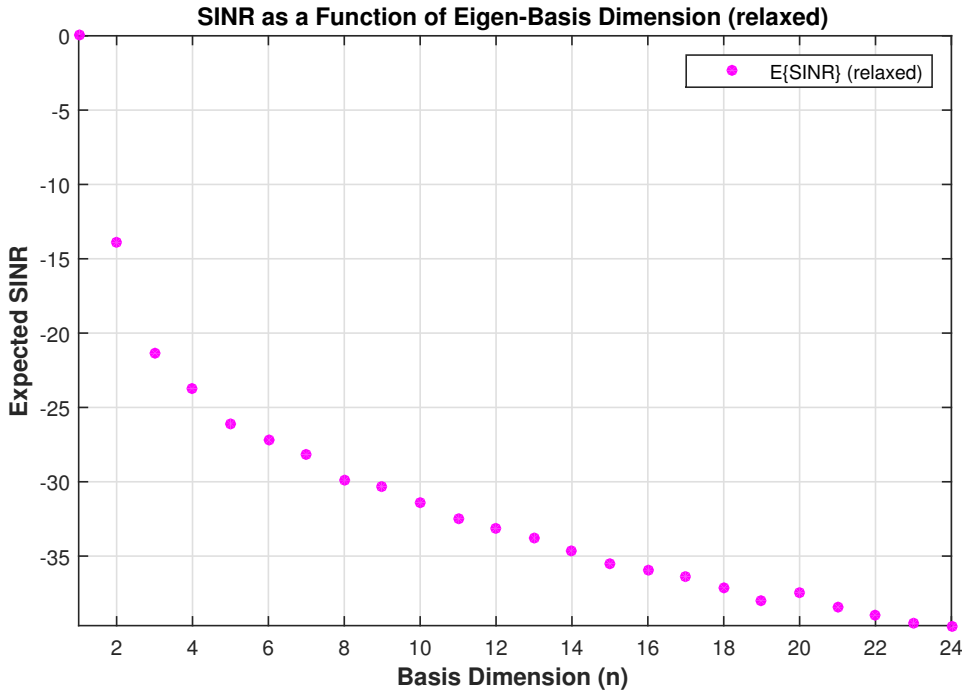


Figure 9.2: Output SINR of (9.45) with the lowest ISL rank-1 solution as a function of the Eigen-basis dimension.

# Bibliography


[1] M. Rangaswamy, "Sam challenges for fully adaptive radar," AFRL Sensors Directorate, Hoboken, NJ, Tech. Rep., June 2012.

[2] G. Scalzi, "Afrl sensors directorate rf range measurement capabilities," Presentation, October 2014.

[3] L. Patton, S. Frost, and B. Rigling, "Efficient design of radar waveforms for optimised detection in coloured noise," *IET Radar, Sonar and Navigation*, vol. 6, no. 1, pp. 22–29, 2012.

[4] J. R. Guerci, "Cognitive radar: A knowledge-aided fully adaptive approach," in *Radar Conference*. Washington, D. C.: IEEE, May 2010, pp. 1365–1370.

[5] ——, *Cognitive Radar: The knowledge-aided fully adaptive approach*. Norwood, MA: Artech House Publishers, 2010.

[6] S. Pillai, K. Y. Li, I. Selesnick, and B. Himed, *Waveform Diversity Theory and Applications*, 1st ed. McGraw-Hill, 2011.

[7] P. Woodward, *Probability and Information Theory, with Applications to Radar*. Pergamon, 1953.

[8] ——, "Theory of radar information," *IEEE Transactions on Information Theory*, vol. 1, no. 1, pp. 108–113, 1953.

[9] J. Benedetto, I. Konstantinidis, and M. Rangaswamy, "Phase-coded waveforms and their design," *IEEE Signal Processing Magazine*, pp. 22–31, January 2009.

[10] L. M. Corporation, "Apg-67 multimode radar," brochure, 2007.

[11] V. V. J. H. and D. Middleton, "A theoretical comparison of the visual , aural, and meter reception of pulsed signals in the presence of noise," *J. Appl. Phys.*, vol. 17, no. 11, pp. 940–971, 1946.

[12] D. K. Barton, *Radars Volume 3*. Dedham, MA: Artech House Publishers, 1975.

[13] P. Antonik, M. Wicks, H. Griffiths, and C. Baker, *Principles of Waveform Diversity and Design*, 1st ed. Raleigh, NC: SciTech Publishing, Inc., 2010.

[14] P. Stoica, H. He, and J. Li, "New algorithms for designing unimodular sequences with good correlation properties," *IEEE Transactions of Signal Processing*, vol. 57, pp. 1415–1425, April 2009.

[15] J. Li, J. Guerci, and L. Xu, "Signal waveform's optimal under restriction design for active sensing," in *Sensor Array and Multichannel Processing, 2006. Fourth IEEE Workshop on*, 2006, pp. 382–386.

[16] A. M. Jones, B. Rigling, and M. Rangaswamy, "Eigen-space analysis of constrained adaptive radar waveform design," in *Proceeedings of the 2014 IEEE Radar Conference*. Cincinnati, OH: IEEE, May 2014, pp. 0829–0824.

[17] J. Albrecht, A. Kane, and T. Chang, "Darpa's microscale power conversion program." IEEE, 2012.

[18] M. Skolnik, *Introduction to radar systems*, 3rd ed. New York, NY: McGraw-Hill, 1980.

[19] S. Haykin, "Cognitive radar: a way of the future," *Signal Processing Magazine, IEEE*, vol. 23, no. 1, pp. 30–40, February 2006.

[20] J. R. Guerci, R. M. Guerci, M. Rangaswamy, J. S. Bergin, and M. C. Wicks, "Cofar: Cognitive fully adaptive radar," in *Radar Conference*. Cincinnati, OH: IEEE, May 2014, pp. 984–989.

[21] I. Reed, J. Mallett, and L. Brennan, "Rapid convergence rate in adaptive arrays," *IEEE Transactions on Aerospace and Electronic Systems*, vol. 10, no. 6, pp. 853–863, November 1974.

[22] G. Wang and Y. Lu, "Designing single/multiple sparse frequency waveforms with sidelobe constraint," *Radar, Sonar, Navigation IET*, vol. 5, no. 1, pp. 32–38, 2011.

[23] A. M. Jones, B. D. Rigling, and M. Rangaswamy, "Eigen-basis analysis of expected modulus perturbation for constrained signal design," in *Signal, Systems and Computers, 48th Asilomar conference on*. Pacific Grove, CA: IEEE, Nov. 2014, pp. 2021–2026.

[24] ——, "Performance models for sidelobe constrained signal design with eigen-basis formulation," in *Proceedings of the 2015 IEEE Radar Conference*. Arlington, VA: IEEE, May 2015, pp. 0828–0833.

[25] ——, "Generation of synthetic uhf rfi in urban north american environments," in *Proceedings of the 2016 IEEE Radar Conference*. Philadelphia, PA: IEEE Xplore, 2016, p. to appear.

[26] S. Frost, "Markov chain spectrum representations for sidelobe prediction," 2015, personal Correspondence.

[27] L. Patton, "On the Satisfaction of Modulus and Ambiguity Function Constraints In Radar Waveform Optimization for Detection," Ph.D. dissertation, Wright State University, 2009.

[28] S. Haykin, *Adaptive Filter Theory*, 3rd ed. Upper Saddle River, New Jersey: Prentice Hall, 1996.

[29] A. M. Jones, B. D. Rigling, and M. Rangaswamy, "Signal-to-interference-plus-noise-ratio analysis for constrained radar waveforms," *Aerospace and Electronic Systems, IEEE Transactions on*, May accepted for publication 2016.

[30] S. Sussman, "Least-square synthesis of radar ambiguity functions," *IRE Transactions on Information Theory*, pp. 246–254, April 1961.

[31] R. McAulay and R. Johnson, "Optimal mismatched filter design for radar ranging, detection, and resolution," *IEEE Transactions on Information Theory*, vol. 17, no. 6, pp. 696–701, November 1971.

[32] J. S. Bergin, P. M. Techau, J. E. Don Carlos, and J. R. Guerci, "Radar waveform optimization for colored noise mitigation," in *Radar Conference*. IEEE, May 2005, pp. 1–6.

[33] L. Patton and B. Rigling, "Autocorrelation and modulus constraints in radar waveform optimization," in *International Waveform Diversity and Design Conference*. IEEE, 2009.

[34] P. Stoica, H. He, and J. Li, "On designing sequences with impulse-like periodic correlation," *IEEE Signal Processing Letters*, vol. 16, no. 8, pp. 703–706, August 2009.

[35] S. Frost, "Performance analysis of radar waveforms for congested spectrums," Master's thesis, Wright State University, November 2011.

[36] S. Frost and B. Rigling, "Performance comparison for constrained radar waveform design," in *IEEE RadarCon 2011 Proceedings*. IEEE, 2011, pp. 724–728.

[37] D. Chu, "Polyphase codes with good periodic correlation properties," *IEEE Transactions on Information Theory*, vol. 18, no. 4, pp. 532–532, July 1972.

[38] A. M. Jones, B. D. Rigling, and M. Rangaswamy, "Subspace approach to performance analysis for subspace approach to performance analysis for range-sidelobe suppressed waveforms," *IET Radar, Sonar and Navigation*, In review.

[39] A. Nehorai, V. Gini, A. Greco, A. P. Suppappola, and M. Rangaswamy, "Introduction to the issue on adaptive waveform design for agile sensing and communication," *IEEE J. Sel. Topics in Sig. Proc.*, vol. 1, no. 1, pp. 2–5, June 2007.

[40] A. P. Suppappola, A. Nehorai, and R. Calderbank, "Waveform-agile sensing and processing," *IEEE Signal Processing Magazine*, vol. 26, no. 1, pp. 10–11, January 2009.

[41] N. Levenon and E. Mozeson, *Basic Radar Signals, in Radar Signals*. Hoboken, NJ, USA: John Wiley and Sons, Inc., 2004.

[42] M. Skolnik, *Introduction to Radar Systems*. New York, McGraw Hill Book Co., 1980, vol. 1.

[43] M. Richards, *Fundamentals of radar signal processing*. Tata McGraw-Hill, 2005.

[44] B. Mahafza, *Radar Signal Analysis and Processing Using MATLAB*. CRC Press, New Delhi, 2011.

[45] V. Gini, A. De Maio, and L. Patton, Eds., *Waveform Design and Diversity for Advanced Radar Systems*, 1st ed. The Institution of Engineering and Technology, 2012.

[46] M. Richards, *Principles of Modern Radar, Basic Principles*, 1st ed. SciTech Publishing, Inc., 2010, vol. 1.

[47] P. Stoica, J. Li, and M. Xue, "Transmit codes and receive filters for radar," *IEEE Signal Processing Magazine*, pp. 94–109, November 2008.

[48] S. Sira, Y. Li, A. Papandreou-Suppappola, D. Morrell, D. Cochran, and M. Rangaswamy, "Waveform-agile sensing for tracking," *IEEE Signal Processing Magazine*, pp. 53–64, January 2009.

[49] R. Calderbank, S. Howard, and B. Moran, "Waveform diversity in radar signal processing," *IEEE Signal Processing Magazine*, pp. 32 – 41, January 2009.

[50] R. Mitchell and A. Rihaczek, "Matched-filter responses of the linear fm waveform," *IEEE Transcations on Aerospace and Electronic Systems*, vol. 4, no. 3, pp. 417–432, May 1968.

[51] P. Antonik and M. Wicks, "Waveform diversity: Past, present, and future," in *IET International Conference on Radar Systems*, 2007.

[52] R. H. Barker, *Group Synchronizing of Binary Digital Sequences*. New York: Academic Press, 1953, no. pp 273-287.

[53] S. Ying, S. Weihua, and L. Guosui, "Ambiguity function of chaotic phase modulated radar signals," in *Fourth International Conference on Signal Processings*. ICSP, 1998.

[54] S. De Nicola, Y. Huang, A. De Maio, S. Zhang, and A. Farina, "Code optimization with similarity and accuracy constraints," in *Radar Conference, 2008. RADAR '08. IEEE*, 2008, pp. 1–6.

[55] R. Manasse, "The use of pulse coding to discriminate against clutter," p. 15, 1961.

[56] M. J. E. Golay, "Notes on digital coding," *Proc. IRE*, vol. 37, p. 657, 1949.

[57] R. Gold, "Optimal binary sequences for spread spectrum multiplexing (corresp.)," *IEEE Transactions on Information Theory*, vol. 13, no. 4, pp. 619–621, January 1967.

[58] S. W. Golomb and R. A. Scholtz, "Generalized barker sequences," *IEEE Transactions on Information Theory*, vol. 11, no. 4, pp. 533–537, January 1965.

[59] B. L. Lewis and F. F. Kretschmer Jr., "A new class of polyphase pulse compression codes and techniques," *IEEE Transactions on Aerospace and Electronic Systems*, vol. 17, no. 3, pp. 364–372, May 1981.

[60] R. L. Frank, "Polyphase codes with good nonperiodic correlation properties," *IEEE Transactions on Information Theory*, vol. 9, pp. 43–45, January 1963.

[61] T. Mao, X. Gong, H. Meng, and X. Wang, "Phase-modulated waveform design for the target detection in the presence of signal-dependent clutter," in *Waveform Diversity and Design Conference, 2010 International*, Niagara Falls, ON, August 2010, pp. 100–104.

[62] M. F. Mesiya and P. J. Mclane, "Design of optimal radar signals subject to a fixed amplitude constraint," *IEEE Transcations on Aerospace and Electronic Systems*, vol. 9, no. 5, pp. 679–687, September 1973.

[63] A. De Maio, Y. Huang, M. Piezzo, S. Zhang, and A. Farina, "Design of optimized radar codes with a peak to average power ratio constraint," *IEEE Transactions of Signal Processing*, vol. 59, no. 6, pp. 2683–2697, June 2011.

[64] M. Soltanalian and P. Stoica, "Design of perfect phase-quantized sequences with low peak-to-average-power ratio," in *20th European Signal Processing Conference*. EUSIPCO, August 2012.

[65] F. Schweppe and D. Gray, "Radar signal design subject to simultaneous peak and average power constraints," *IEEE Transactions on Information Theory*, vol. 12, no. 1, pp. 13–26, January 1966.

[66] D. Tufts and D. Shnidman, "Optimum waveforms subject to both energy and peak-value constraints," *Proceedings of the IEEE*, pp. 1002 – 1007, September 1964.

[67] M. I. Skolnik, *Radar Handbook*, 3rd ed. McGraw-Hill Professional, February 2008.

[68] M. Soltanalian, "Signal design for active sensing and communications," Ph.D. dissertation, Uppsala University, 2014.

[69] M. A. Richards, "Time and frequency domain windowing of lfm pulses," 29 September 2006.

[70] L. Patton and B. Rigling, "Phase retrieval for radar waveform optimization," *IEEE Transcations on Aerospace and Electronic Systems*, vol. 48, no. 4, pp. 3287–3301, October 2012.

[71] R. A. Romero and N. A. Goodman, "Information-theoretic matched waveform in signal dependent interference." IEEE, 2008.

[72] M. Bell, "Information theory and radar waveform design," *IEEE Transactions on Information Theory*, vol. 39, no. 5, pp. 1578–1597, September 1993.

[73] H. Trees, "Optimum signal design and processing for reverberation-limited environments," *IEEE Transactions on Military Electronics*, pp. 212–229, July-October 1965.

[74] D. DeLong and E. Hofstetter, "On the design of optimum radar waveforms for clutter rejection," *IEEE Transactions on Information Theory*, vol. 13, no. 3, pp. 454–463, July 1967.

[75] L. Patton and B. Rigling, "Optimal signal/filter design for multi-target detection in colored noise," *IEEE*, pp. 276–281, 2011.

[76] S. Pillai, D. Youla, H. Oh, and J. Guerci, "Optimum transmit-receiver design in the presence of signal-dependent interference and channel noise," *IEEE*, pp. 870–875, 1999.

[77] S. Kay, "Optimal signal design for detection of gaussian point targets in stationary gaussian clutter/reverberation," *IEEE J. Sel. Topics in Sig. Proc.*, vol. 1, no. 1, pp. 31–41, June 2007.

[78] L. Spafford, "Optimum radar signal processing in clutter," *IEEE Transactions on Information Theory*, vol. 14, no. 5, pp. 734 – 742, September 1968.

[79] L. Sibul and E. Tittlebaum, "Signal design for detection of targets in clutter," *Proceedings of the IEEE*, vol. 69, no. 4, pp. 481–482, April 1981.

[80] R. A. Romero and N. A. Goodman, "Waveform design in signal-dependent interfernece and application to target recognition with multiple transmissions," *IET Radar, Sonar and Navigation*, vol. 3, no. 4, pp. 328–340, 2009.

[81] S. Pillai, H. Oh, and J. Guerci, "Multichannel matched transmit-receiver design in presence of signal-dependent interference and noise," in *Sensor Array and Multichannel Signal Processing Workshop. 2000. Proceedings of the 2000 IEEE*, 2000, pp. 385–389.

[82] M. Cook, S. Blunt, and J. Jakabosky, "Optimization of waveform diversity and performance for pulse-agile radar." IEEE, 2011.

[83] W. Rummler, "A technique for improving the clutter performance of coherent pulse train signals," *IEEE Transcations on Aerospace and Electronic Systems*, vol. 3, no. 6, pp. 898–906, November 1967.

[84] ——, "Clutter suppression by complex weighting of coherent pulse trains," *IEEE Transcations on Aerospace and Electronic Systems*, vol. 2, no. 6, pp. 689–699, November 1965.

[85] M. Ares, "Optimum burst waveforms for detection of targets in uniform range-extended clutter," *IEEE Transcations on Aerospace and Electronic Systems*, Jan. 1967.

[86] A. Aubry, A. DeMaio, A. Farina, and M. Wicks, "Knowledge-aided (potentially cognitive) transmit signal and receive filter design in signal-dependent clutter," *Aerospace and Electronic Systems, IEEE Transactions on*, vol. 49, no. 1, pp. 93–117, January 2013.

[87] C. W. Rossler and L. Patton, "Rapid waveform adaptation for nearly optimal detection in colored interference," in *2nd International Workshop on Cognitive Information Processing*, 2010, pp. 232–236.

[88] K. Wong, "Adaptive pulse-diverse radar/sonar waveform design," *IEEE*, pp. 105–110, 1998.

[89] S. Kay, "Optimal transmit signal design for active sonar/radar," in *IEEE International Conference on Acoutstics, Speech, and Signal Processing*, vol. 2, Orlando, FL, 13-17 May 2002, pp. II–1513 – II–1516.

[90] M. Lindenfeld, "Sparse frequency transmit and receive waveform design," *IEEE Transcations on Aerospace and Electronic Systems*, vol. 40, no. 3, pp. 851 – 861, July 2004.

[91] N. A. Goodman, P. Venkata, and M. A. Neifeld, "Adaptive waveform design and sequential hypothesis for target recognition with active sensors," *IEEE J. Sel. Topics in Sig. Proc.*, vol. 1, no. 1, pp. 105–113, june 2007.

[92] A. Sowelam, Sameh; Tewfik, "Waveform selection in radar target classification," *IEEE Transactions on Information Theory*, vol. 46, no. 3, pp. 1014–1029, May 2000.

[93] Q. Liang, "Automatic target recognition using waveform diversity in radar sensor networks," *Pattern Recognition Letters*, vol. 29, pp. 377–381, Nov. 2007.

[94] L. Patton, C. Bryant, and B. Himed, "Radar-centric design of waveforms with disjoint spectral support," in *Radar Conference, 2012 IEEE*. IEEE, 2012.

[95] W. Chung and K. Wong, "Pulse-diverse radar waveform design for accurate joint estimation of time delay and doppler shift," *IEEE*, pp. 3037 – 3040, 2000.

[96] L. Patton and B. Rigling, "Nonquadratic regularization for waveform optimization." IEEE, 2006, pp. 763–768.

[97] B. Friedlander, "A subspace framework for adaptive radar waveform design," 2005.

[98] R. Kassab, M. Lesturgie, and J. Fiorina, "Alternate projections technique for radar waveform design," 2009.

[99] Multiple, "Gerchber-saxton algorithm," March 2012. [Online]. Available: http://en.wikipedia.org/wiki/GerchbergSaxton_algorithm

[100] P. Swerling, "Probability of detection for fluctuating targets," RAND Corporation, Research Memorandum, 1954.

[101] S. Frost and B. Rigling, "Sidelobe predictions for spectrally-disjoint radar," Radar Conference. IEEE, May 2012.

[102] J. M. Loomis, "Army radar requirements for the 21st century," in *Radar Conference, 2007 IEEE*, April 2007, pp. 1–6.

[103] P. M. Baggenstoss, "Class specific classifier: Avoiding the curse of dimensionality," *IEEE Aerospace and Electronic Systems Magazine*, vol. 19, no. 1, pp. 37–52, January 2004.

[104] V. Marcenko and L. Pastur, "Distribution of eigenvalues for some sets of random matrices," *Math USSR-Sbornik*, vol. 1, no. 4, pp. 457–483, 1967.

[105] R. Gray, "On the asymptotic eigenvalue distribution of toeplitz matrices," *IEEE Transactions on Information Theory*, vol. 18, no. 6, pp. 725–730, November 1972.

[106] ——, "Toeplitz and circulant matrices: A review," *Journal of Communications and Information Theory*, vol. 2, no. 3, pp. 1567–2190, August 2005.

[107] ——, *Toeplitz and Circulant Matrices: A Review*. The Netherlands: Now Publishers Inc, 2005, vol. 2, no. 3.

[108] A. van den Bos, "Complex gradient and hessian," *IEE Proceedings - Vis. Image Signal Processing*, vol. 141, no. 6, pp. 380 – 382, December 1994.

[109] A. Hjorungnes and D. Gesbert, "Complex-valued matrix differentiation: Techniques and key results," *IEEE Transactions of Signal Processing*, vol. 55, no. 6, pp. 2740–2746, June 2007.

[110] MATLAB, *Version 7.14.0.739 (2013b)*. The MathWorks Inc., 2012.

[111] H. Zhou, B. Wen, and W. S, "Dense radio frequency interference suppression in hf radars," *IEEE Signal Processing Letters*, vol. 12, no. 5, pp. 361–364, May 2005.

[112] L. Devroye, "Sample-based non-uniform random variate gerneration," in *Proceedings of the 18th Conference on Winter Simulation*. ACM, 1986, pp. 260–265.

[113] T. K. Moon and W. C. Stirling, *Mathematical methods and algorithms for signal processing*. New York: Prentice Hall, 2000, vol. 1.

[114] D. Messerschmitt, "Autocorrelation matrix eigenvalues and the power spectrum," EECS Department, University of California, Berkeley, Tech. Rep. UCB/EECS-2006-90, June 2006.

[115] J. Proakis, *Digital Communications*, 3rd ed. McGraw-Hill, March 1994.

[116] M. Wax and Kailath, "Detection of signals by information theoretic criteria," *IEEE Transactions Acoust. Speech Signal Processing*, vol. 33, no. 2, pp. 387–392, April 1985.

[117] K. Sunggon, J. Lee, and D. Sung, "A shifted gamma distribution model for long-range dependent internet traffic," *IEEE Communications Letters*, vol. 7, no. 3, pp. 124–126, March 2003.

[118] K. S. Shanmugan and A. M. Breipohl, *Random Signals: Detection, Estimation and Data Analysis*, 1st ed. New York: John Wiley and Sons, 1988.

[119] T. Cover and J. Thomas, *Elements of Information Theory*, 2nd ed. Wiley, 2006.

[120] P. Setlur and M. Rangaswamy, "Joint filter and waveform design for radar stap in signal dependent interference," AFRL Sensors Directorate, Tech. Rep. AFRL-RY-WP-TP-2015-0170, October 2015.

[121] S. Boyd and L. Vandenberghe, *Convex Optimization*. Cambridge University Press, 2004.

[122] J. Guerci, *Space-Time Adaptive Processing for Radar*. Artech House Publishers, July 2003.

[123] S. Kay, *Fundamentals of Statistical Signal Processing: Detection Theory*. Upper Saddle River, New Jersey: Prentice Hall, 1998.

[124] J. R. Guerci, R. W. Schutz, and J. D. Hulsmann, "Constrained optimum matched illumination-reception radar," *United States Patent*, p. 8, September 1992.

[125] P. Antonik, M. Wicks, H. Griffiths, and C. Baker, "Multi-mission multi-mode waveform diversity," in *Radar, 2006 IEEE Conference on*. IEEE, 2006, p. 3.

[126] B. Kang, "L1 optimization of cumulative modulus," Nov. 2015, personal Correspondence.

[127] G. Lame, *Examen Des Differentes Methodes Employees Pour Resoudre Les Problemes de Geometrie: Paris, Vve Courcier, 1818*. Paris A. Hermann, 1903.

[128] M. E. J. Newman, "Power laws, pareto distributions and zipf's law," *Contemporary Physics*, vol. 46, no. 5, pp. 323–351, December 2005.

[129] M. Grant and S. Boyd, "Cvx: Matlab software for disciplined convex programming, version 2.1," http://cvxr.com/cvx, March 2014.

[130] ——, "Graph implementations for nonsmooth convex programs," in *Recent Advances in Learning and Control*, ser. Lecture Notes in Control and Information Sciences, V. Blondel, S. Boyd, and H. Kimura, Eds. Springer-Verlag Limited, 2008, pp. 95–110.

[131] A. M. Jones, B. D. Rigling, and M. Rangaswamy, "Motivations to develop performance prediction for adaptive radar," in *IEEE National Aerospace and Electronics Conference and Ohio Innovation Summit (NAECON-OIS)*. Dayton, OH: IEEE, June 2015.

[132] N. R. Goodman, "The distribution of the determinnant of a complex wishart distributed matrix," *The Annals of Mathematical Statistics*, vol. 34, no. 1, pp. 178–180, March 1963.

[133] A. Beck and Y. Eldar, "Strong duality in noncovex quadratic optimization with two quadratic constraints," *SIAM Journal On Optimization*, vol. 17, no. 3, pp. 844–860, 2006.

[134] A. Hjorungnes, *Complex-Valued Matrix Derivatives*. The Edinburgh Building, Cambridge CB2 8RU, UK: Cambridge University Press, 2011.